U.S. GEOLOGICAL SURVEY
Reston, VA 22092

Memorandum

Date 3/17/80

To: Branch of Plans and Program Management
Publications Division

From: Chief, Office of Scientific Publications

Subject: New USGS open-file report

The following report was authorized by Henry Spall for the Director

on 4/6/79 for release in the open files:

TITLE: Polarization of bay-type geomagnetic disturbances in the Rio Grande Rift, New Mexico

AUTHOR(S): James N. Towle

CONTENTS: 67 p., _____ over-size sheets (i.e., larger than 8½ x 11 inches)

Map scale: _____

Depositories:

(NC) USGS Library, Room 4A100, 12201 Sunrise Valley Dr., Reston, VA 22092
(Da) USGS Library, 1526 Cole Blvd. at West Colfax Ave., Golden, CO
(Mail address: Stop 914, Box 25046, Federal Center, Denver, CO 80225)
(M) USGS Library, 345 Middlefield Rd., Menlo Park, CA 94025
(U) USGS, Room 8105, Federal Bldg., 125 South State St., Salt Lake City, UT 84138
(T) USGS, Room 1-C-45, 1100 Commerce St., Dallas, TX 75242
USGS, 7th Floor, 505 Marquette NW (P.O. Box 26659), Albuquerque, NM 87125
New Mexico Bur. Mines & Mineral Resources, Campus Station, Socorro, NM 87801

PRICE:	ORIGINATING OFFICE	
Fiche $_____	Name: DTRU, USGS, Stop 902, Box 25046	Release date: APRIL 1980
Paper $_____	Address: DEC, Denver, CO	Area: NEW MEXICO
	Telephone: FTS- 234-2445	OFR No. 80-377

UNITED STATES DEPARTMENT OF THE INTERIOR

GEOLOGICAL SURVEY

Polarization of geomagnetic bay-type disturbances in the Rio Grande rift

by

James N. Towle

Open-File Report 80-377

1980

Table of Contents

Abstract

Data recorded by six three-component fluxgate magnetometers located across the Rio Grande Rift are presented as time records and hodographs of the three geomagnetic components. Differential field calculations indicate that the geomagnetic variation anomaly associated with the Rio Grande Rift is due to local concentration of current flow in a regionally induced telluric current system.

Polarization of bay-type geomagnetic disturbances

in the Rio Grande rift, New Mexico

by

James N. Towle

Introduction

The first investigations of geomagnetic variations across the Rio Grande Rift, a system of en echelon rift valleys extending from southern Colorado to Mexico through the central portion of New Mexico, were conducted by Schmucker (1964, 1970) in order to determine the extent to which the surface expression of rifting was manifest in the structure of the lower crust and upper mantle. Schmucker's study suggested the presence of a zone of anomalously high electrical conductivity beneath southern Arizona and New Mexico. More recently, Swift (1967) in a series of deep magnetotelluric soundings reported a shoaling of the 1200°C isotherm beneath the Rio Grande Rift. A summary of these observations and a series of heat flow measurements have been presented by Warren and others (1969).

The relatively wide spacing of instruments in Schmucker's study and other large scale geomagnetic array studies in the Southwest (Reitzel and others, 1970; Porath and Gough, 1971) has precluded a detailed interpretation of the lateral extent of the geomagnetic variation anomaly associated with the Rio Grande Rift. In the spring of 1977 the U.S. Geological Survey (USGS) occupied nine sites across the Rio Grande Rift in central New Mexico in order to conduct a detailed study of this geomagnetic variation anomaly. The general geologic setting of the Rio

Grande Rift and the station locations of the USGS study are shown in figure 1. This report presents data selected from three periods of geomagnetic activity during the spring of 1977 during which isolated bay-type geomagnetic disturbances were observed. Time records and hodographs of data for these events are presented in the Appendices. During the selected events only six of the nine stations were operating properly.

Instrumentation

The instrumentation used in this study was designed by the USGS for detailed investigations of geomagnetic induction anomalies (Towle and others, 1979). The instrument package consists of an EDA Model FM 100B fluxgate magnetometer* modified to provide ±500 nT dynamic range and a Sea Data Model 651-2 digital data acquisition system. The noise level of the combined magnetometer-data logging system is less than 1 nT. The instrumentation is self contained and designed to operate unattended for periods of up to 45 days. Data are recorded on digital tape cassettes which are subsequently transcribed for data processing on a dedicated minicomputer system. The sampling interval for the data presented in this report was 8 seconds.

Field Observations

The three components of the time-varying geomagnetic field, X(t), Y(t), and Z(t), (magnetic northward, magnetic eastward and downward components respectively) at Gallup, N. Mex. (GAL) are shown in Figures

*Use of brand names in this report is for descriptive purposes only and does not constitute endorsement by the U.S. Geological Survey.

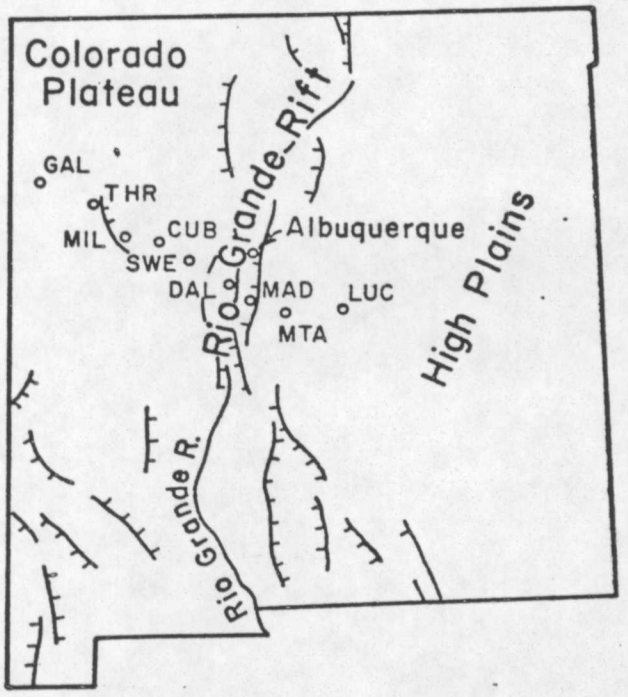

Figure 1. Index map of New Mexico showing recording sites, major geologic provinces, and faults bounding the Rio Grande rift. Station locations abbreviated as follows: GAL (Gallup), THR (Thoreau), MIL (Milan), CUB (Cubero), SWE (Swanee), DAL (Dalies), MAD (Madrone), MTA (Mountainair), LVC (Lucy).

A.1.1, A.2.1 and A.3.1 for the three data intervals processed in this study. Each interval was selected to contain at least one isolated baytype geomagnetic disturbance.

An alternative presentation of this data which emphasizes the directional variations associated with a geomagnetic field disturbance, is the hodographic projection, or hodograph, of the three dimensional path that is traced by the tip of the geomagnetic field vector during a disturbance. At each recording site the time-varying geomagnetic field can be described by the field vector, $\bar{F}(t)$, where

$$\bar{F}(t) = X(t)i + Y(t)j + Z(t)k. \qquad (1)$$

In conventional geomagnetic notation, the unit vector $\hat{i}$ is directed to the magnetic north, the unit vector $\hat{j}$ is directed to the magnetic east and the unit vector $\hat{k}$ is directed downward. A hodograph is then the projection of F(t) on an appropriate reference plane. In this study the X-Y plane (top view), the Y-Z plane (end view) and X-Z plane (side view) have been selected as the reference planes, as illustrated in Figure 2.

Figures A.1.2 through A.1.7 show hodographs of geomagnetic field variations that occurred from 0100 thru 0430 u.t. on April 25, 1977. This bay-type geomagnetic disturbance, which is identified as Event 1 in this study, is characterized by a predominantly NW-SE horizontal polarization.

Hodographs of the geomagnetic variations that occurred from 0600 through 1400 u.t. on May 3, 1977 are shown in figures A.2.2 thru A.2.7. This data interval is identified as Event 2 in this report. Two geomagnetic bay-type disturbances were recorded during this interval, each of which has an approximately E-W polarization.

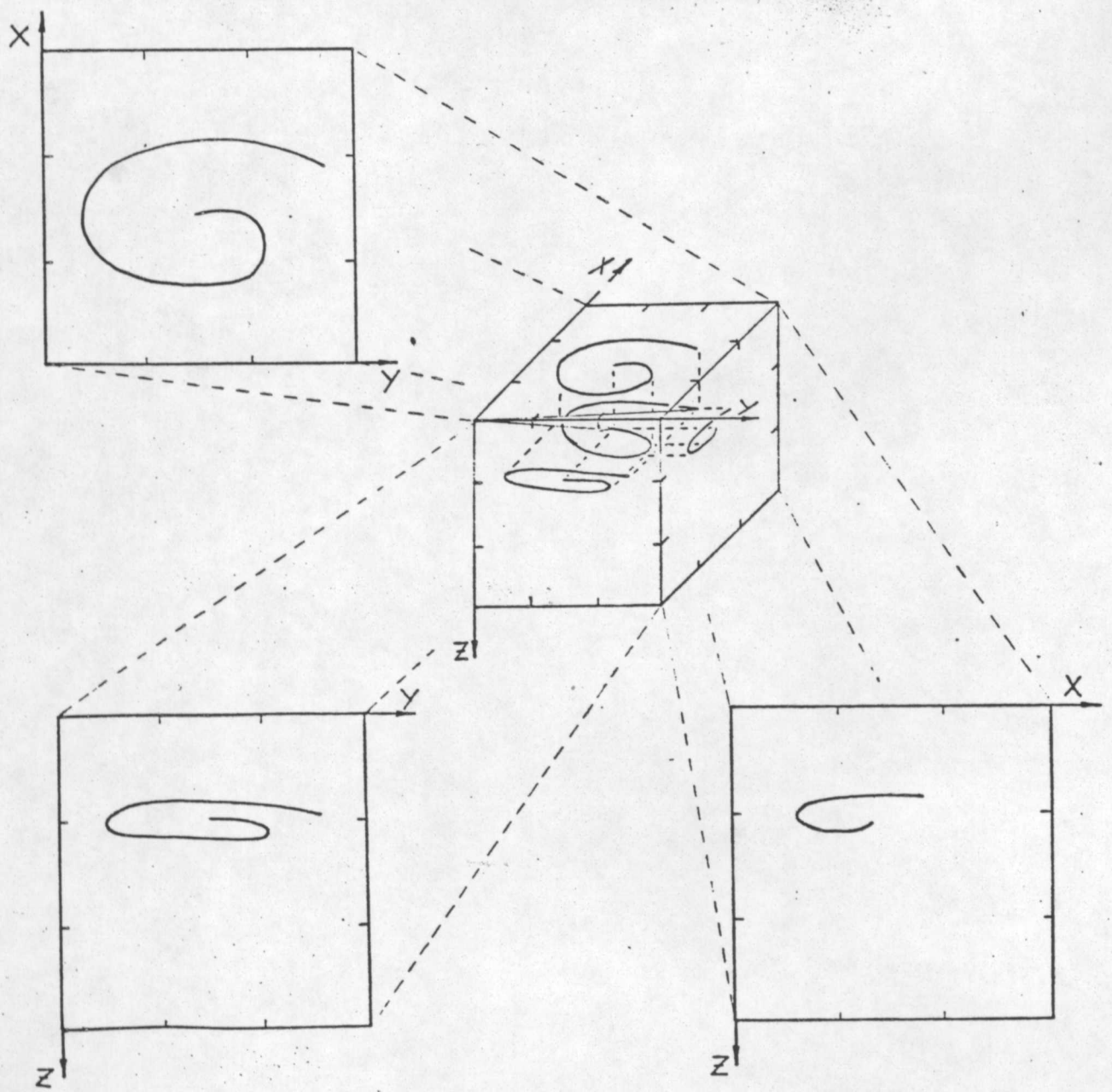

Figure 2. Hodographic projection of geomagnetic field variation showing, in three dimensions, the path traced by the tip of the geomagnetic field vector during a geomagnetic disturbance. Direction X is magnetic northward, Y is magnetic eastward, and Z is downward.

Figures A.3.2 through A.3.7 are hodographs of geomagnetic variations during Event 3, which occurred from 0530 to 0730 u.t. on May 5, 1977. This geomagnetic disturbance does not indicate a preferred direction of horizontal polarization.

Differential Field Calculation

Studies by Wilhjelm and Friis-Christensen (1974) and Babour and Mosnier (1977) have demonstrated that lateral variations in telluric current density can be detected by calculation of the differential geomagnetic field. The geomagnetic variation field is composed of a source component, $\bar{F}^s$, a "normal" component, $\bar{F}^n$, produced by laterally uniform telluric current flow, and an anomalous component, $\bar{F}^a$, produced by lateral variations or concentrations of the induced telluric current system. The observed geomagnetic variation field can be written as the sum of these component fields:

$$\bar{F}_i^o = \bar{F}_i^{sn} + \bar{F}_i^a. \qquad (2)$$

The source field and normal field cannot be separated in geomagnetic array studies of limited areal extent. The anomalous field, which is produced by both regional and local geomagnetic induction, depends upon many factors, including the conductivity structure of regions well removed from the study area and the frequency spectrum of the source field. In this study, in order to investigate the anomalous field and the structure of the local telluric current system, a differential field is calculated, which, under ideal conditions (a "normal" reference station), will closely approximate the anomalous field. At midlatitudes the source field can be considered uniform over distances of 100 km and greater. Consequently, for regional studies of this scale, the difference or differential field between location i and a

reference location, j, is written

$$\bar{F}_{ij} = \bar{F}_i^o - \bar{F}_j^o = \bar{F}_i^a - \bar{F}_j^a \qquad (3)$$

since by definition the normal field, and the source field, are both laterally uniform.

When the anomalous field is produced by lateral variations in a regional telluric current system, temporal variations in the anomalous field at all observation points will be directly proportional to temporal variations in the telluric current system. Babour and Mosnier (1977) first discussed this property of the anomalous field in detail and described the separation of spatial and temporal variations in the anomalous field by the expression

$$\bar{F}_{ij}(t) = (x_i,y_i)i + (x_i,y_i)j + (x_i,y_i)k \cdot R(t), \qquad (4)$$

where R(t) is a function describing the temporal variations of the anomalous field and (x_i,y_i), (x_i,y_i) and (x_i,y_i) are coefficients describing the spatial variations of the anomalous field. Babour and Mosnier observed this property of the anomalous field in experiments in Brittany and the Pyrenees, which are both locations that are strongly affected by ocean induced telluric current systems. At each of their stations in these studies, the anomalous field was strongly polarized in a direction that was independent of time. Temporal variations of the anomalous field were similar at all stations in accordance with equation 4.

To study the regionally induced telluric current system producing local geomagnetic variation anomalies in a region that is not so clearly affected by the ocean-induced current system, differential field variations were calculated from the observations of bay-type geomagnetic disturbances presented in the previous section. Gallup, New Mexico (GAL), was selected as the reference site for these calculations.

Time records of the differential field variations during Event 1 are

shown in Figures B.1.1 through B.1.5, and hodographs of variations during this event are shown in Figures B.1.6 through B.1.10.

Figures B.2.1 through B.2.10 and B.3.1 through B.3.10 present similar calculations for Events 2 and 3, respectively.

Discussion

The data clearly support the concept of a regionally induced telluric current system, lateral variations of which produce local variations in the geomagnetic variation field. For each of the three events analyzed in this study the differential geomagnetic field variations are linearly polarized and exhibit a marked similarity in their temporal variations.

The polarization of differential field variations is unchanged during the significantly different source polarizations of Events 1, 2, and 3. This is a clear indication of a telluric current concentrating structure associated with the Rio Grande Rift and illustrates the usefulness of differential field measurements in mapping lateral variations of the electrical conductivity of the crust and upper mantle.

References Cited

Babour, K. and Mosnier, J., 1977, Differential geomagnetic sounding: Geophysics, v. 42, p. 66-76.

Porath, H. and Gough, D. I., 1971, Mantle conductive structures in the western United States from magnetometer array studies: Geophysical Journal of the Royal Astronomical Society, v. 22, p. 261-275.

Reitzel, J. S., Gough, D. I., Porath, H., and Anderson, C. W. III, 1970, Geomagnetic deep sounding and upper mantle structure in the western United States: Geophysical Journal of the Royal Astronomical Society, v. 19, p. 213-235.

Schmucker, U., 1964, Anomalies of geomagnetic variations in the southwestern United States: Journal of Geomagnetism, v. 15, p. 193-121.

Schmucker, U., 1970, Anomalies of geomagnetic variations in the southwestern United States: Bulletin of the Scripps Institution of Oceanography, v. 13, 165 p.

Towle, J. N., D. V. Fitterman, and Lescelius, R., 1979, A digital recording field system for geomagnetic-telluric array studies: IEEE Transactions in Geoscience Electronics, v. GE-17, no. 2, p. 41-45.

Warren, R. E., Sclater, J. G., Vacquier, V., and Roy, R. F., 1969, A comparison of terrestrial heat flow and geomagnetic fluctuations in the southwestern United States: Geophysics, v. 34, p. 463-478.

Wilhjelm, J. and Friis-Christensen, E., 1974, The Igdlorssuit geomagnetic variation anomaly in the rift-fault zone of northern West Greenland: Journal of Geomagnetism and Geoelectricity, v. 26, p. 173-189.

Appendix A.1

Geomagnetic field variations during Event 1

Figure A.1.1 Geomagnetic field variations during Event 1 at Gallup, N. Mexico {GAL}. Vertical tick interval is 20 nT. Horizontal scale in seconds.

Figures A.1.2-A.1.7 Hodographs of geomagnetic field variations during Event 1. Horizontal and vertical tick interval is 20 nT.

Station	Figure
GAL	A.1.2
CUB	A.1.3
SWE	A.1.4
MAD	A.1.5
MTA	A.1.6
LUC	A.1.7

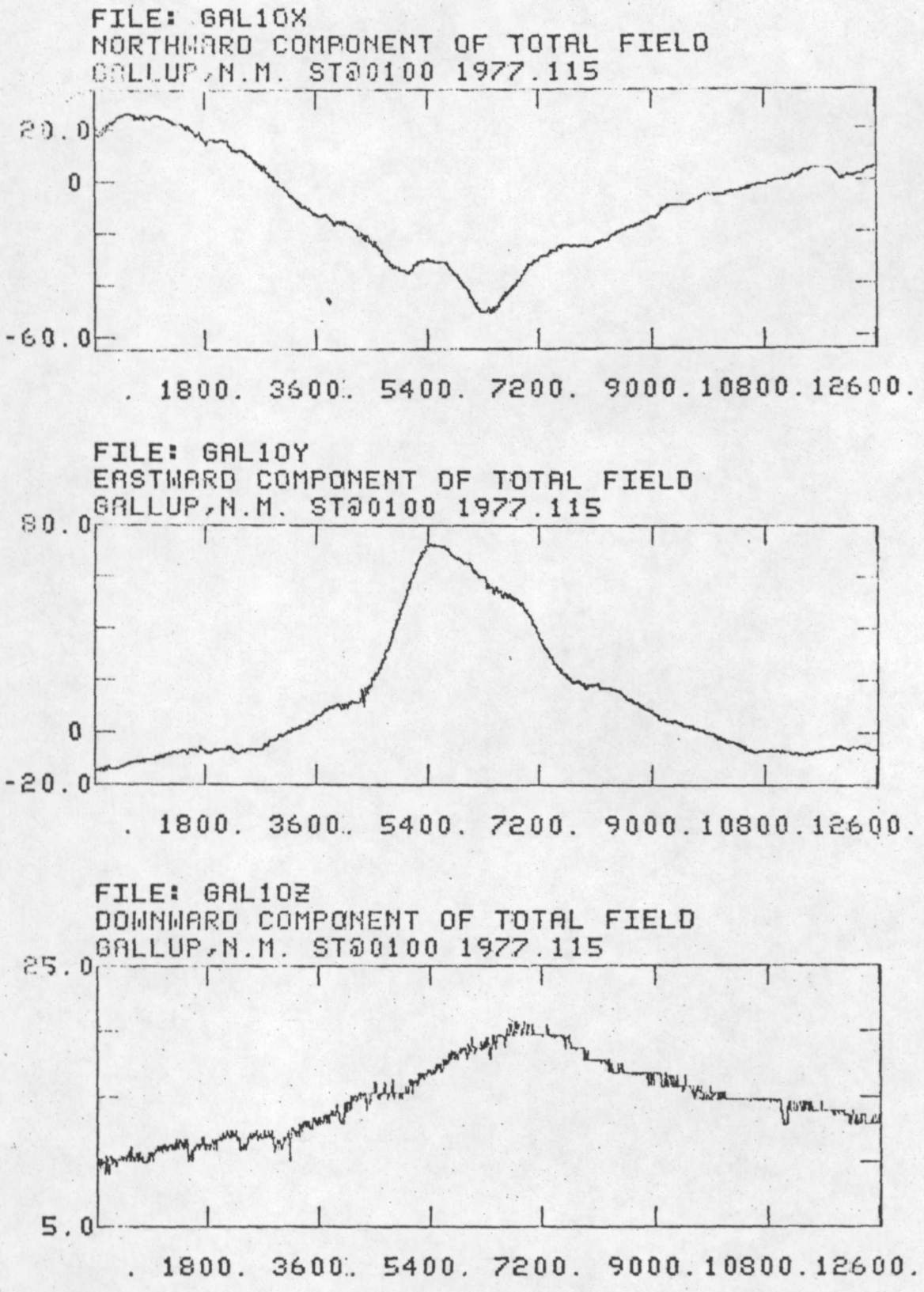
FILE: GAL10X
NORTHWARD COMPONENT OF TOTAL FIELD
GALLUP,N.M. ST@0100 1977.115
20.0
0
-60.0
1800. 3600. 5400. 7200. 9000. 10800. 12600.
FILE: GAL10Y
EASTWARD COMPONENT OF TOTAL FIELD
GALLUP,N.M. ST@0100 1977.115
80.0
0
-20.0
1800. 3600. 5400. 7200. 9000. 10800. 12600.
FILE: GAL10Z
DOWNWARD COMPONENT OF TOTAL FIELD
GALLUP,N.M. ST@0100 1977.115
25.0
5.0
1800. 3600. 5400. 7200. 9000. 10800. 12600.

Figure A.1.1

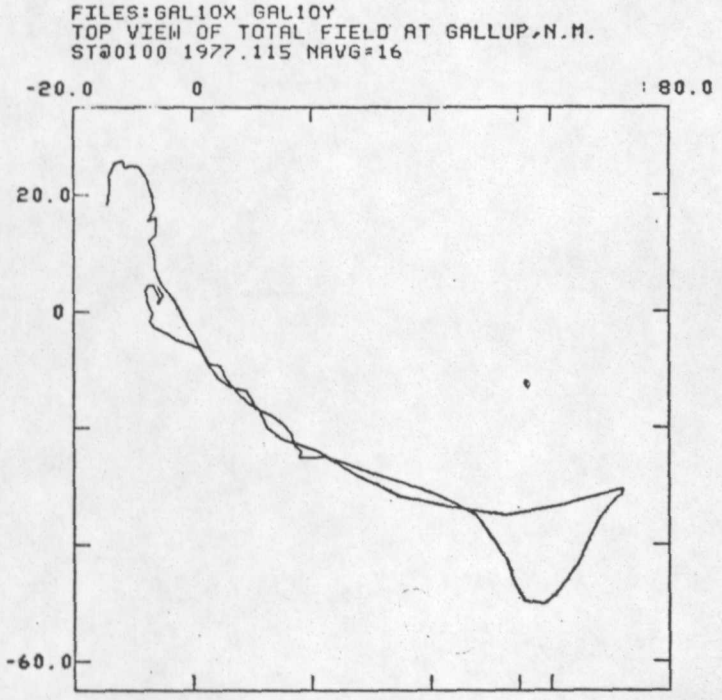
FILES:GAL10X GAL10Y
TOP VIEW OF TOTAL FIELD AT GALLUP,N.M.
ST@0100 1977.115 NAVG=16
-20.0
0
80.0
20.0
0
-60.0

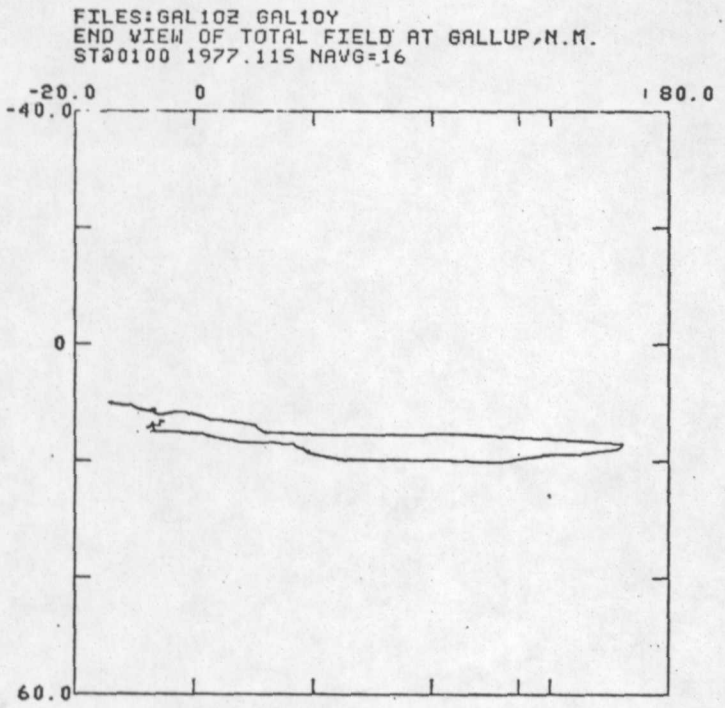
FILES:GAL10Z GAL10Y
END VIEW OF TOTAL FIELD AT GALLUP,N.M.
ST@0100 1977.115 NAVG=16
-20.0
0
80.0
-40.0
0
60.0

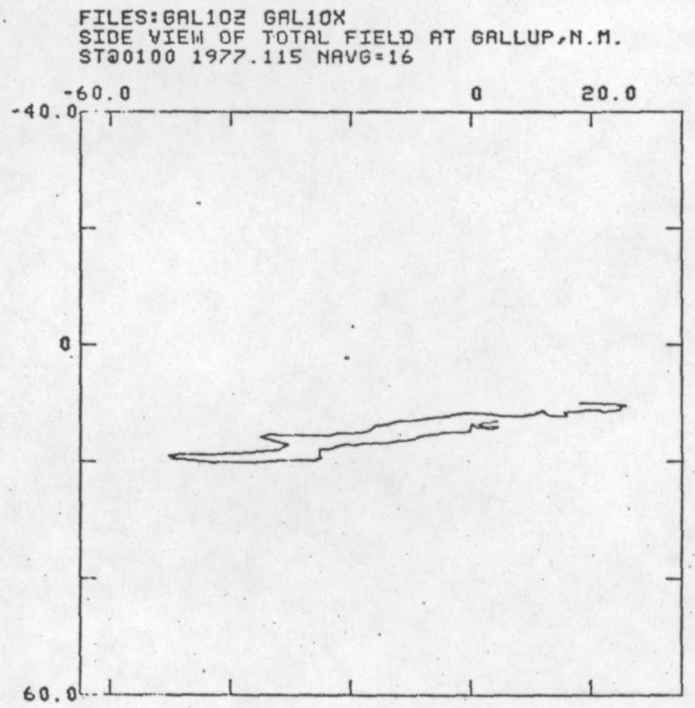
FILES:GAL10Z GAL10X
SIDE VIEW OF TOTAL FIELD AT GALLUP,N.M.
ST@0100 1977.115 NAVG=16
-60.0
0
20.0
-40.0
0
60.0

Figure A.1.2

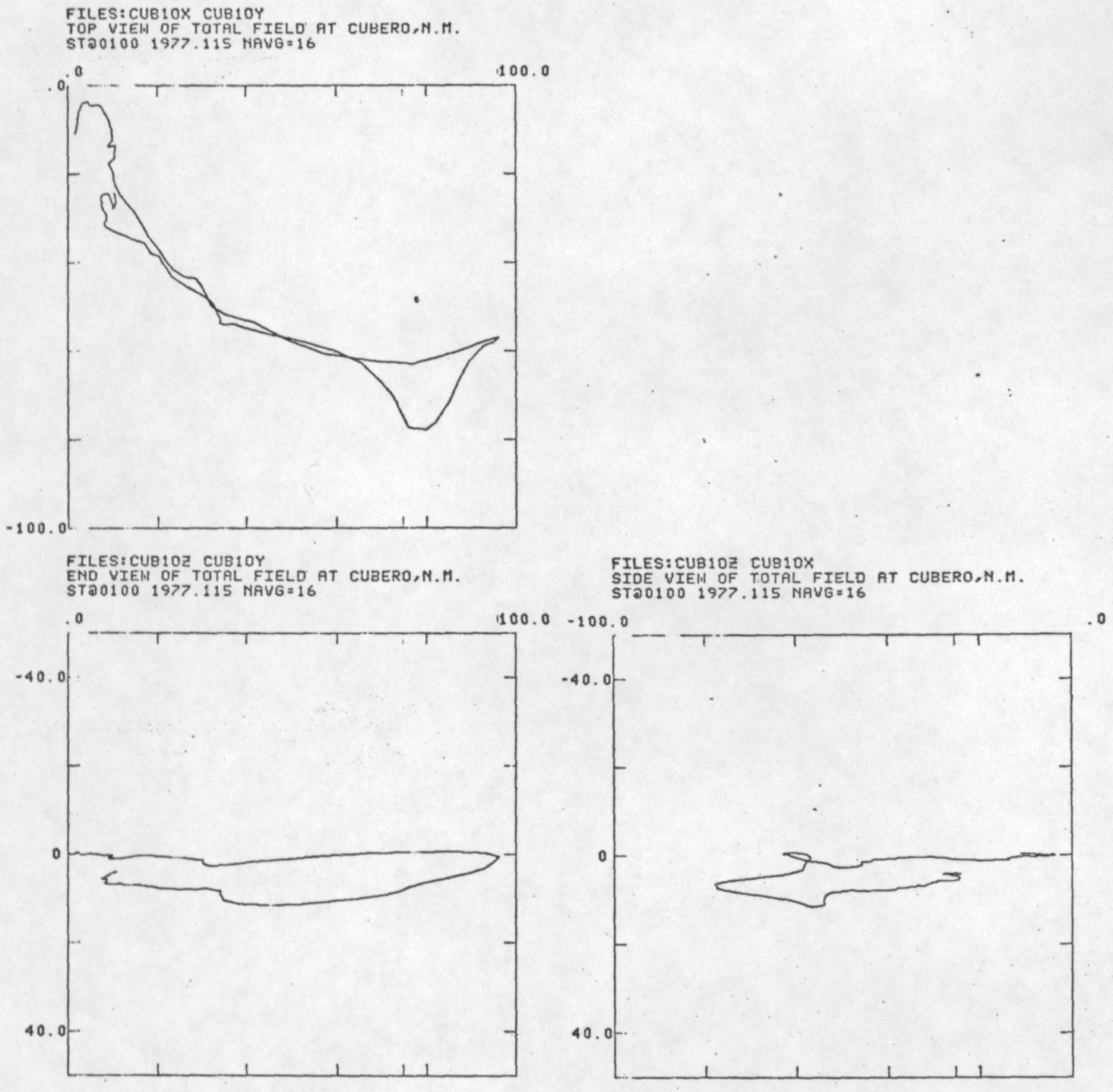
FILES:CUB10X CUB10Y
TOP VIEW OF TOTAL FIELD AT CUBERO,N.M.
ST@0100 1977.115 NAVG=16
.0
100.0
.0
-100.0
FILES:CUB10Z CUB10Y
END VIEW OF TOTAL FIELD AT CUBERO,N.M.
ST@0100 1977.115 NAVG=16
.0
100.0
-40.0
0
40.0
FILES:CUB10Z CUB10X
SIDE VIEW OF TOTAL FIELD AT CUBERO,N.M.
ST@0100 1977.115 NAVG=16
-100.0
.0
-40.0
0
40.0

Figure A.1.3

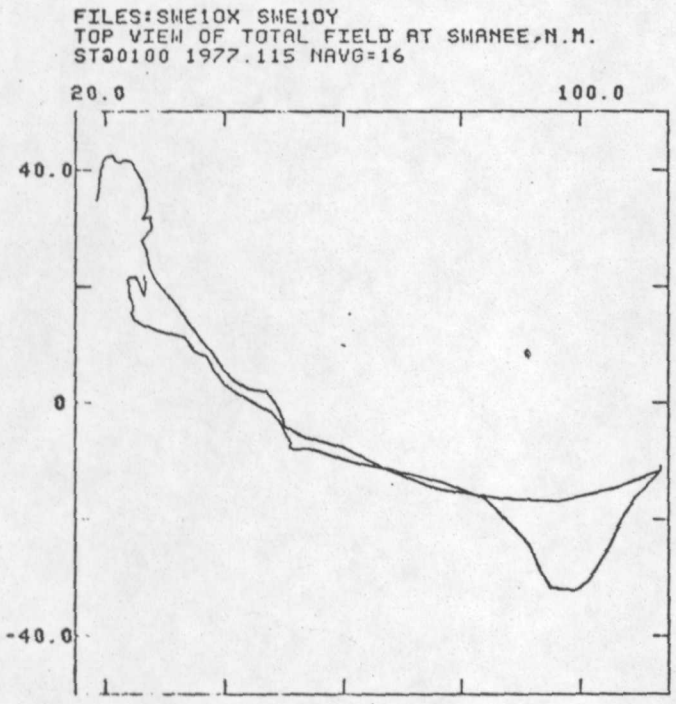
FILES:SWE10X SWE10Y
TOP VIEW OF TOTAL FIELD AT SWANEE,N.M.
ST@0100 1977.115 NAVG=16
20.0
100.0
40.0
0
-40.0

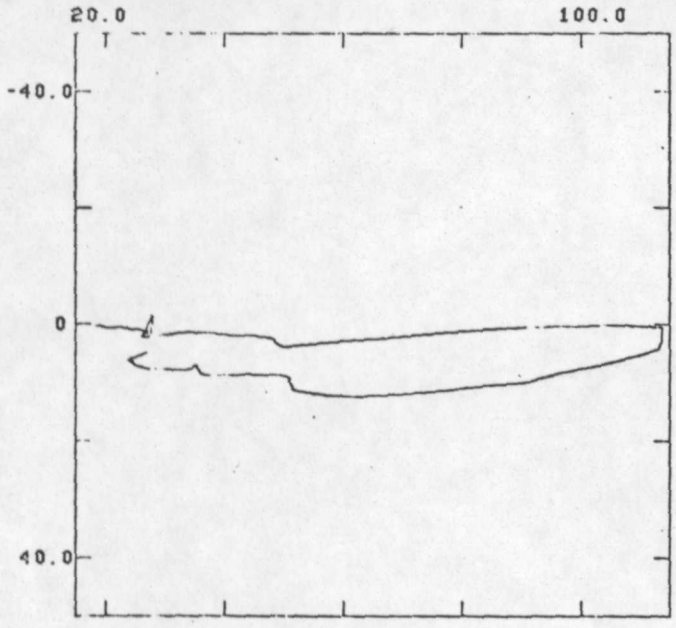
FILES:SWE10Z SWE10Y
END VIEW OF TOTAL FIELD AT SWANEE,N.M.
ST@0100 1977.115 NAVG=16
20.0
100.0
-40.0
0
40.0

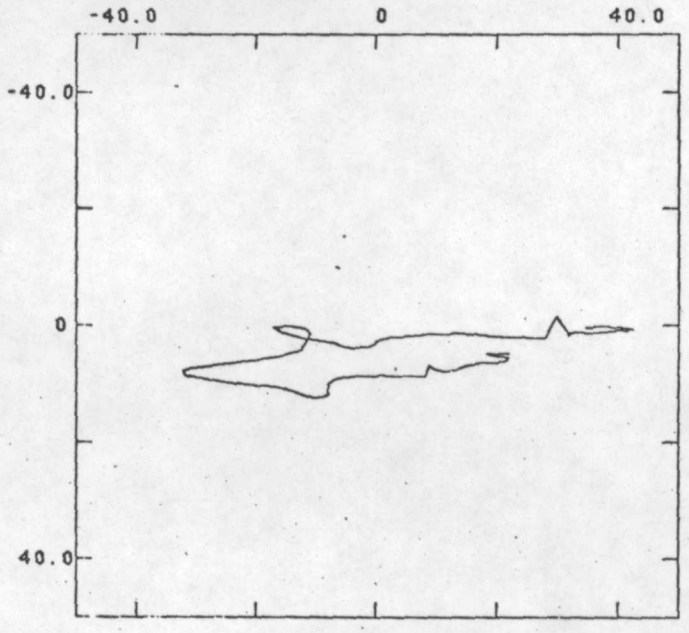
FILES:SWE10Z SWE10X
SIDE VIEW OF TOTAL FIELD AT SWANEE,N.M.
ST@0100 1977.115 NAVG-16
-40.0
0
40.0
-40.0
0
40.0

Figure A.1.4

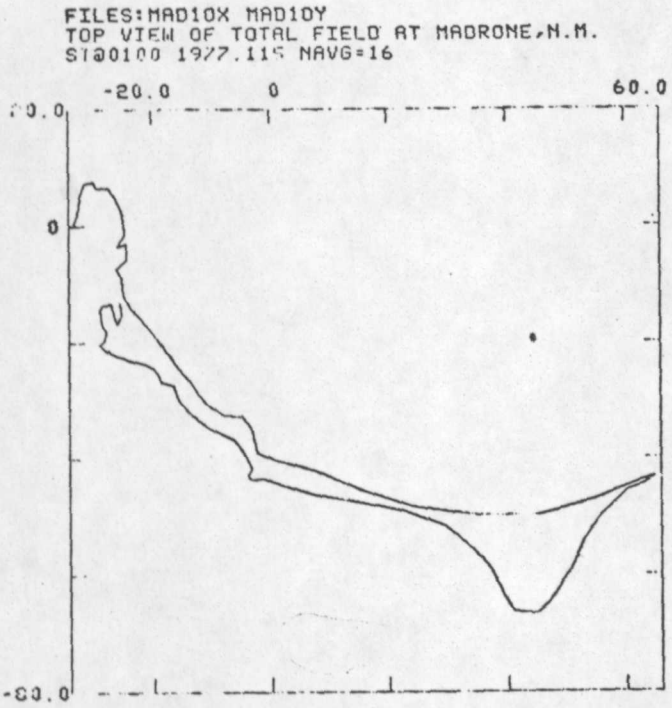
FILES:MAD10X MAD10Y
TOP VIEW OF TOTAL FIELD AT MADRONE,N.M.
ST@0100 1977.115 NAVG=16
-20.0
0
60.0
0
-40.0

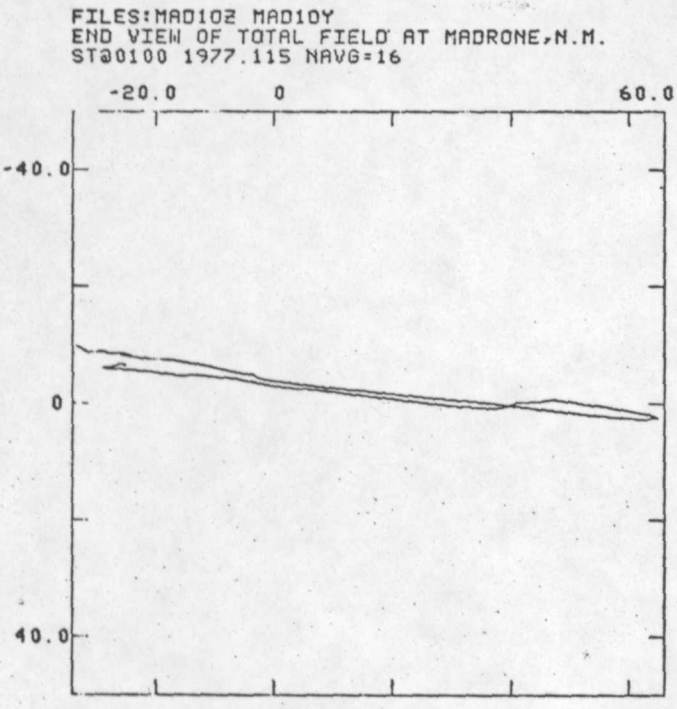
FILES:MAD10Z MAD10Y
END VIEW OF TOTAL FIELD AT MADRONE,N.M.
ST@0100 1977.115 NAVG=16
-20.0
0
60.0
-40.0
0
40.0

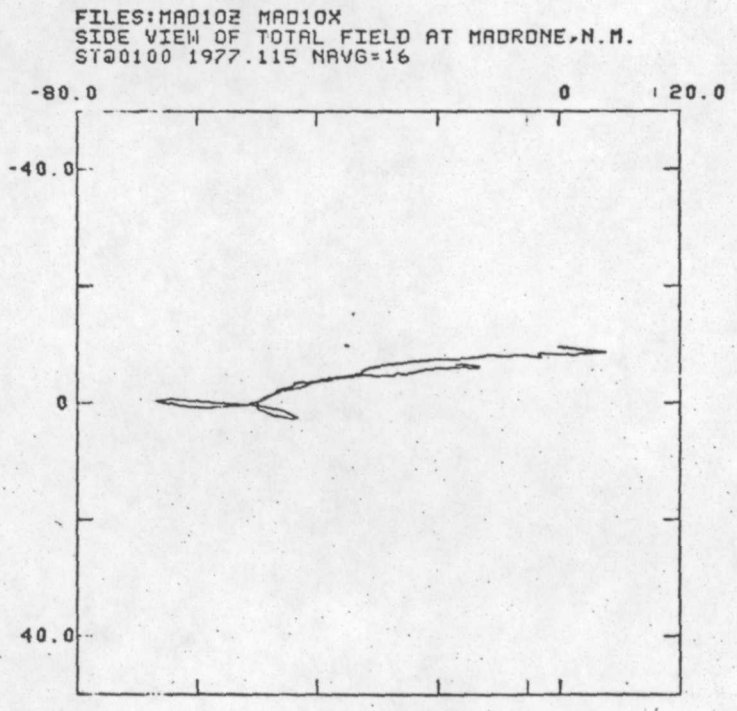
FILES:MAD10Z MAD10X
SIDE VIEW OF TOTAL FIELD AT MADRONE,N.M.
ST@0100 1977.115 NAVG=16
-80.0
0
120.0
-40.0
0
40.0

Figure A.1.5

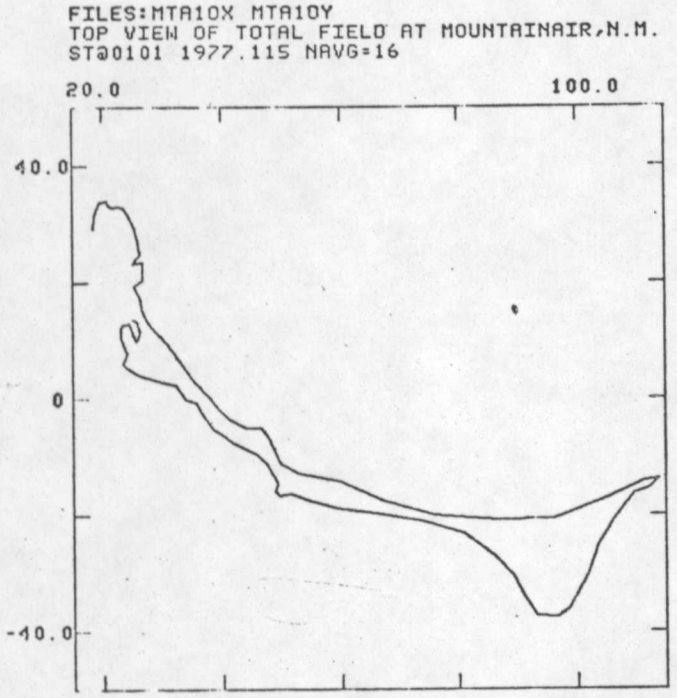
FILES:MTA10X MTA10Y
TOP VIEW OF TOTAL FIELD AT MOUNTAINAIR,N.M.
ST@0101 1977.115 NAVG=16
20.0
100.0
40.0
0
-40.0

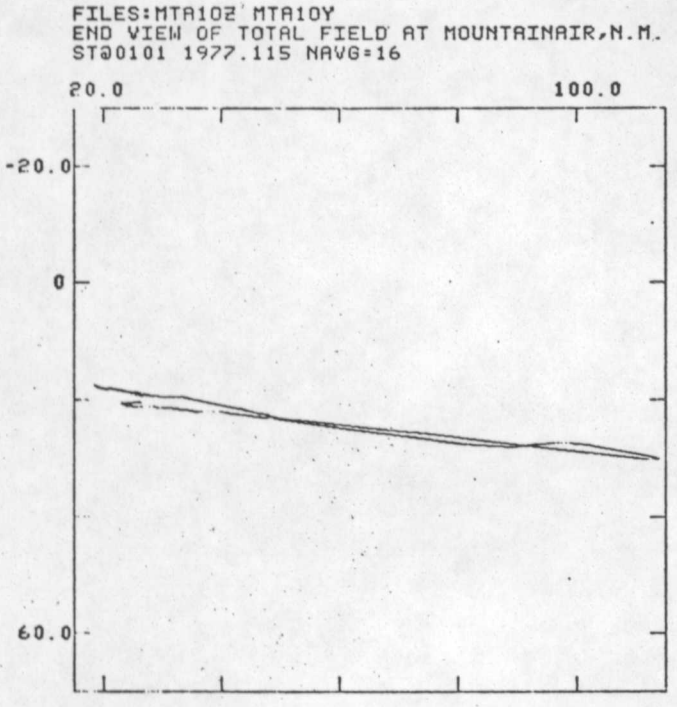
FILES:MTA10Z MTA10Y
END VIEW OF TOTAL FIELD AT MOUNTAINAIR,N.M.
ST@0101 1977.115 NAVG=16
20.0
100.0
-20.0
0
60.0

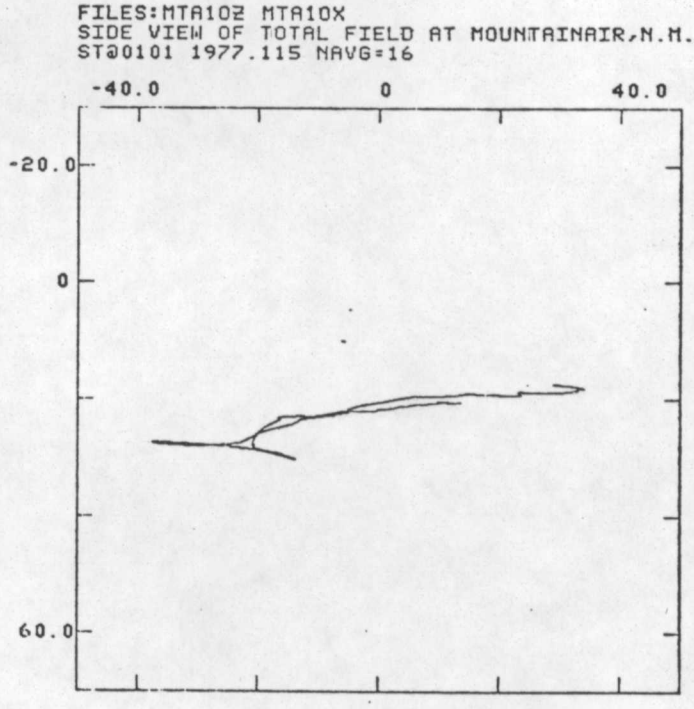
FILES:MTA10Z MTA10X
SIDE VIEW OF TOTAL FIELD AT MOUNTAINAIR,N.M.
ST@0101 1977.115 NAVG=16
-40.0
0
40.0
-20.0
0
60.0

Figure A.1.6

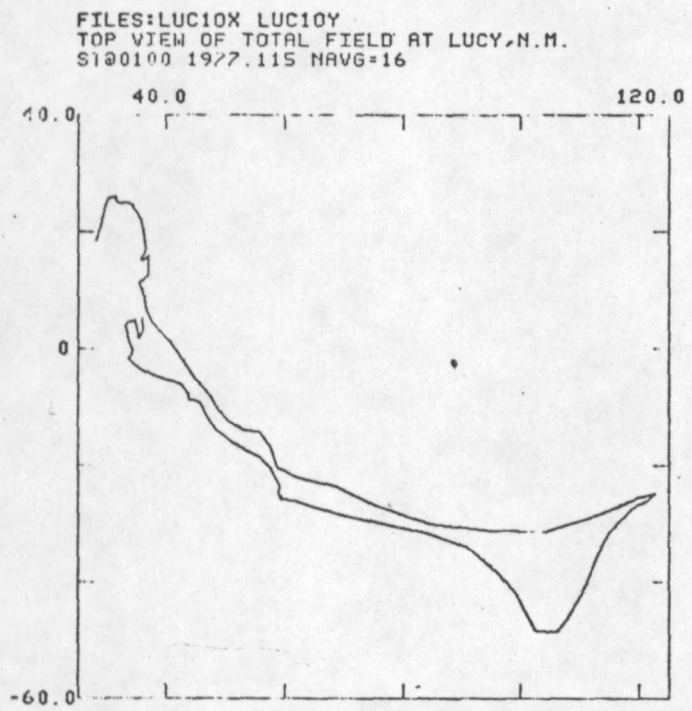
FILES:LUC10X LUC10Y
TOP VIEW OF TOTAL FIELD AT LUCY,N.M.
ST@0100 1977.115 NAVG=16
40.0
120.0
40.0
0
-60.0

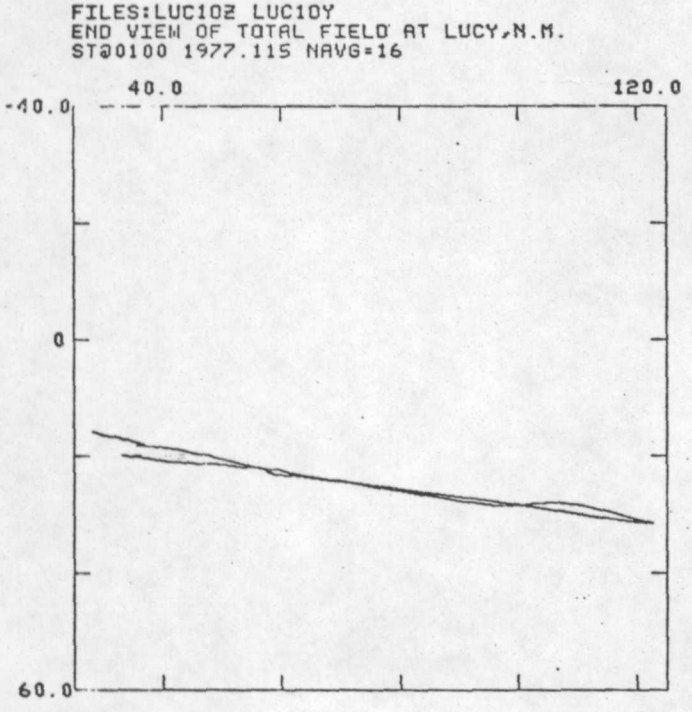
FILES:LUC10Z LUC10Y
END VIEW OF TOTAL FIELD AT LUCY,N.M.
ST@0100 1977.115 NAVG=16
40.0
120.0
-40.0
0
60.0

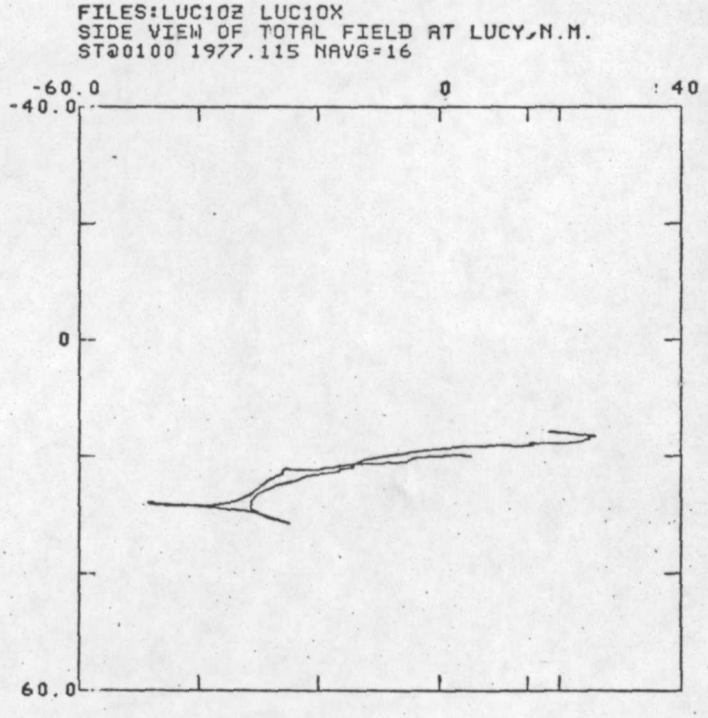
FILES:LUC10Z LUC10X
SIDE VIEW OF TOTAL FIELD AT LUCY,N.M.
ST@0100 1977.115 NAVG=16
-60.0
0
40
-40.0
0
60.0

Figure A.1.7

Appendix A.2

Geomagnetic field variations during Event 2

Figure A.2.1 Geomagnetic field variations during Event 2 at Gallup, N. Mexico {GAL}. Vertical tick interval is 20 nT. Horizontal scale in seconds.

Figures A.2.2-A.2.7 Hodographs of geomagnetic field variations during Event 1. Horizontal and vertical tick interval is 20 nT.

Station	Figure
GAL	A.1.2
CUB	A.2.3
SWE	A.2.4
MAD	A.2.5
MTA	A.2.6
LUC	A.2.7

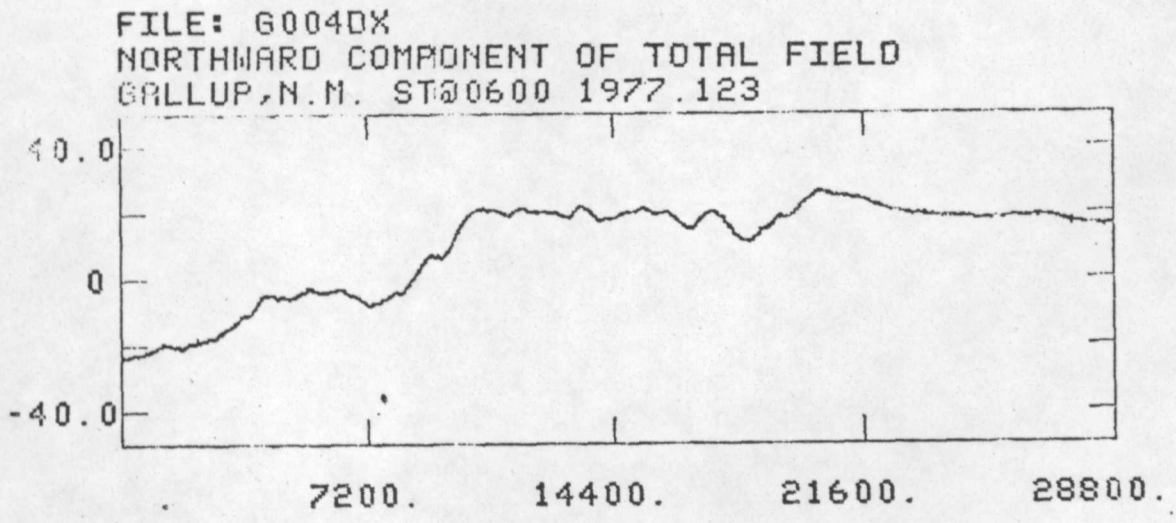
FILE: G004DX
NORTHWARD COMPONENT OF TOTAL FIELD
GALLUP,N.M. ST@0600 1977.123
40.0
0
-40.0
7200.
14400.
21600.
28800.

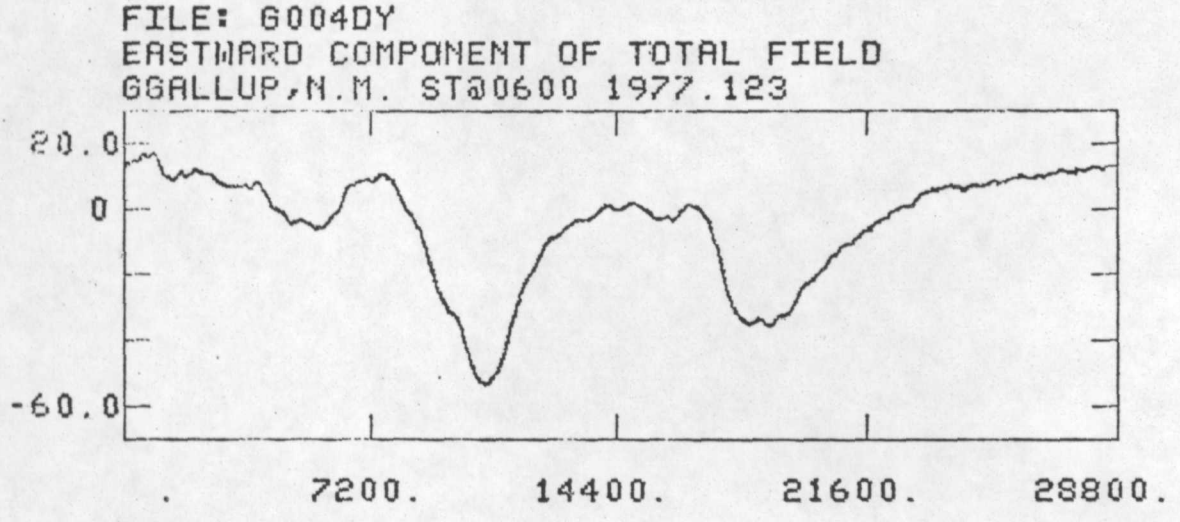
FILE: G004DY
EASTWARD COMPONENT OF TOTAL FIELD
GGALLUP,N.M. ST@0600 1977.123
20.0
0
-60.0
7200.
14400.
21600.
28800.

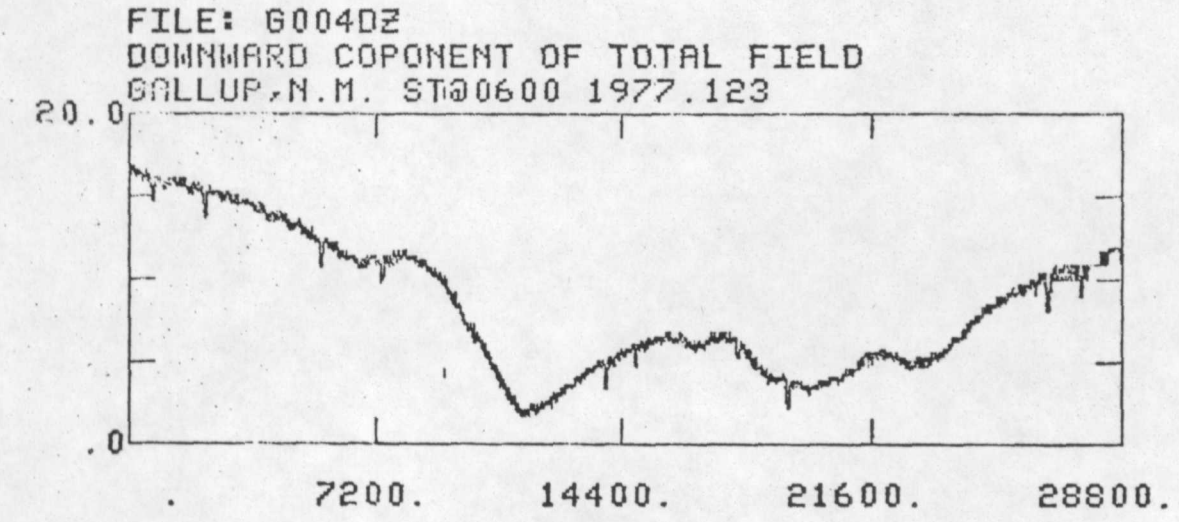
FILE: G004DZ
DOWNWARD COPONENT OF TOTAL FIELD
GALLUP,N.M. ST@0600 1977.123
20.0
.0
7200.
14400.
21600.
28800.

Figure A.2.1

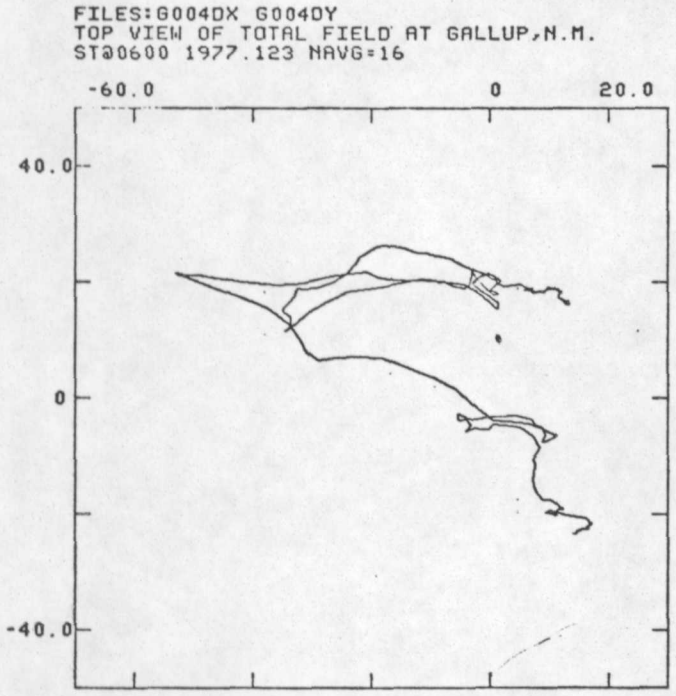
FILES:G004DX G004DY
TOP VIEW OF TOTAL FIELD AT GALLUP,N.M.
ST@0600 1977.123 NAVG=16
-60.0
0
20.0
40.0
0
-40.0

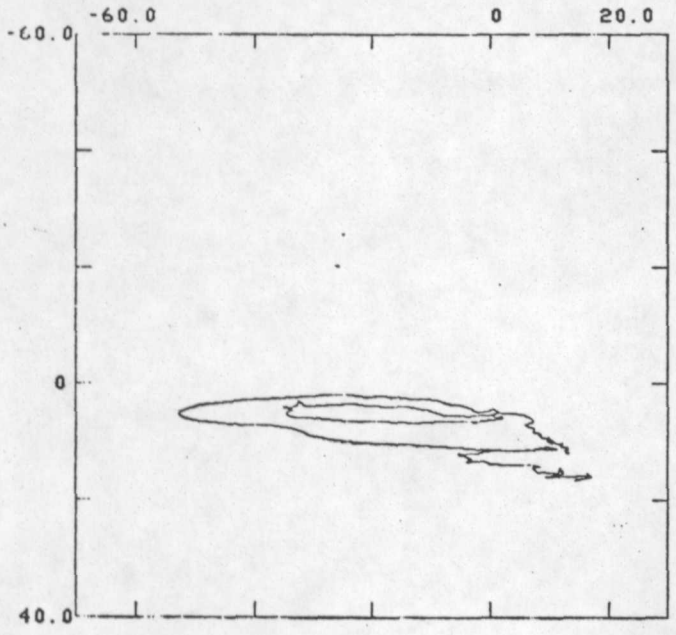
FILES:G004DZ G004DY
END VIEW OF TOTAL FIELD AT GALLUP,N.M.
ST@0600 1977.123 NAVG-16
-60.0
0
20.0
0
40.0

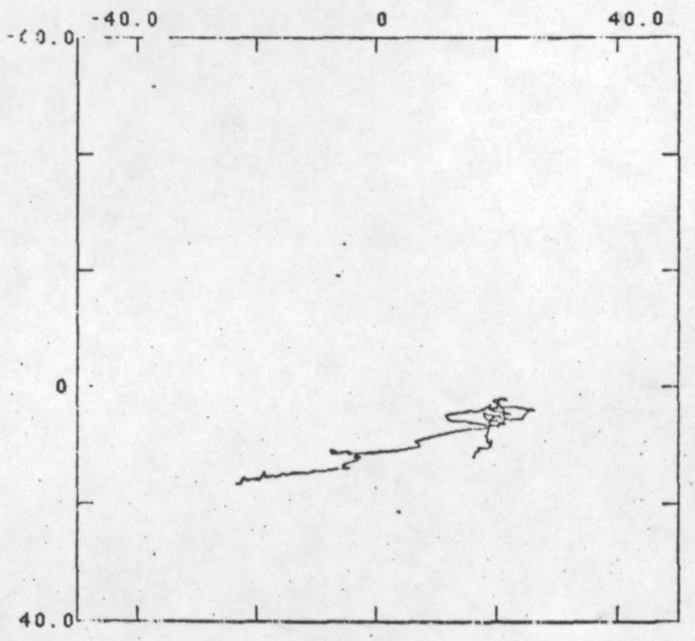
FILES:G004DZ G004DX
SIDE VIEW OF TOTAL FIELD AT GALLUP,N.M.
ST@0600 1977.123 NAVG=16
-40.0
0
40.0
0
40.0

Figure A.2.2

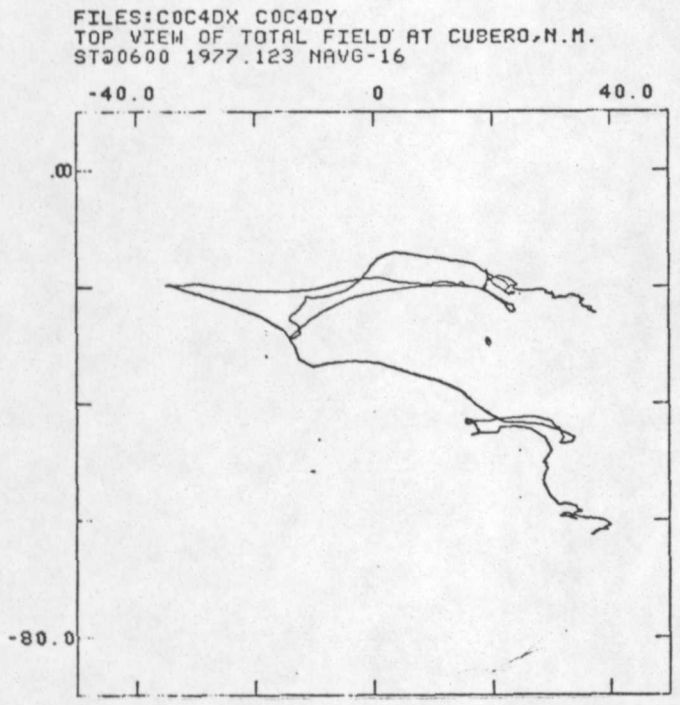
FILES:C0C4DX C0C4DY
TOP VIEW OF TOTAL FIELD AT CUBERO,N.M.
ST@0600 1977.123 NAVG-16
-40.0
0
40.0
.00
-80.0

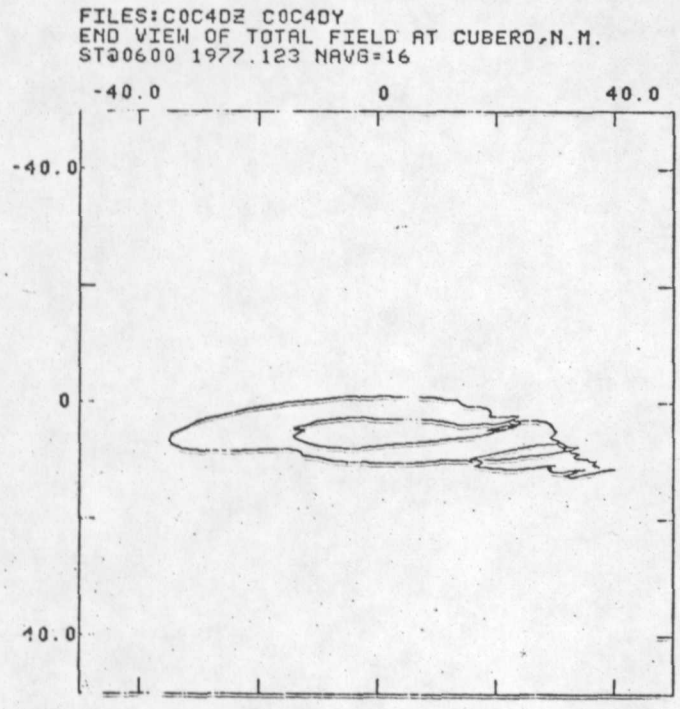
FILES:C0C4DZ C0C4DY
END VIEW OF TOTAL FIELD AT CUBERO,N.M.
ST@0600 1977.123 NAVG=16
-40.0
0
40.0
-40.0
0
40.0

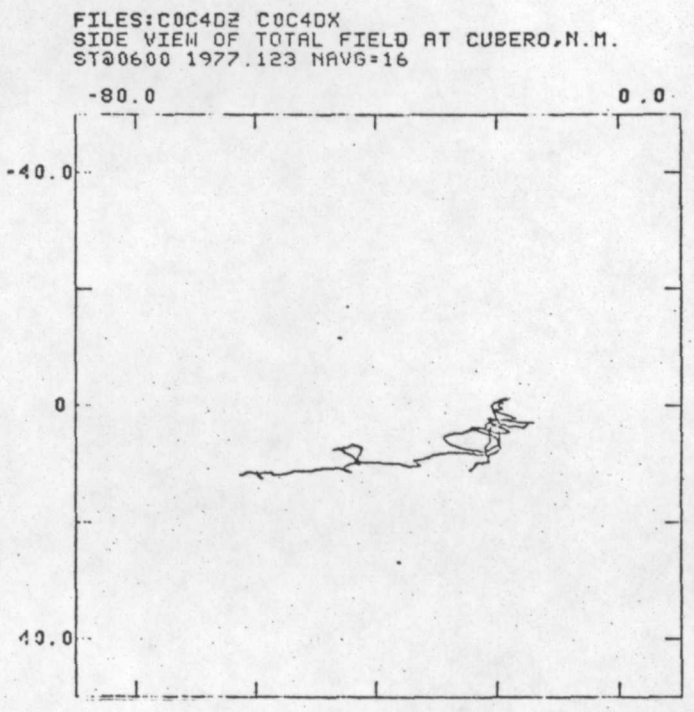
FILES:C0C4DZ C0C4DX
SIDE VIEW OF TOTAL FIELD AT CUBERO,N.M.
ST@0600 1977.123 NAVG=16
-80.0
0.0
-40.0
0
40.0

Figure A.2.3

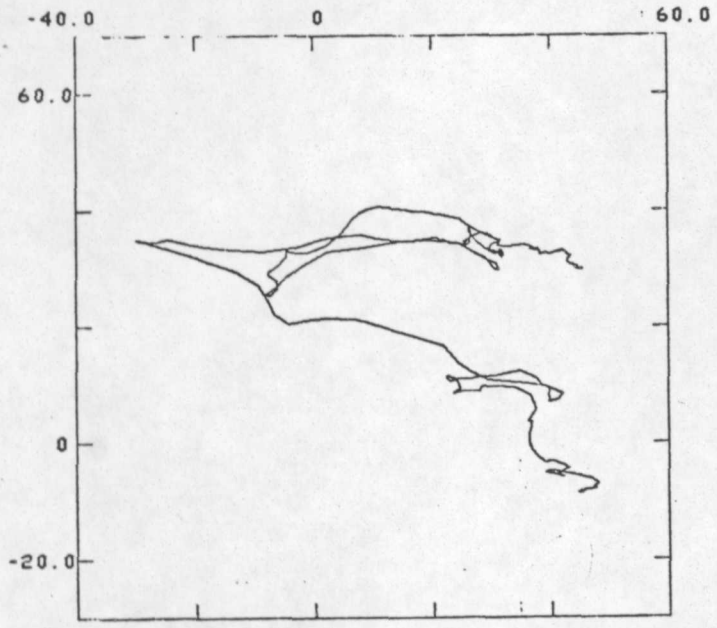
FILES:S0C4DX S0C4DY
TOP VIEW OF TOTAL FIELD AT SWANEE,N.M.
ST@0600 1977.123 NAVG=16
-40.0
0
60.0
60.0
0
-20.0

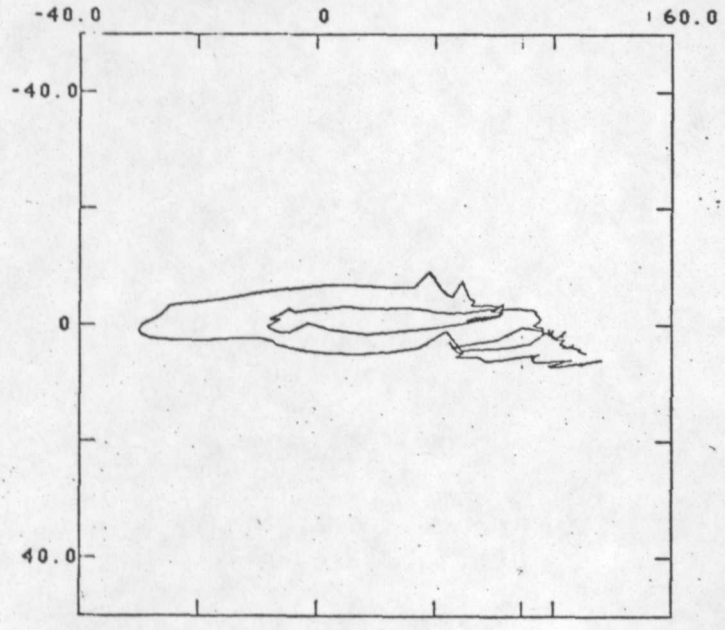
FILES:S0C4DZ S0C4DY
END VIEW OF TOTAL FIELD AT SWANEE,N.M.
ST@0600 1977.123 NAVG=16
-40.0
0
60.0
-40.0
0
40.0

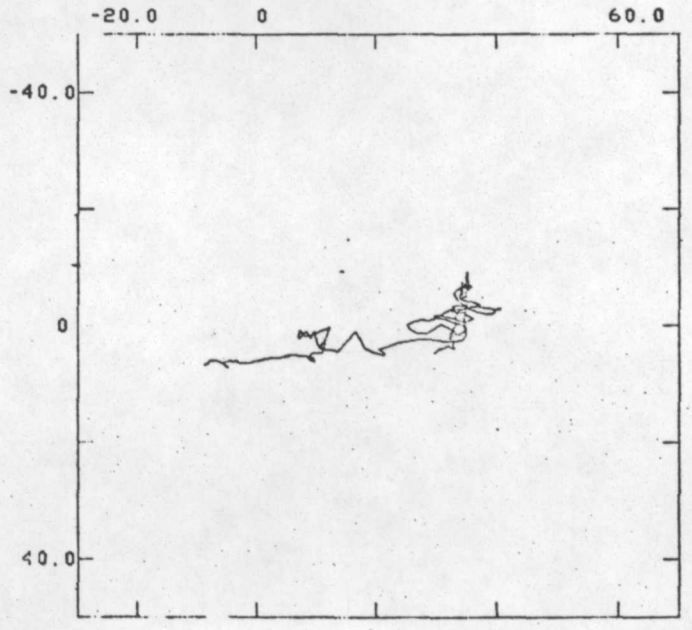
FILES:S0C4DZ S0C4DX
SIDE VIEW OF TOTAL FIELD AT SWANEE,N.M.
ST@0600 1977.123 NAVG=16
-20.0
0
60.0
-40.0
0
40.0

Figure A.2.4

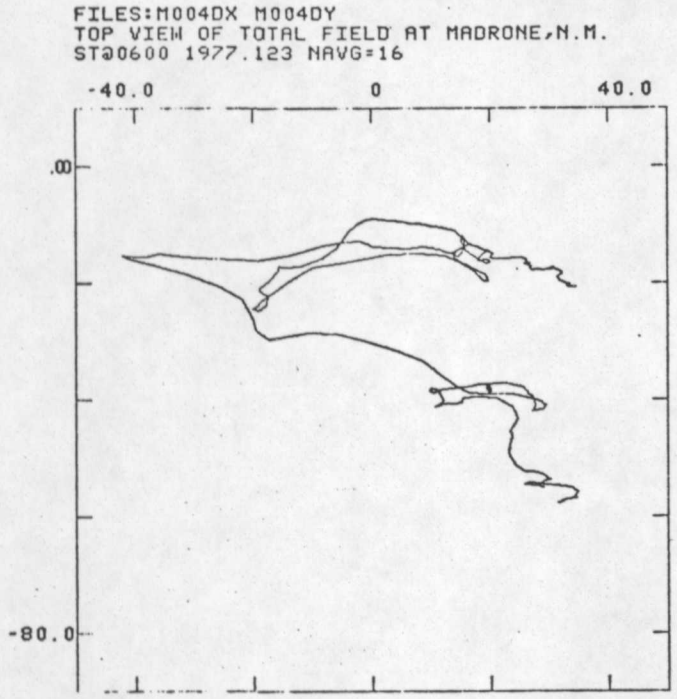
FILES:M004DX M004DY
TOP VIEW OF TOTAL FIELD AT MADRONE,N.M.
ST@0600 1977.123 NAVG=16
-40.0
0
40.0
-80.0

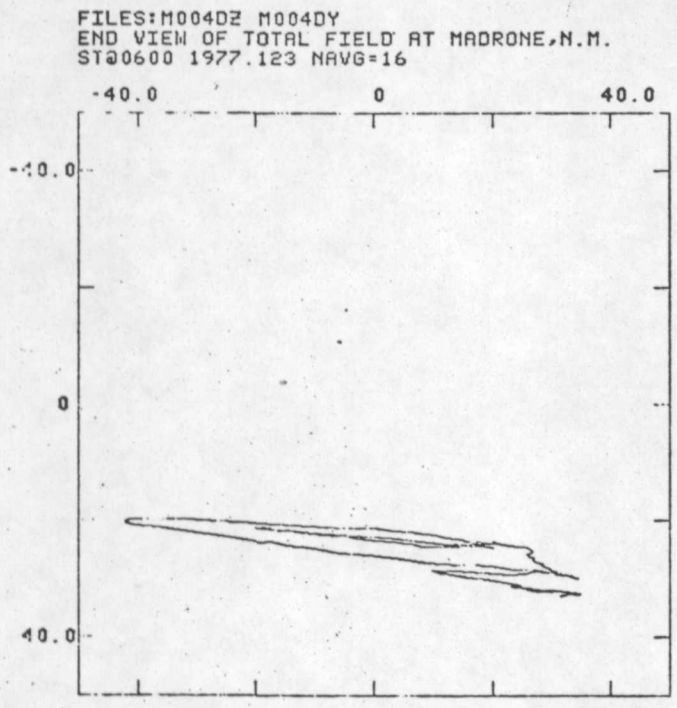
FILES:M004DZ M004DY
END VIEW OF TOTAL FIELD AT MADRONE,N.M.
ST@0600 1977.123 NAVG=16
-40.0
0
40.0
0
40.0

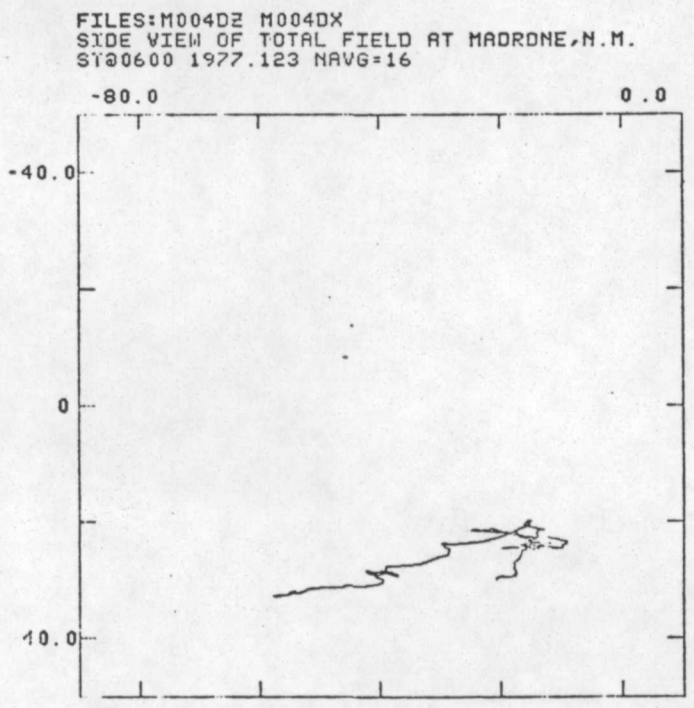
FILES:M004DZ M004DX
SIDE VIEW OF TOTAL FIELD AT MADRONE,N.M.
ST@0600 1977.123 NAVG=16
-80.0
0.0
-40.0
0
40.0

Figure A.2.5

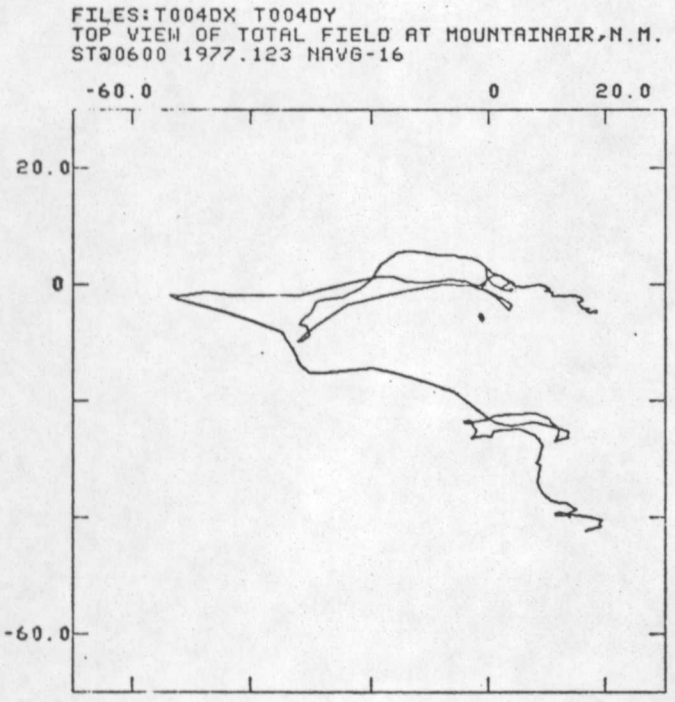
FILES:T004DX T004DY
TOP VIEW OF TOTAL FIELD AT MOUNTAINAIR,N.M.
ST@0600 1977.123 NAVG-16
-60.0
0
20.0
20.0
0
-60.0

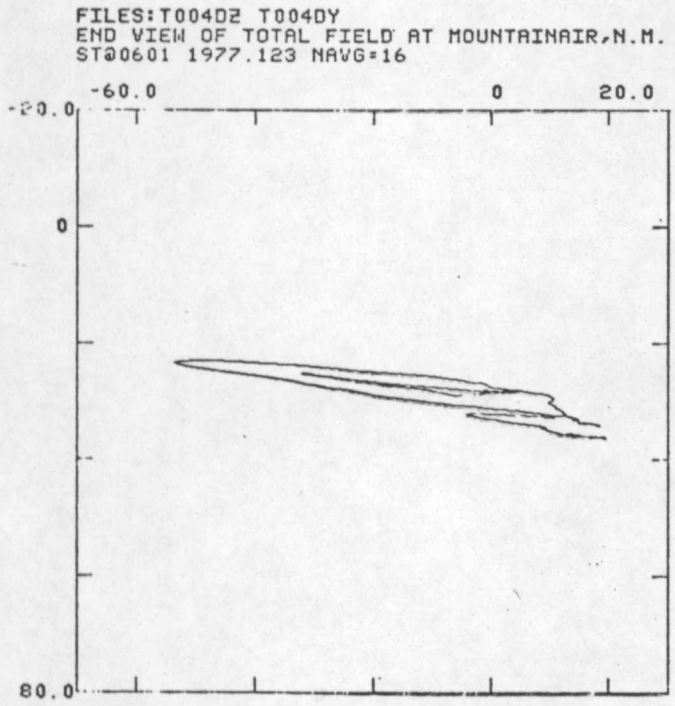
FILES:T004DZ T004DY
END VIEW OF TOTAL FIELD AT MOUNTAINAIR,N.M.
ST@0601 1977.123 NAVG=16
-60.0
0
20.0
0
80.0

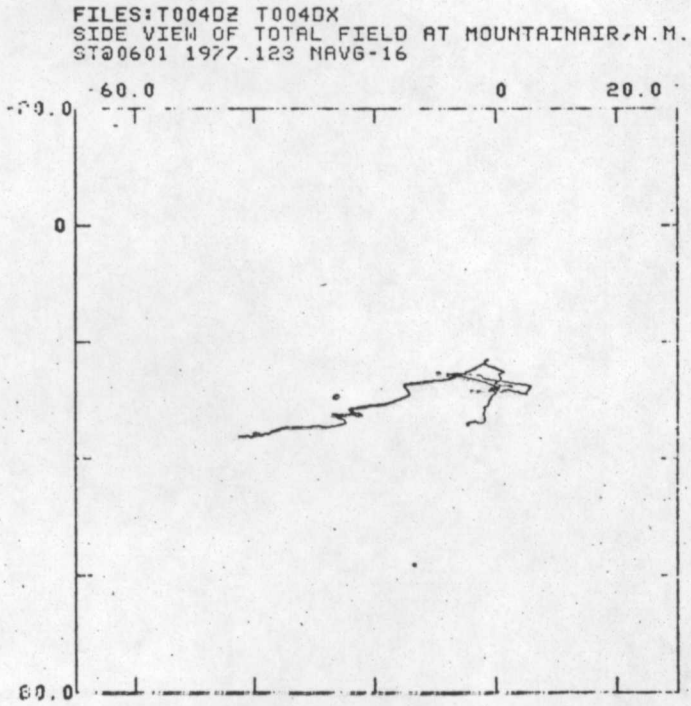
FILES:T004DZ T004DX
SIDE VIEW OF TOTAL FIELD AT MOUNTAINAIR,N.M.
ST@0601 1977.123 NAVG-16
-60.0
0
20.0
0
80.0

Figure A.2.6

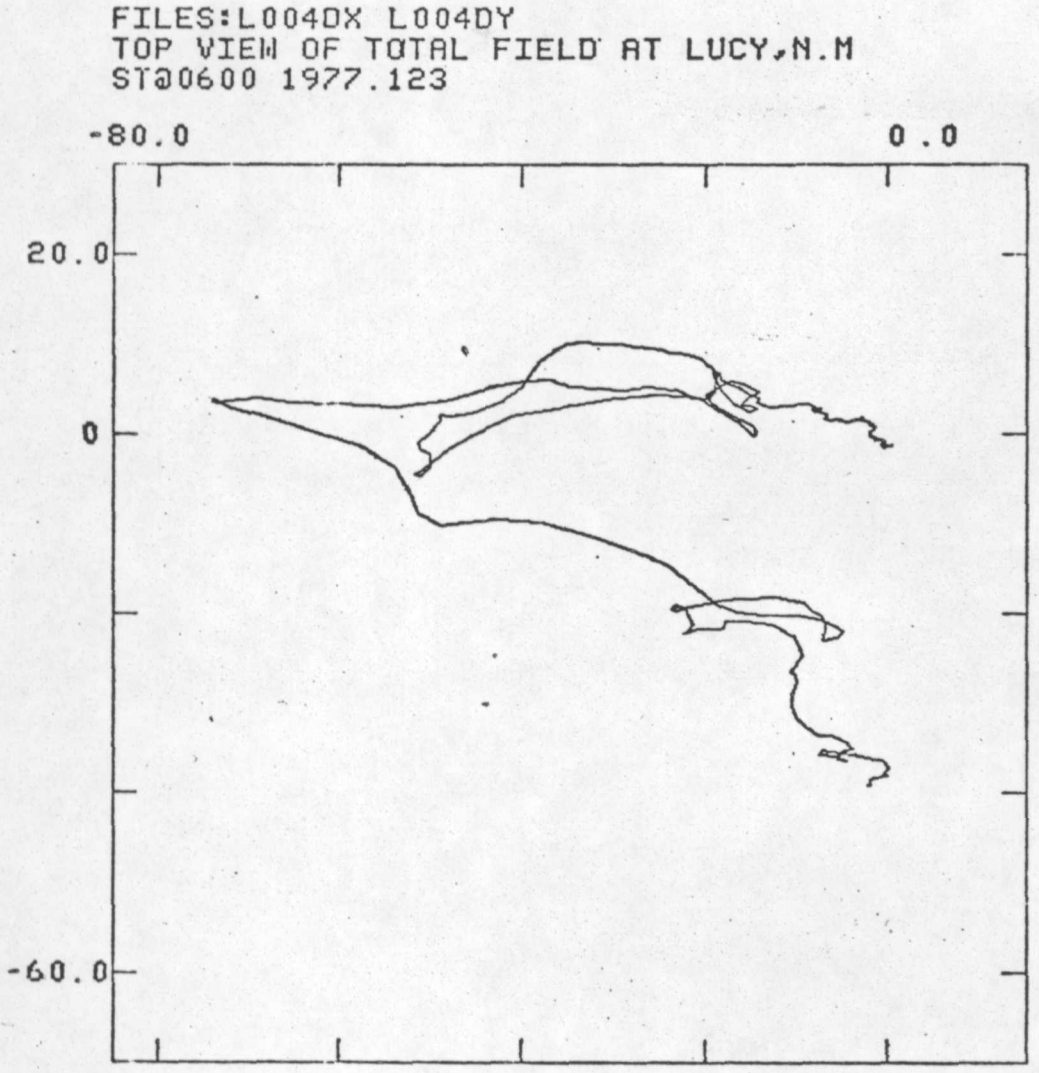
FILES:L004DX L004DY
TOP VIEW OF TOTAL FIELD AT LUCY,N.M
ST@0600 1977.123
-80.0
0.0
20.0
0
-60.0

Figure A.2.7

Appendix A.3

Geomagnetic field variations during Event 3

Figure A.3.1 Geomagnetic field variations during Event 3 at Gallup, N. Mexico {GAL}. Vertical tick interval is 20 nT. Horizontal scale in seconds.

Figures A.3.2-A.3.7 Hodographs of geomagnetic field variations during Event 1. Horizontal and vertical tick interval is 20 nT.

Station	Figure
GAL	A.3.2
CUB	A.3.3
SWE	A.3.4
MAD	A.3.5
MTA	A.3.6
LUC	A.3.7

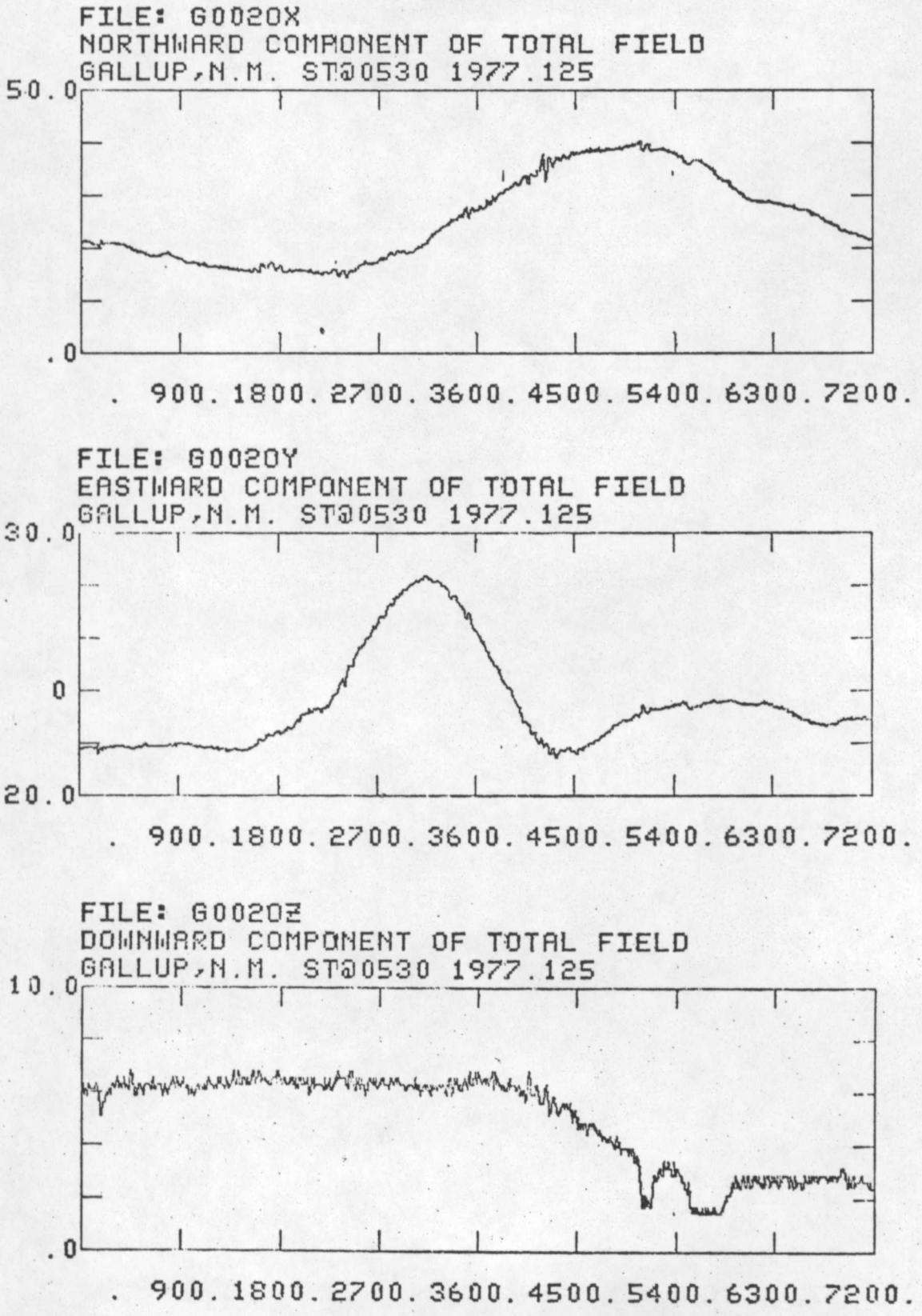
FILE: G0020X
NORTHWARD COMPONENT OF TOTAL FIELD
GALLUP,N.M. ST@0530 1977.125
50.0
.0
. 900. 1800. 2700. 3600. 4500. 5400. 6300. 7200.
FILE: G0020Y
EASTWARD COMPONENT OF TOTAL FIELD
GALLUP,N.M. ST@0530 1977.125
30.0
0
-20.0
. 900. 1800. 2700. 3600. 4500. 5400. 6300. 7200.
FILE: G0020Z
DOWNWARD COMPONENT OF TOTAL FIELD
GALLUP,N.M. ST@0530 1977.125
10.0
.0
. 900. 1800. 2700. 3600. 4500. 5400. 6300. 7200.

Figure A.3.1

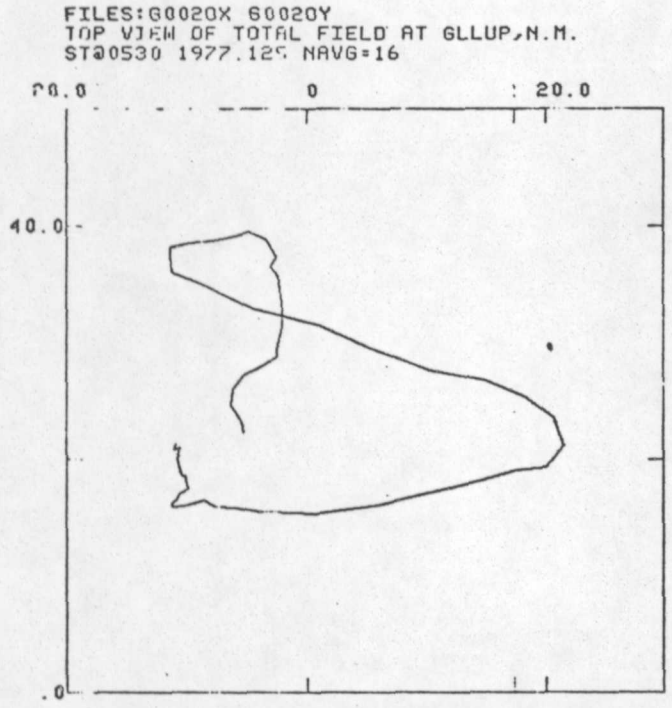
FILES:G0020X G0020Y
TOP VIEW OF TOTAL FIELD AT GLLUP,N.M.
ST@0530 1977.125 NAVG=16
-20.0
0
20.0
40.0
0

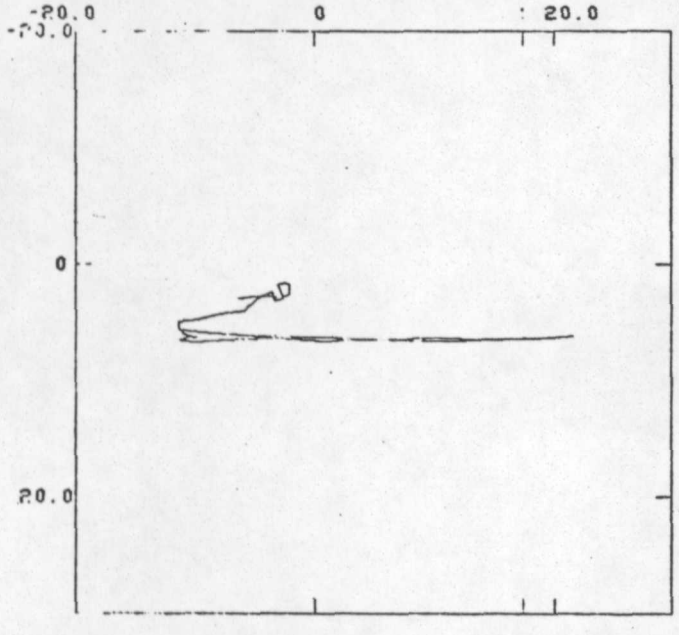
FILES:G0020Z G0020Y
END VIEW OF TOTAL FIELD AT GALLUP,N.M.
ST@0530 1977.125 NAVG=16
-20.0
0
20.0
0
20.0

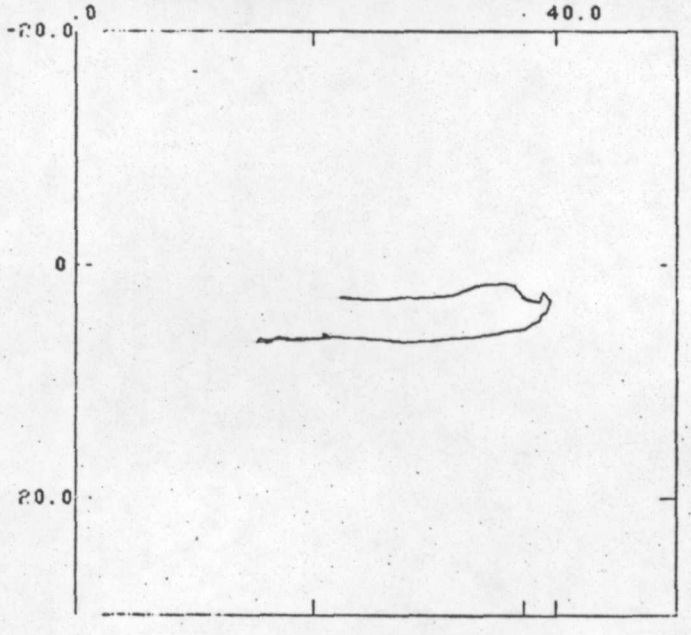
FILES:G0020Z G0020X
SIDE VIEWOF TOTAL FIELD AT GALLUP,N.M.
ST@0530 1977.125 NAVG=16
0
40.0
-20.0
0
20.0

Figure A.3.2

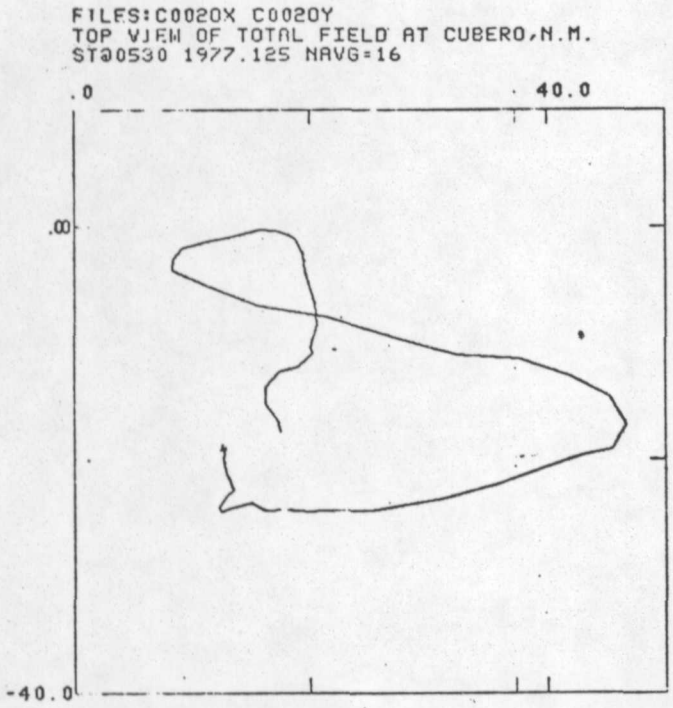
FILES:C0020X C0020Y
TOP VIEW OF TOTAL FIELD AT CUBERO,N.M.
ST@0530 1977.125 NAVG=16
.0
40.0
.00
-40.0

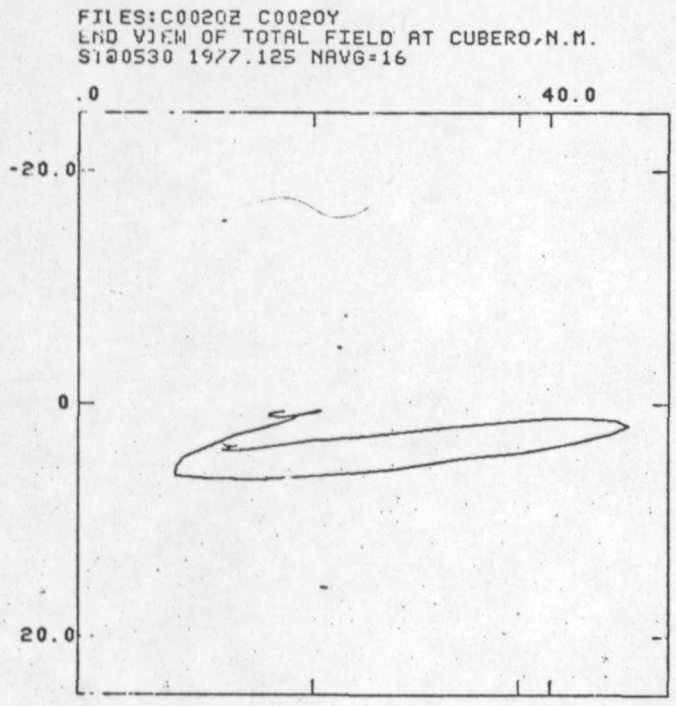
FILES:C0020Z C0020Y
END VIEW OF TOTAL FIELD AT CUBERO,N.M.
ST@0530 1977.125 NAVG=16
.0
40.0
-20.0
0
20.0

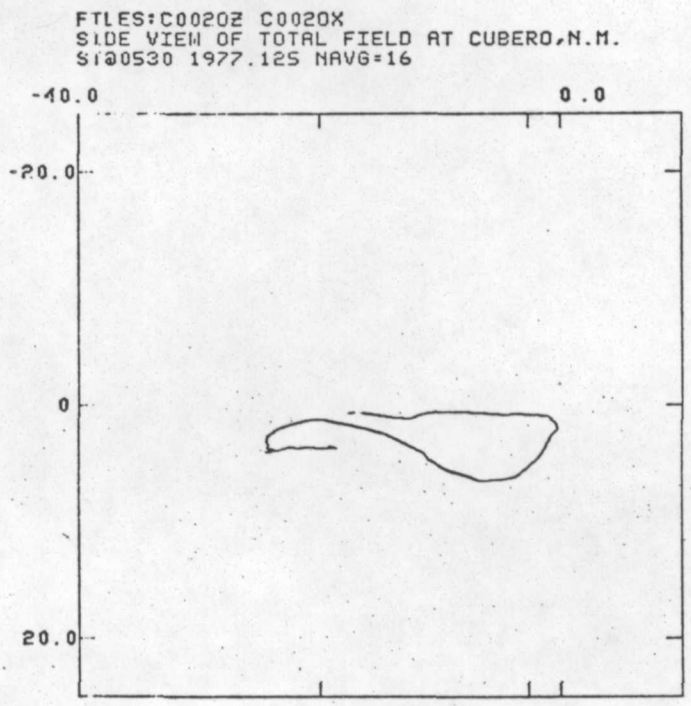
FILES:C0020Z C0020X
SIDE VIEW OF TOTAL FIELD AT CUBERO,N.M.
ST@0530 1977.125 NAVG=16
-40.0
0.0
-20.0
0
20.0

Figure A.3.3

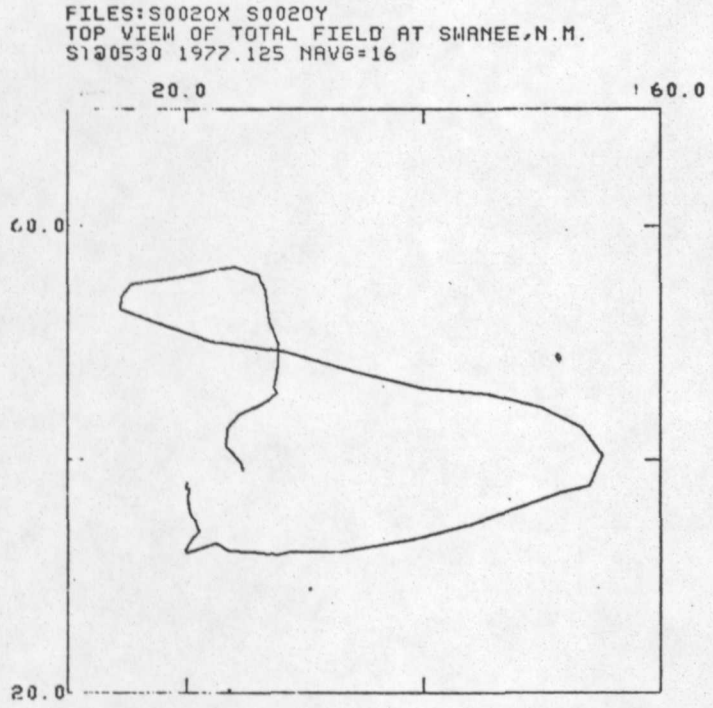
FILES:S0020X S0020Y
TOP VIEW OF TOTAL FIELD AT SWANEE,N.M.
S1@0530 1977.125 NAVG=16
20.0
60.0
60.0
20.0

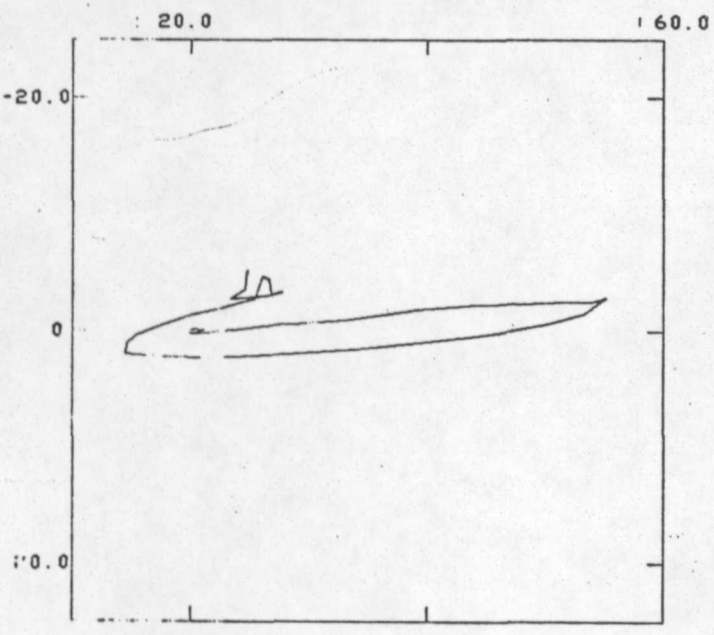
FILES:S0020Z S0020Y
END VIEW OF TOTAL FIELD AT SWANEE,N.M.
ST@0530 1977.125 NAVG=16
20.0
60.0
-20.0
0
20.0

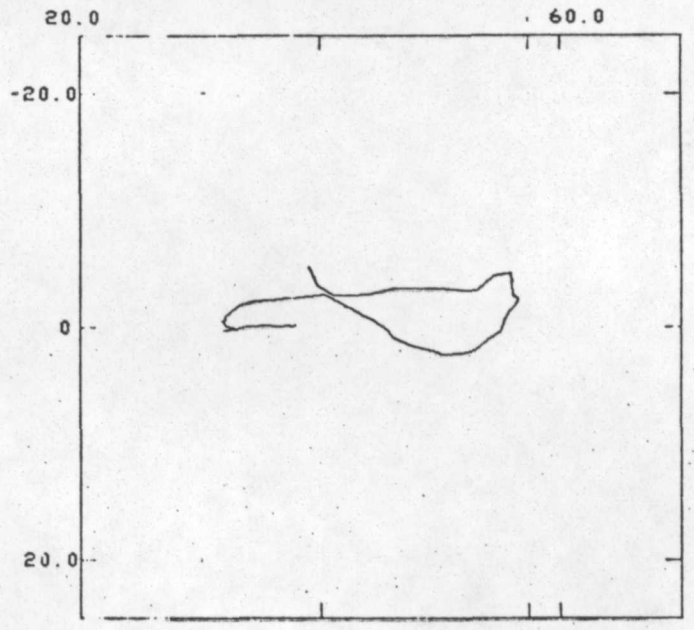
FILES:S0020Z S0020X
SIDE VIEW OF TOTAL FIELD AT SWANEE,N.M.
S1@0530 1977.125 NAVG=16
20.0
60.0
-20.0
0
20.0

Figure A.3.4

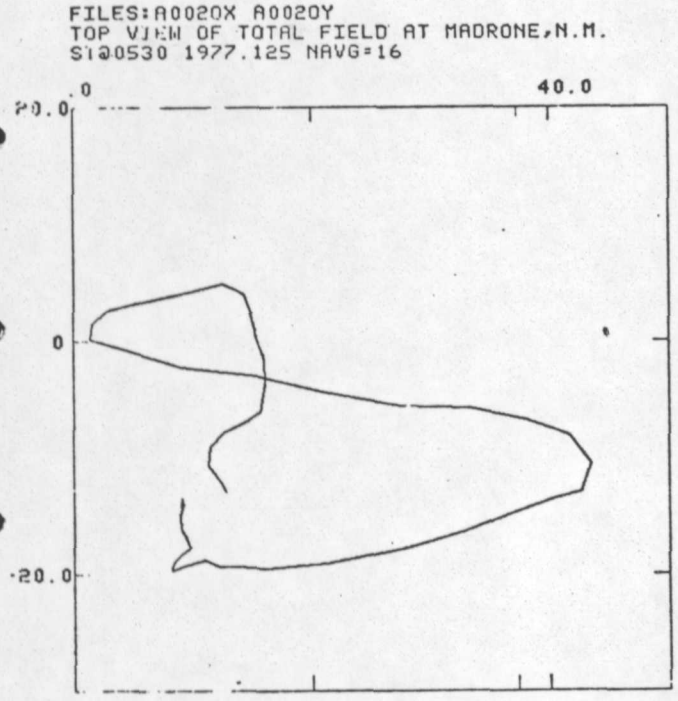
FILES:A0020X A0020Y
TOP VIEW OF TOTAL FIELD AT MADRONE,N.M.
ST@0530 1977.125 NAVG=16
.0
40.0
20.0
0
-20.0

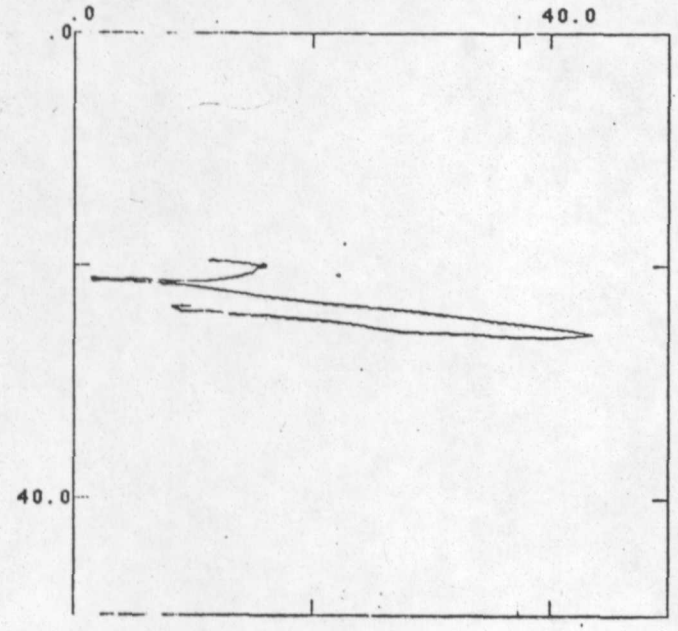
FILES:A0020Z A0020Y
END VIEW OF TOTAL FIELD AT MADRONE,N.M.
ST@0530 1977.125 NAVG=16
.0
40.0
.0
40.0

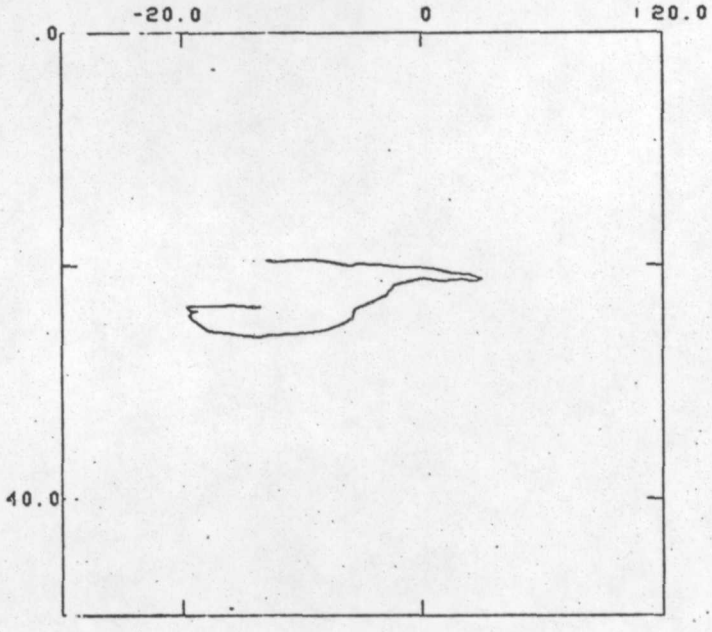
FILES:A0020Z A0020X
SIDE VIEW OF TOTAL FIELD AT MADRONE,N.M.
ST@0530 1977.125 NAVG=16
-20.0
0
20.0
.0
40.0

Figure A.3.5

FILES:T0020X T0020Y
TOP VIEW OF TOTAL FIELD AT MOUNTAINAIR,N.M.
ST@0531 1977.125 NAVG=16

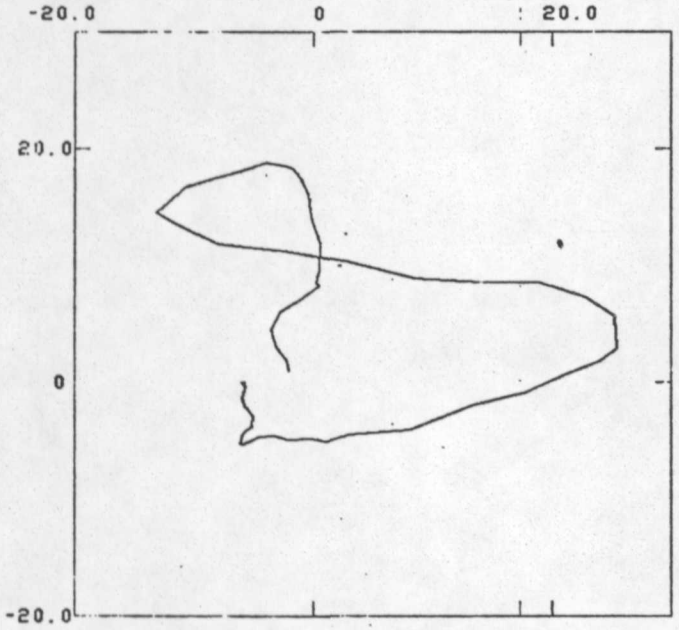

FILES:T0020Z T0020Y
END VIEW OF TOTAL FIELD AT MOUNTAINAIR,N.M.
ST@0531 1977.125 NAVG=16

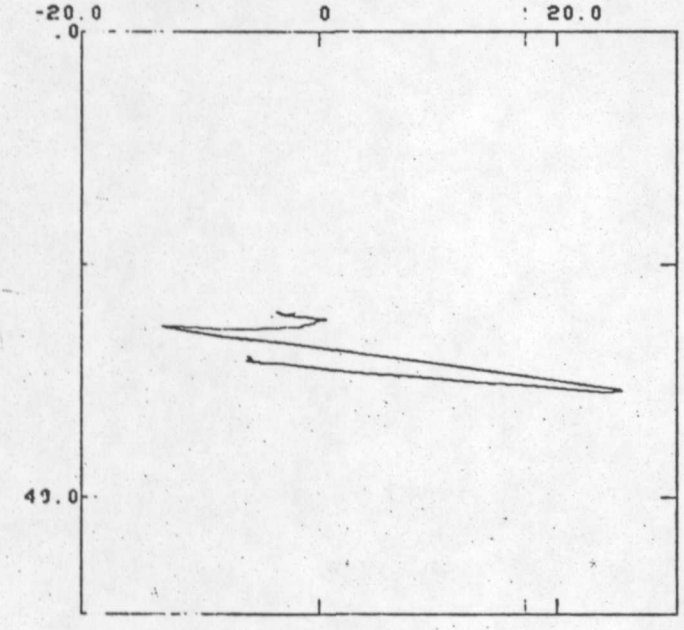

FILES:T0020Z T0020X
SIDE VIEW OF TOTAL FIELD AT MOUNTAINAIR,N.M.
ST@0531 1977.125 NAVG=16

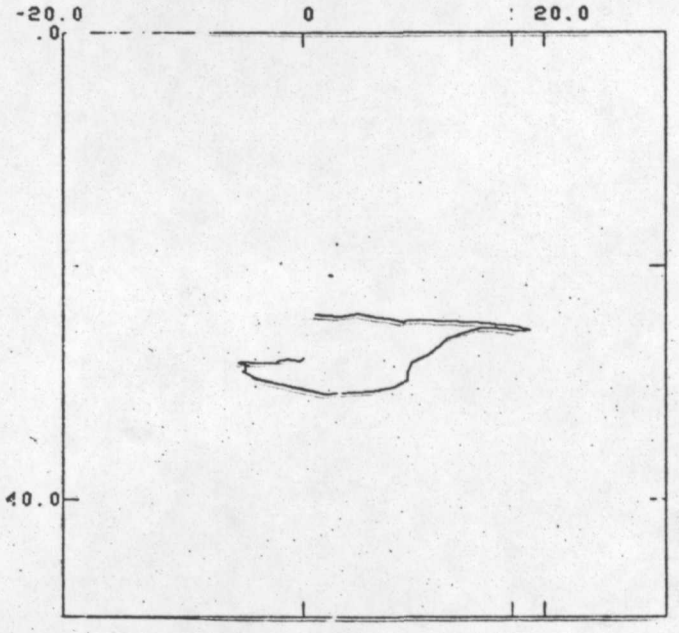

Figure A.3.6

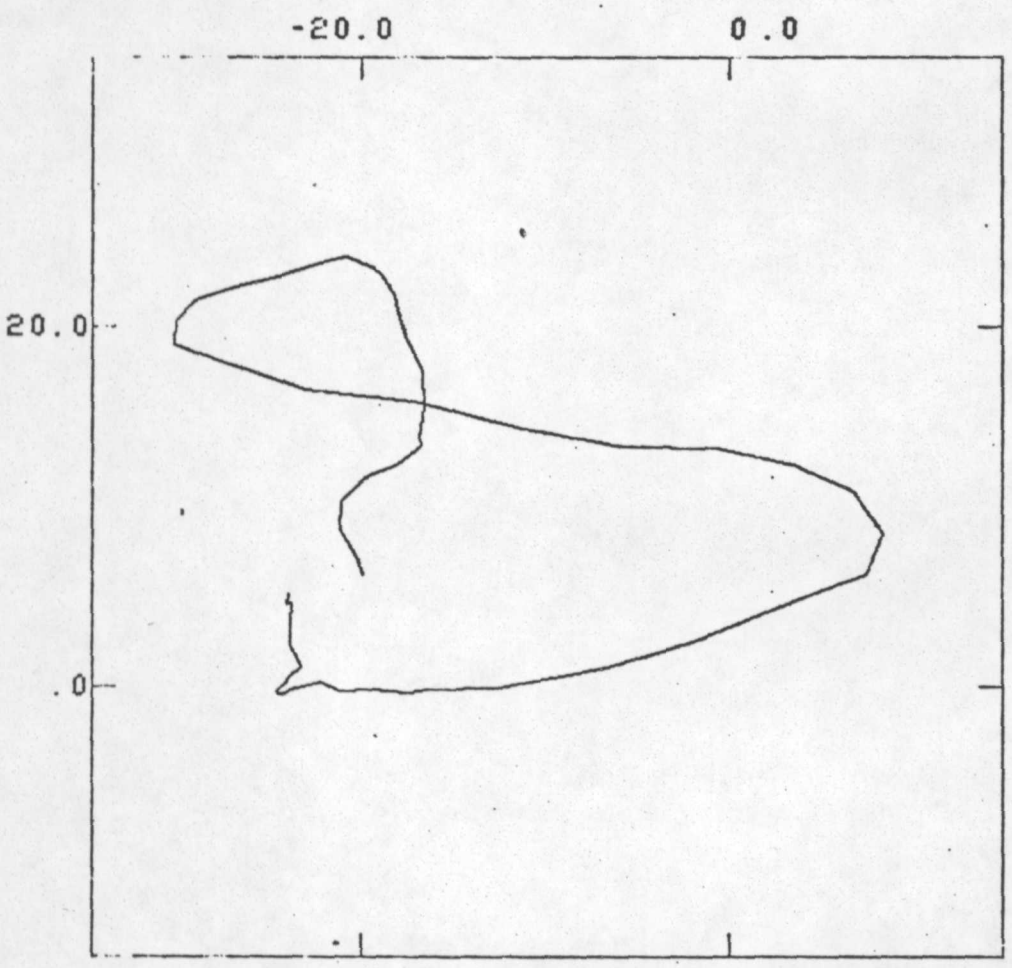
FILES:L0020X L0020Y
TOP VIEW OF TOTAL FIELD AT LUCY,N.M.
S1@0530 1977.125 NAVG=16
-20.0
0.0
20.0
.0

Figure A.3.7

Differential geomagnetic field variations during Event 1

Figures B.1.1-B.1.5 Differential geomagnetic fields during Event 1. Reference station is Gallup, N. Mexico {GAL}. Vertical tick interval is 2nT. Horizontal scale in seconds.

Station	Figure
CUB	B.1.1
SWE	B.1.2
MAD	B.4.3
MTA	B.1.4
LUC	B.1.5

Figures B.1.6-B.1.10 Hodographs of differential geomagnetic field during Event 1. Reference station is Gallup, N. Mexico {GAL}. Both horizontal and vertical intervals are 2nT.

Station	Figure
CUB	B.1.6
SWE	B.1.7
MAD	B.1.8
MTA	B.1.9
LUC	B.1.10

Appendix B.1

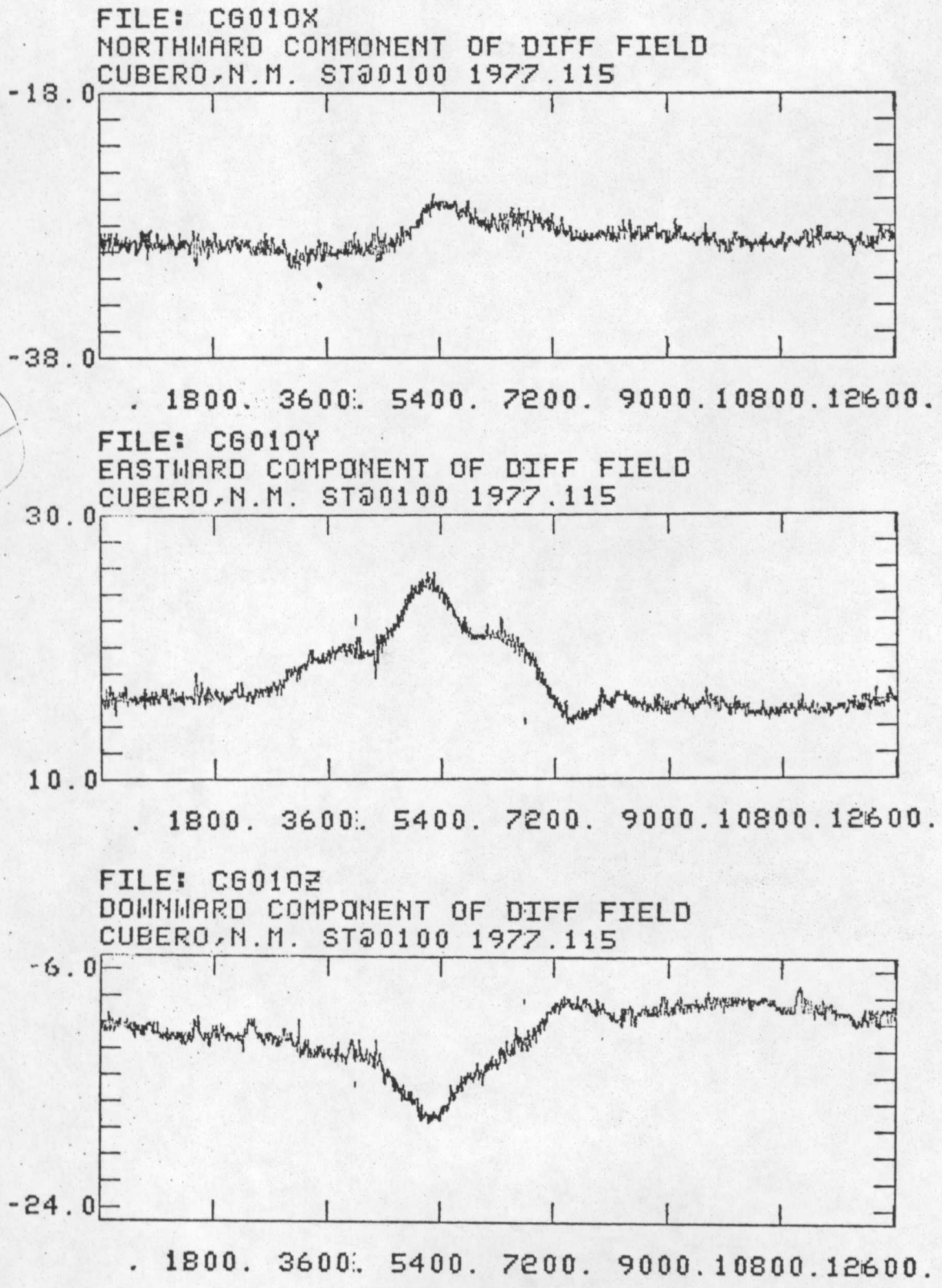
FILE: CG010X
NORTHWARD COMPONENT OF DIFF FIELD
CUBERO,N.M. ST@0100 1977.115
-18.0
-38.0
1800. 3600. 5400. 7200. 9000. 10800. 12600.
FILE: CG010Y
EASTWARD COMPONENT OF DIFF FIELD
CUBERO,N.M. ST@0100 1977.115
30.0
10.0
1800. 3600. 5400. 7200. 9000. 10800. 12600.
FILE: CG010Z
DOWNWARD COMPONENT OF DIFF FIELD
CUBERO,N.M. ST@0100 1977.115
-6.0
-24.0
1800. 3600. 5400. 7200. 9000. 10800. 12600.

Figure B.1.1

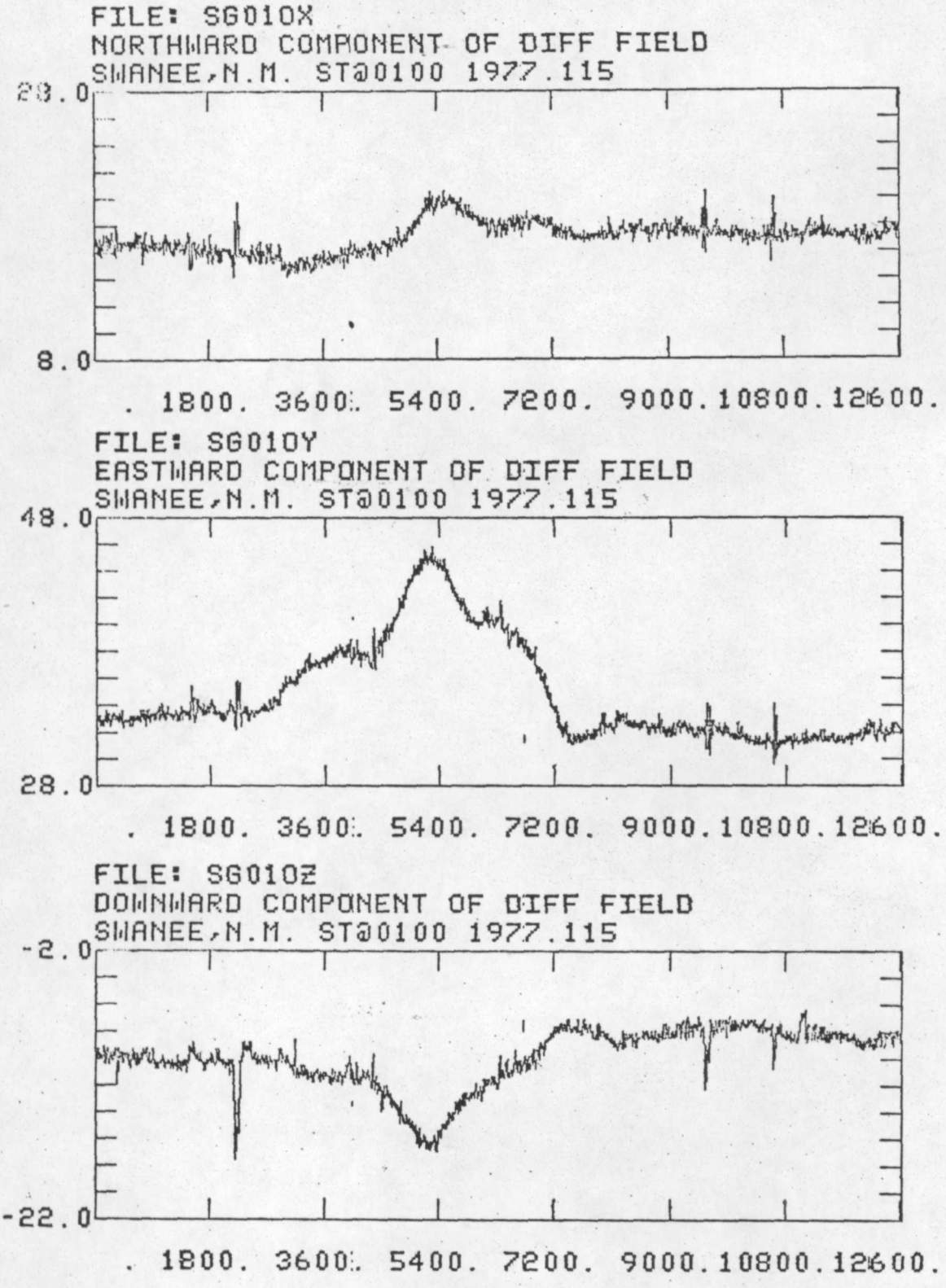
FILE: SG010X
NORTHWARD COMPONENT OF DIFF FIELD
SWANEE,N.M. ST@0100 1977.115
28.0
8.0
1800. 3600. 5400. 7200. 9000. 10800. 12600.
FILE: SG010Y
EASTWARD COMPONENT OF DIFF FIELD
SWANEE,N.M. ST@0100 1977.115
48.0
28.0
1800. 3600. 5400. 7200. 9000. 10800. 12600.
FILE: SG010Z
DOWNWARD COMPONENT OF DIFF FIELD
SWANEE,N.M. ST@0100 1977.115
-2.0
-22.0
1800. 3600. 5400. 7200. 9000. 10800. 12600.

Figure B.1.2

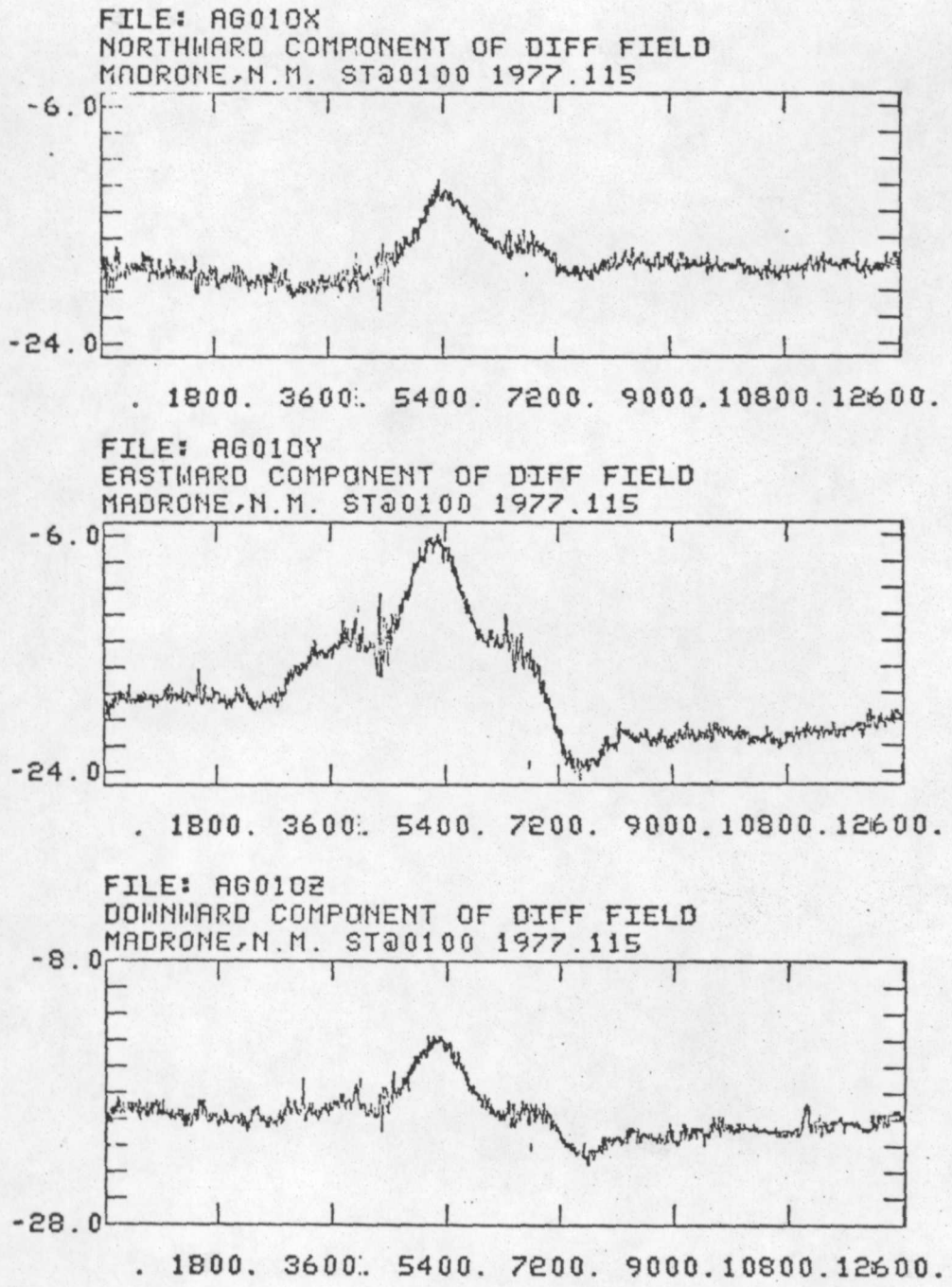
FILE: AG010X
NORTHWARD COMPONENT OF DIFF FIELD
MADRONE,N.M. ST@0100 1977.115
-6.0
-24.0
. 1800. 3600. 5400. 7200. 9000.10800.12600.
FILE: AG010Y
EASTWARD COMPONENT OF DIFF FIELD
MADRONE,N.M. ST@0100 1977.115
-6.0
-24.0
. 1800. 3600. 5400. 7200. 9000.10800.12600.
FILE: AG010Z
DOWNWARD COMPONENT OF DIFF FIELD
MADRONE,N.M. ST@0100 1977.115
-8.0
-28.0
. 1800. 3600. 5400. 7200. 9000.10800.12600.

Figure B.1.3

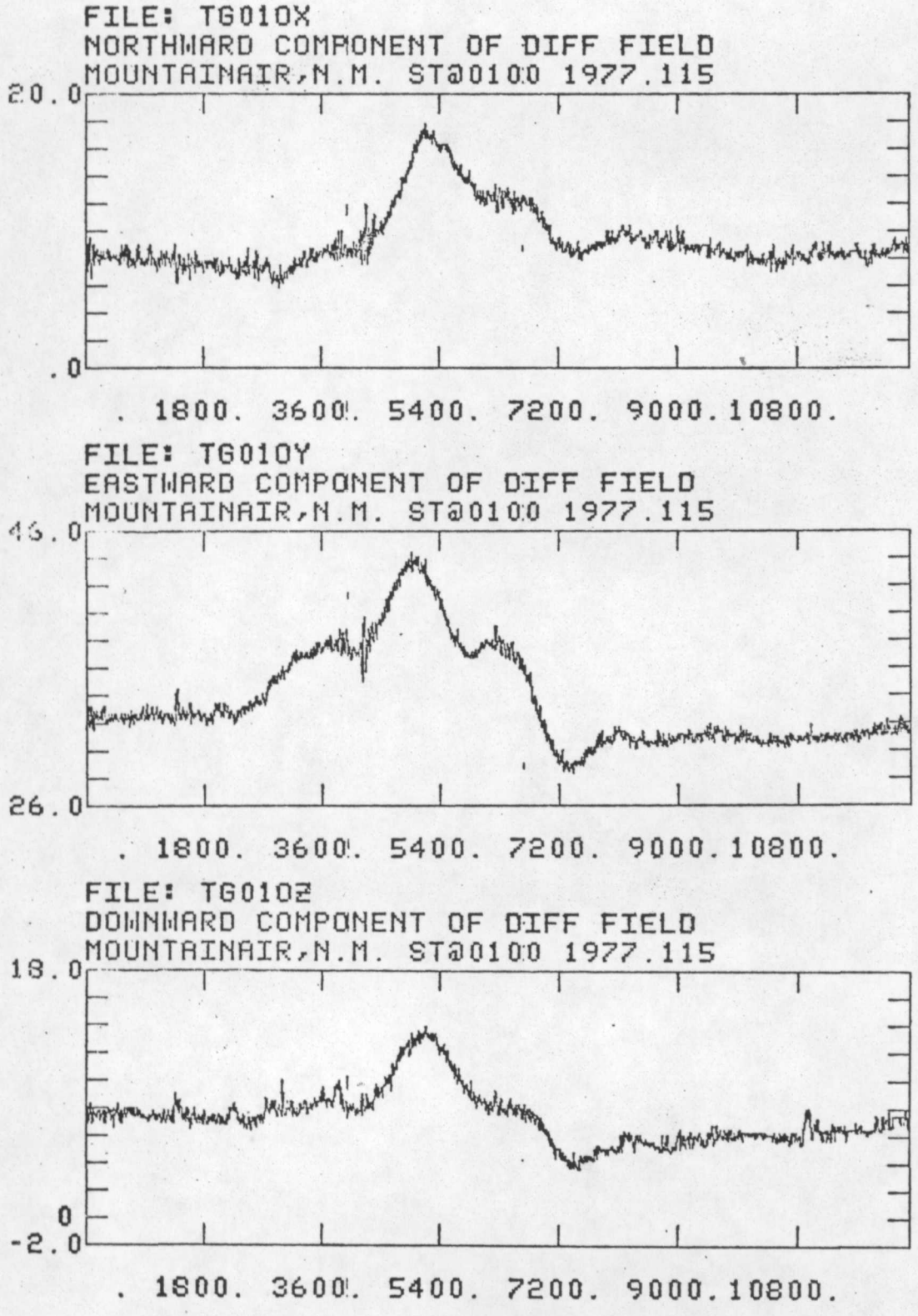
FILE: TG010X
NORTHWARD COMPONENT OF DIFF FIELD
MOUNTAINAIR,N.M. ST@0100 1977.115
20.0
.0
. 1800. 3600. 5400. 7200. 9000.10800.
FILE: TG010Y
EASTWARD COMPONENT OF DIFF FIELD
MOUNTAINAIR,N.M. ST@0100 1977.115
16.0
26.0
. 1800. 3600. 5400. 7200. 9000.10800.
FILE: TG010Z
DOWNWARD COMPONENT OF DIFF FIELD
MOUNTAINAIR,N.M. ST@0100 1977.115
18.0
0
-2.0
. 1800. 3600. 5400. 7200. 9000.10800.

Figure B.1.4

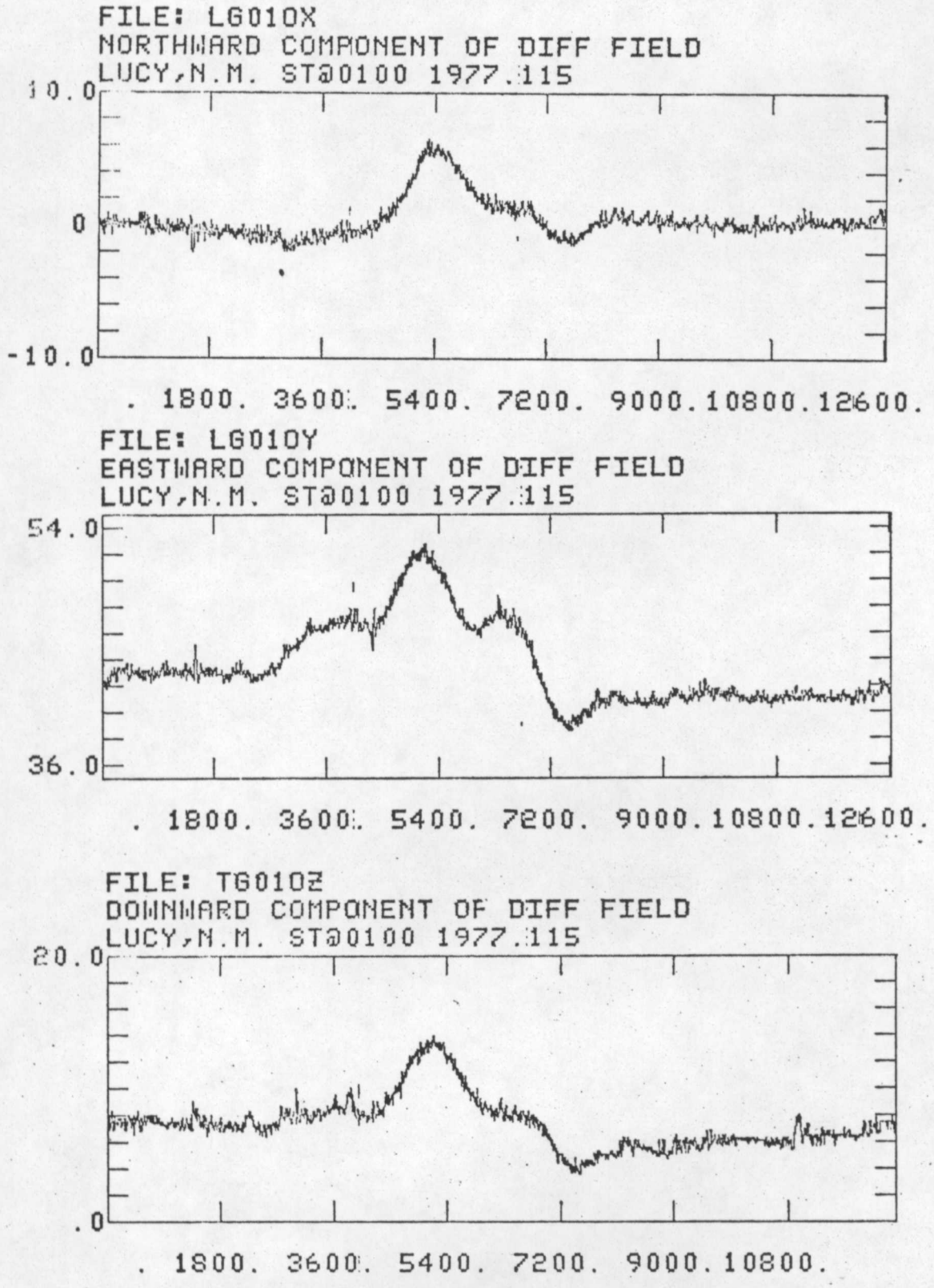
FILE: LG010X
NORTHWARD COMPONENT OF DIFF FIELD
LUCY,N.M. ST@0100 1977.115
10.0
0
-10.0
. 1800. 3600. 5400. 7200. 9000.10800.12600.
FILE: LG010Y
EASTWARD COMPONENT OF DIFF FIELD
LUCY,N.M. ST@0100 1977.115
54.0
36.0
. 1800. 3600. 5400. 7200. 9000.10800.12600.
FILE: TG010Z
DOWNWARD COMPONENT OF DIFF FIELD
LUCY,N.M. ST@0100 1977.115
20.0
.0
. 1800. 3600. 5400. 7200. 9000.10800.

Figure B.1.5

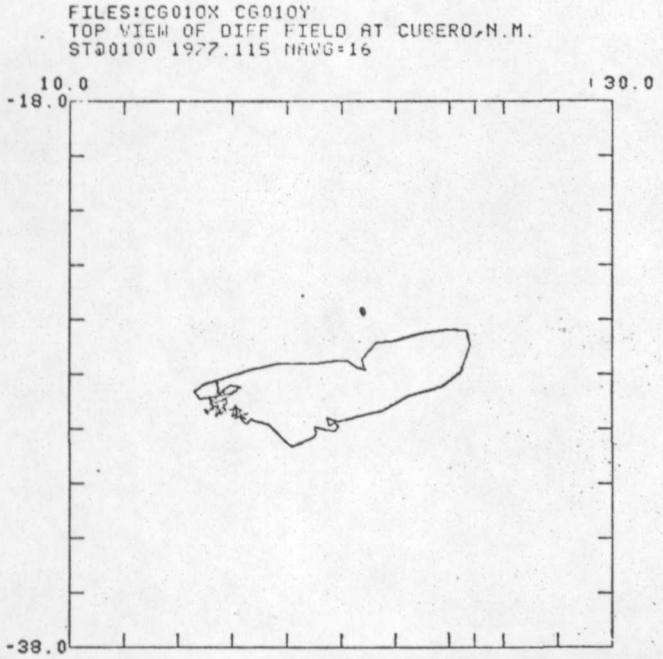
FILES:CG010X CG010Y
TOP VIEW OF DIFF FIELD AT CUBERO,N.M.
ST@0100 1977.115 NAVG=16
10.0
30.0
-18.0
-38.0

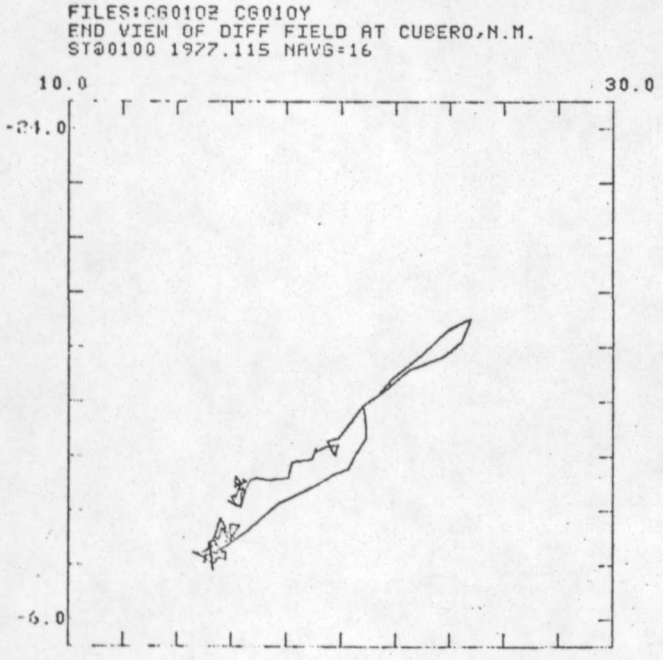
FILES:CG010Z CG010Y
END VIEW OF DIFF FIELD AT CUBERO,N.M.
ST@0100 1977.115 NAVG=16
10.0
30.0
-24.0
-6.0

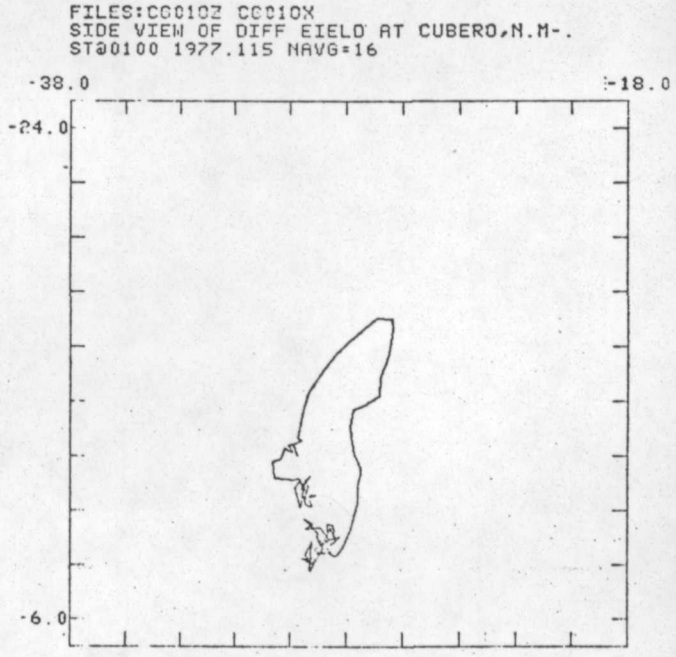
FILES:CG010Z CG010X
SIDE VIEW OF DIFF FIELD AT CUBERO,N.M.
ST@0100 1977.115 NAVG=16
-38.0
-18.0
-24.0
-6.0

Figure B.1.6

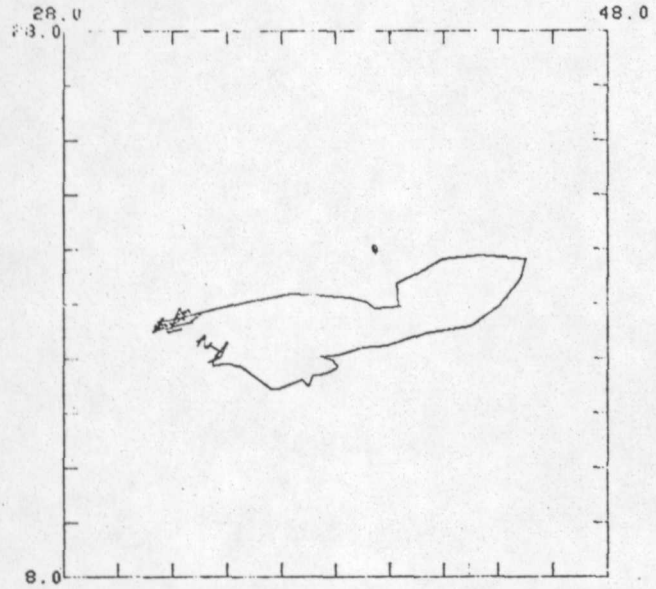
FILES:SG010X SG010Y
TOP VIEW OF DIFF FIELD AT SWANEE,N.M.
ST@0100 1977.115 NAVG=16
28.0
48.0
8.0

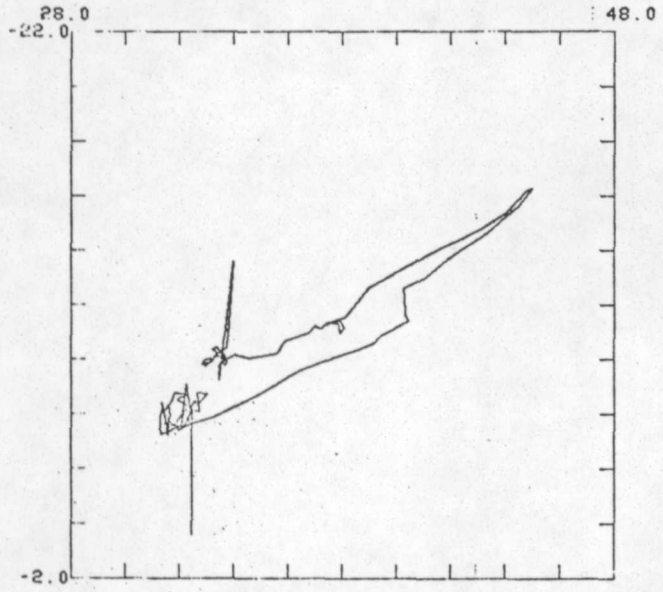
FILES:SG010Z SG010Y
END VIEW OF DIFF FIELD AT SWANEE,N.M.
ST@0100 1977.115 NAVG-16
28.0
48.0
-22.0
-2.0

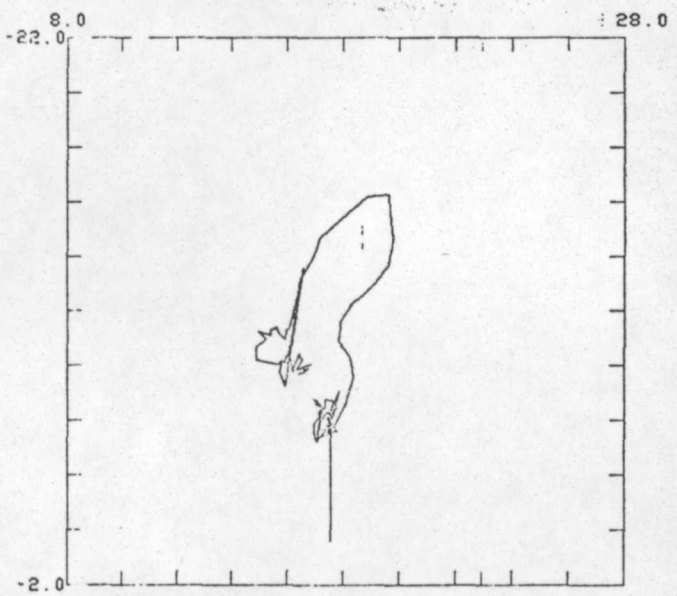
FILES:SG010Z SG010X
SIDE VIEW OF DIFF FIELD AT SWANEE,N.M.
ST@0100 1977.115 NAVG=16
8.0
28.0
-22.0
-2.0

Figure C.1.7

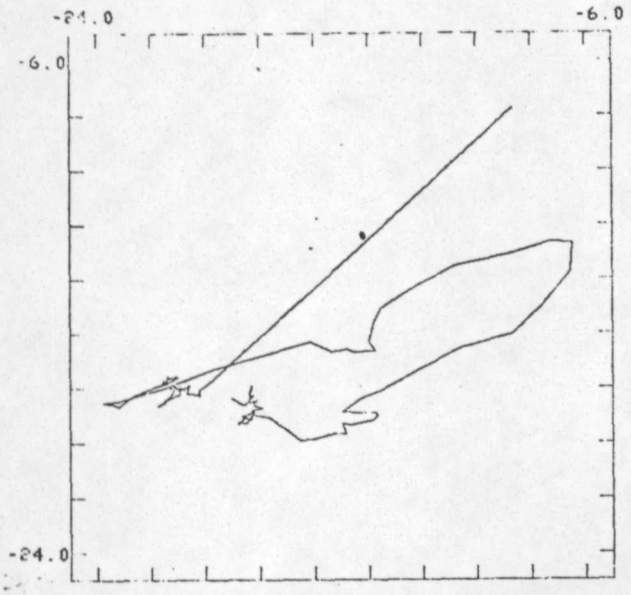
FILES:AG010X AG010Y
TOP VIEW OF DIFF FIELD AT MADRONE,N.M.
ST@0100 1977.115 NAVG=16
-24.0
-6.0
-6.0
-24.0

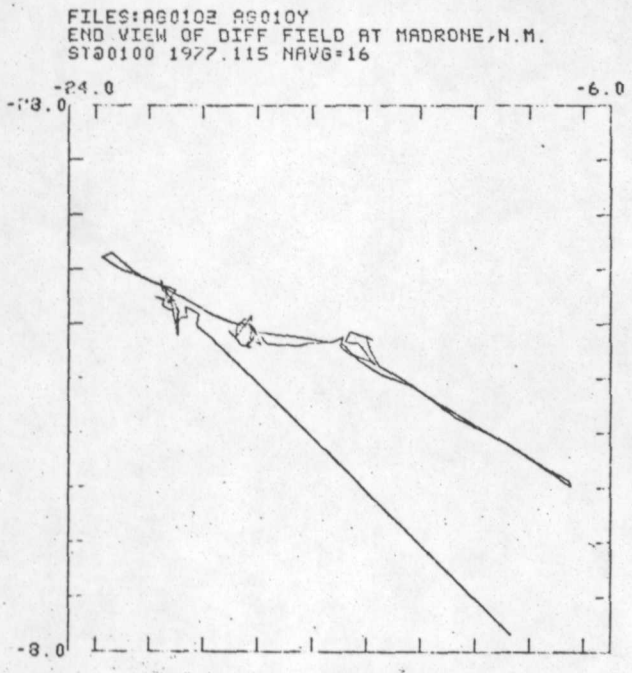
FILES:AG010Z AS01OY
END VIEW OF DIFF FIELD AT MADRONE,N.M.
ST@0100 1977.115 NAVG=16
-24.0
-6.0
-8.0

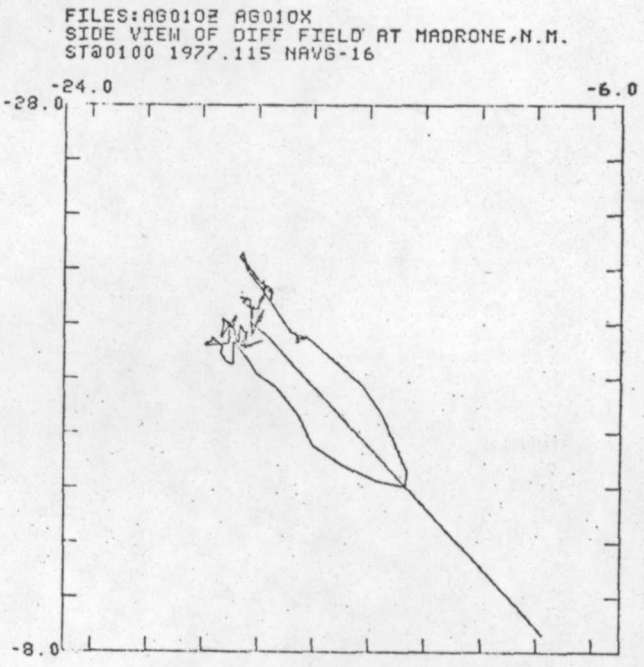
FILES:AG010Z AG010X
SIDE VIEW OF DIFF FIELD AT MADRONE,N.M.
ST@0100 1977.115 NAVG-16
-24.0
-6.0
-28.0
-8.0

Figure B.1.8

FILES:TG010X TG010Y
TOP VIEW OF DIFF FIELD AT MOUNTAINAIR,N.M.
ST@0102 1977.115 NAVG=16

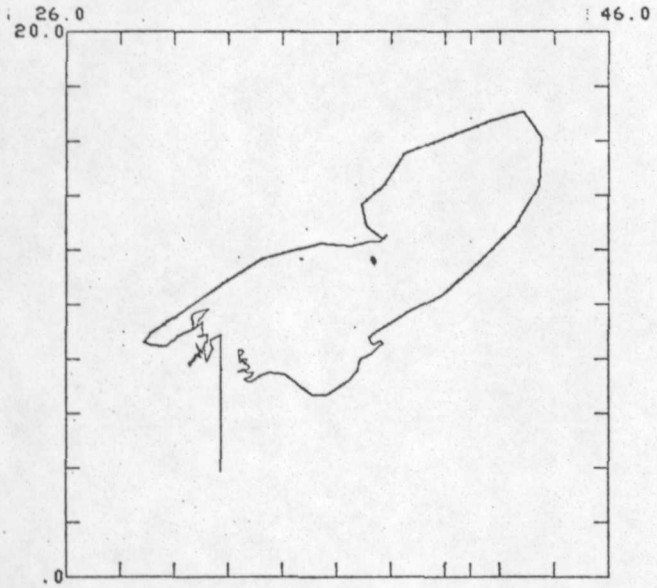

FILES:TG010Z TG010Y
END VIEW OF DIFF FIELD AT MOUNTAINAIR,N.M.
ST@0602 1977.115 NAVG=16

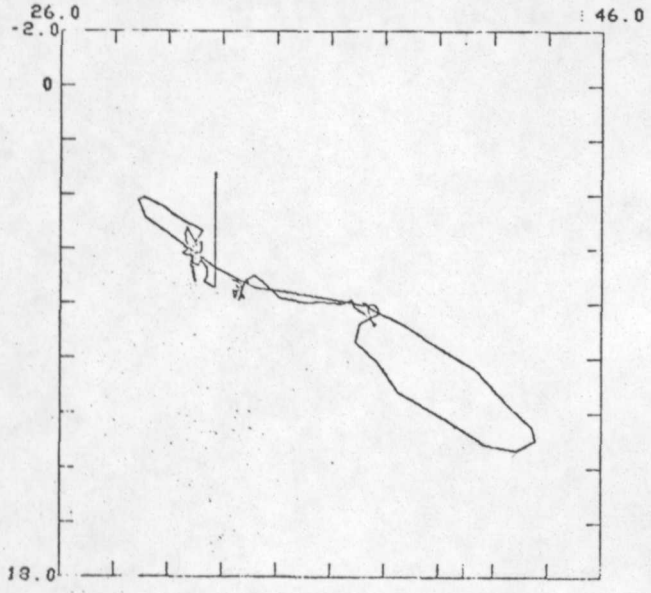

FILES:TG010Z TG010X
SIDE VIEW OF DIFF FIELD AT MOUNTAINAIR,N.M.
ST@0102 1977.115 NAVG=16

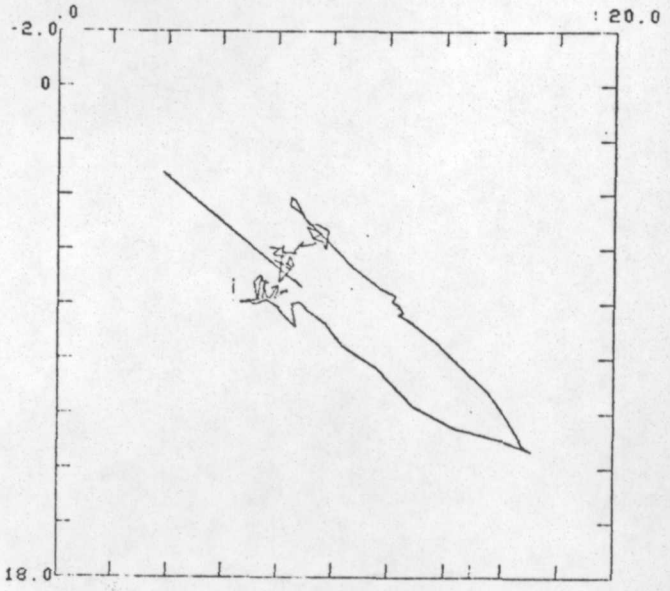

Figure B.1.9

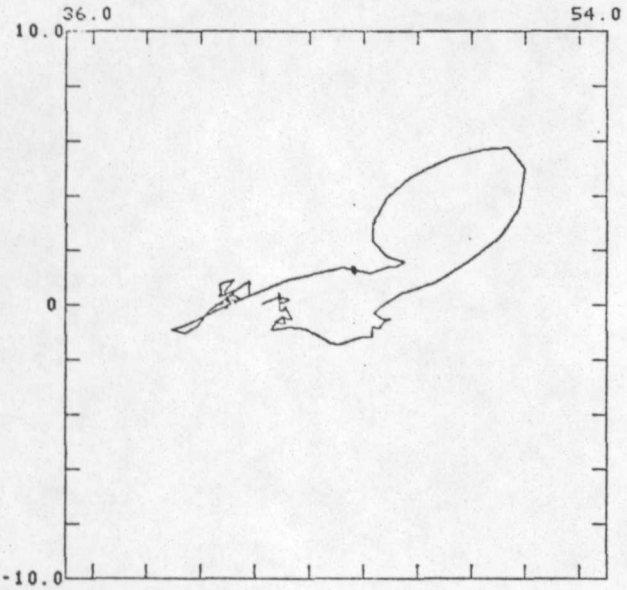
FILES:LG010X LG010Y
TOP VIEW OF DIFF FIELD AT LUCY,N.M.
ST@0100 1977.115 NAVG=16
36.0
54.0
10.0
0
-10.0

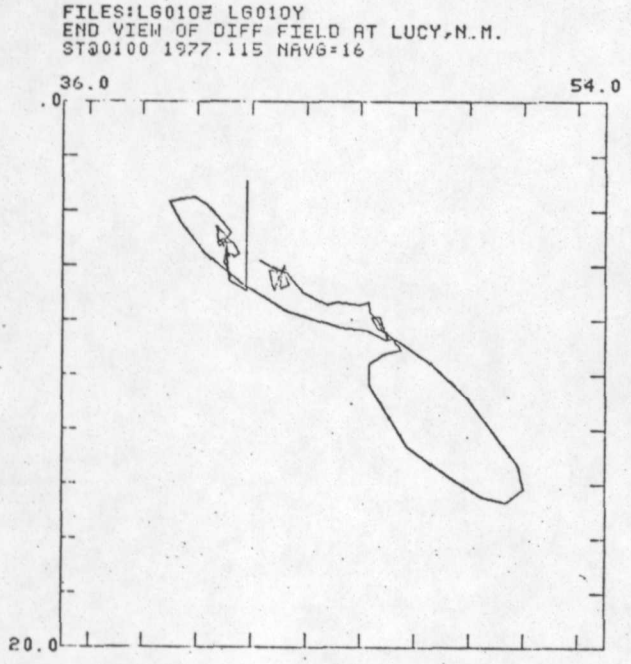
FILES:LG010Z LG010Y
END VIEW OF DIFF FIELD AT LUCY,N.M.
ST@0100 1977.115 NAVG=16
36.0
54.0
.0
20.0

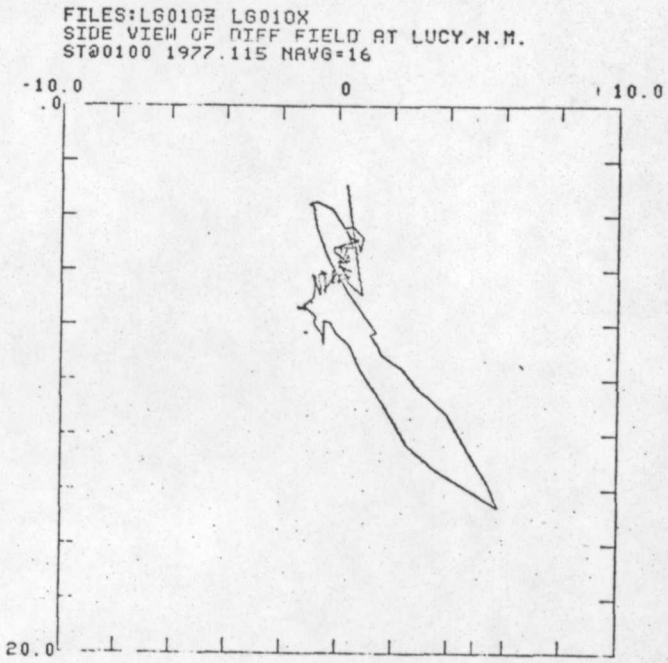
FILES:LG010Z LG010X
SIDE VIEW OF DIFF FIELD AT LUCY,N.M.
ST@0100 1977.115 NAVG=16
-10.0
0
10.0
.0
20.0

Figure B.1.10

Differential geomagnetic field variations during Event 2

Figures B.2.1-B.2.5 Differential geomagnetic fields during Event 2. Reference station is Gallup, N. Mexico {GAL}. Vertical tick interval is 2nT. Horizontal scale in seconds.

Station	Figure
CUB	B.2.1
SWE	B.2.2
MAD	B.2.3
MTA	B.2.4
LUC	B.2.5

Figures B.2.6-B.2.10 Hodographs of differential geomagnetic field during Event 2. Reference station is Gallup, N. Mexico {GAL}.

Station	Figure
CUB	B.2.6
SWE	B.2.7
MAD	B.2.8
MTA	B.2.9
LUC	B.2.10

Appendix B.2

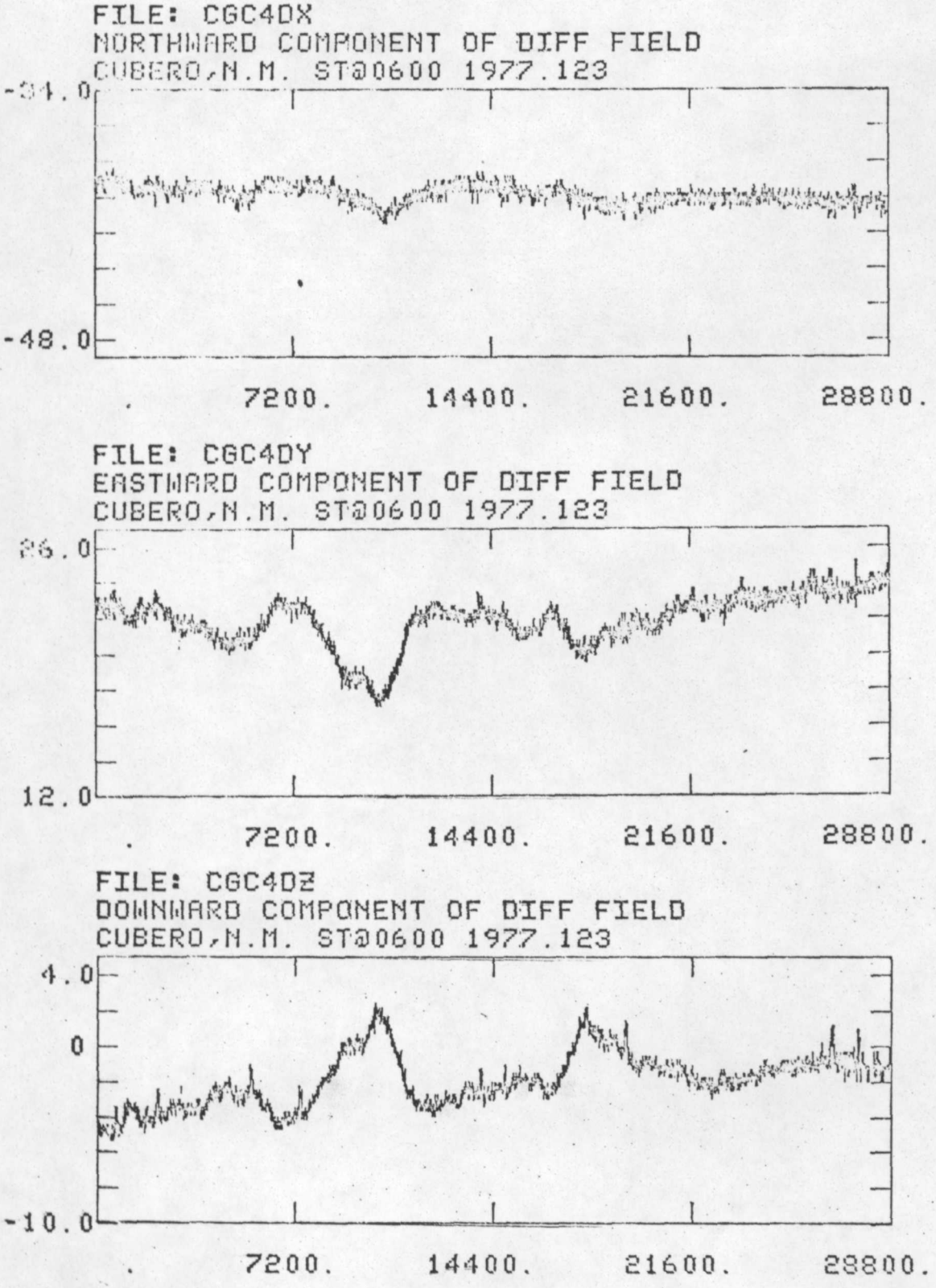
FILE: CGC4DX
NORTHWARD COMPONENT OF DIFF FIELD
CUBERO,N.M. ST@0600 1977.123
-34.0
-48.0
7200.
14400.
21600.
28800.
FILE: CGC4DY
EASTWARD COMPONENT OF DIFF FIELD
CUBERO,N.M. ST@0600 1977.123
26.0
12.0
7200.
14400.
21600.
28800.
FILE: CGC4DZ
DOWNWARD COMPONENT OF DIFF FIELD
CUBERO,N.M. ST@0600 1977.123
4.0
0
-10.0
7200.
14400.
21600.
28800.

Figure B.2.1

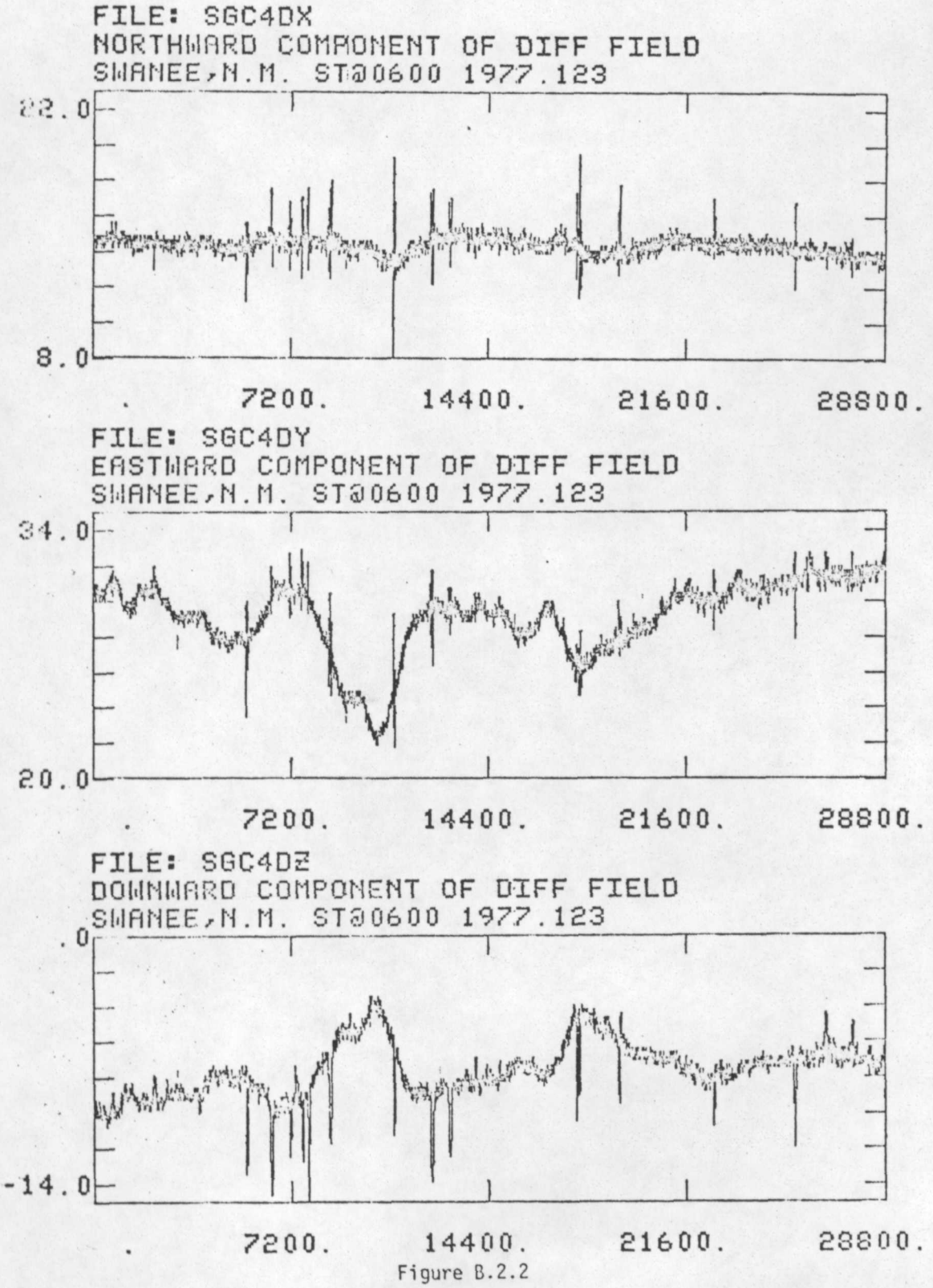
FILE: SGC4DX
NORTHWARD COMPONENT OF DIFF FIELD
SWANEE,N.M. ST@0600 1977.123
22.0
8.0
7200.
14400.
21600.
28800.
FILE: SGC4DY
EASTWARD COMPONENT OF DIFF FIELD
SWANEE,N.M. ST@0600 1977.123
34.0
20.0
7200.
14400.
21600.
28800.
FILE: SGC4DZ
DOWNWARD COMPONENT OF DIFF FIELD
SWANEE,N.M. ST@0600 1977.123
.0
-14.0
7200.
14400.
21600.
28800.

Figure B.2.2

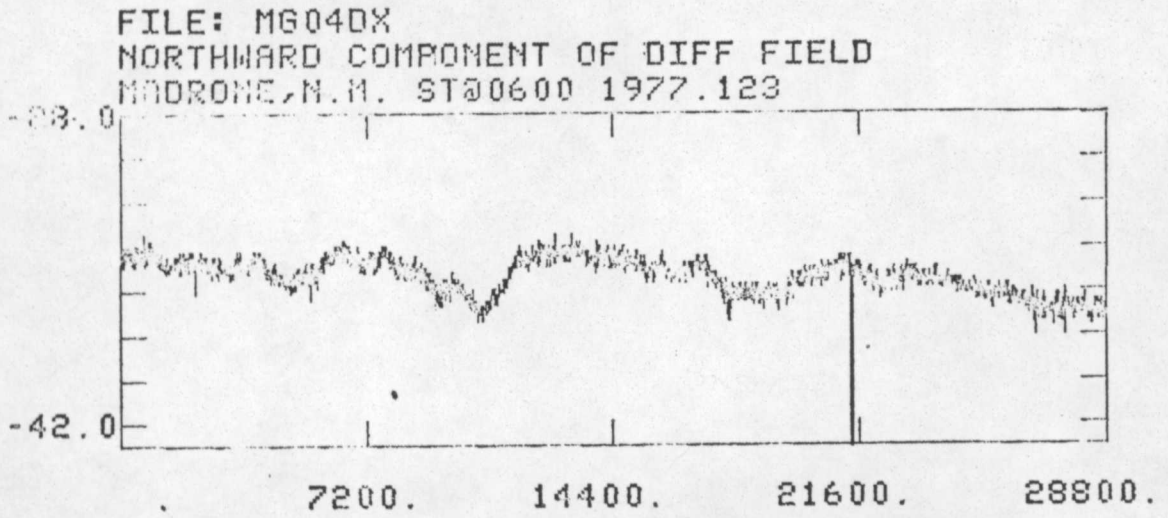
FILE: MG04DX
NORTHWARD COMPONENT OF DIFF FIELD
MADRONE,N.M. ST@0600 1977.123
-28.0
-42.0
7200.
14400.
21600.
28800.

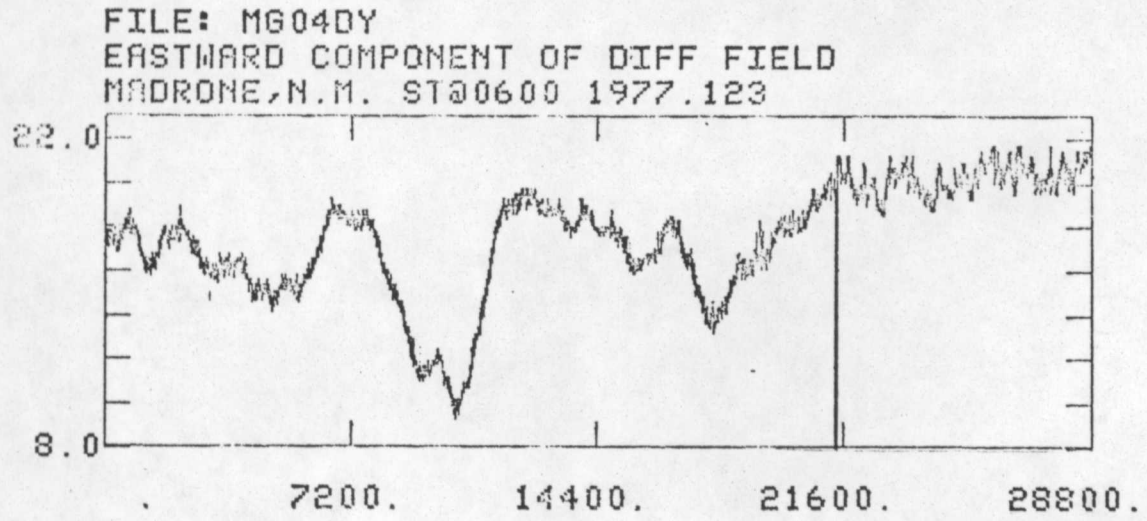
FILE: MG04DY
EASTWARD COMPONENT OF DIFF FIELD
MADRONE,N.M. ST@0600 1977.123
22.0
8.0
7200.
14400.
21600.
28800.

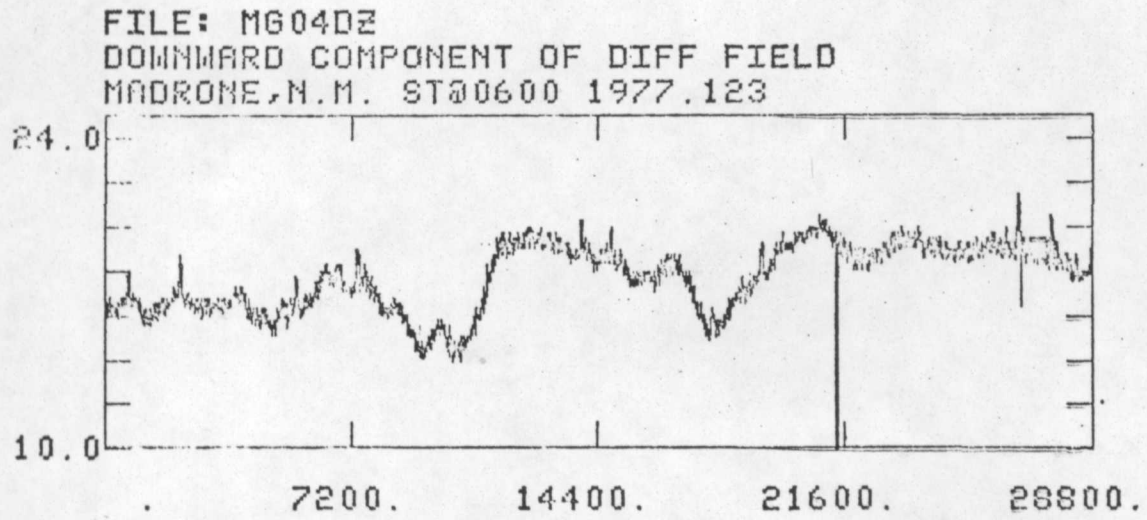
FILE: MG04DZ
DOWNWARD COMPONENT OF DIFF FIELD
MADRONE,N.M. ST@0600 1977.123
24.0
10.0
7200.
14400.
21600.
28800.

Figure B.2.3

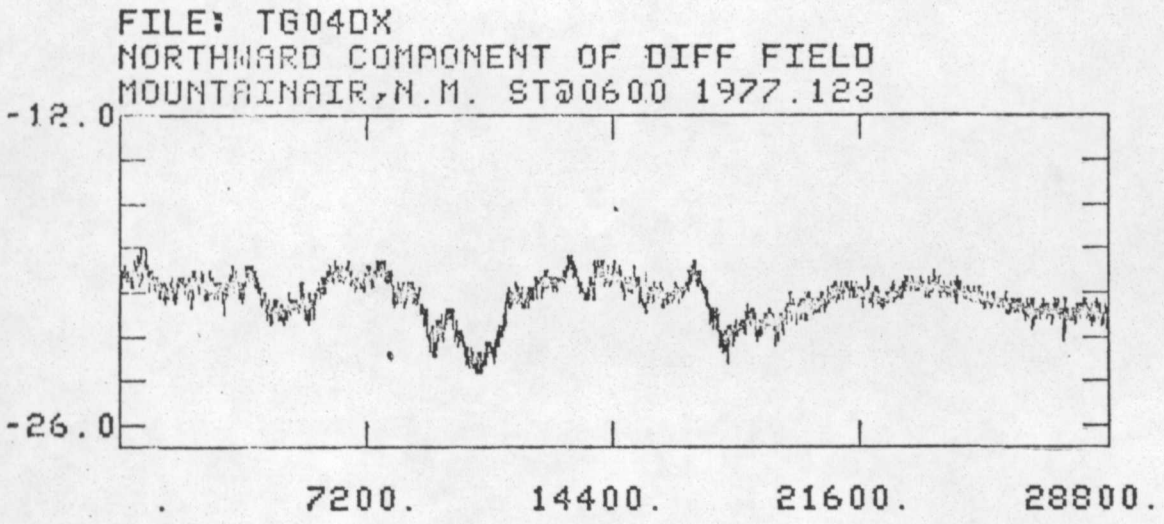
FILE: TG04DX
NORTHWARD COMPONENT OF DIFF FIELD
MOUNTAINAIR,N.M. ST@0600 1977.123
-12.0
-26.0
7200.
14400.
21600.
28800.

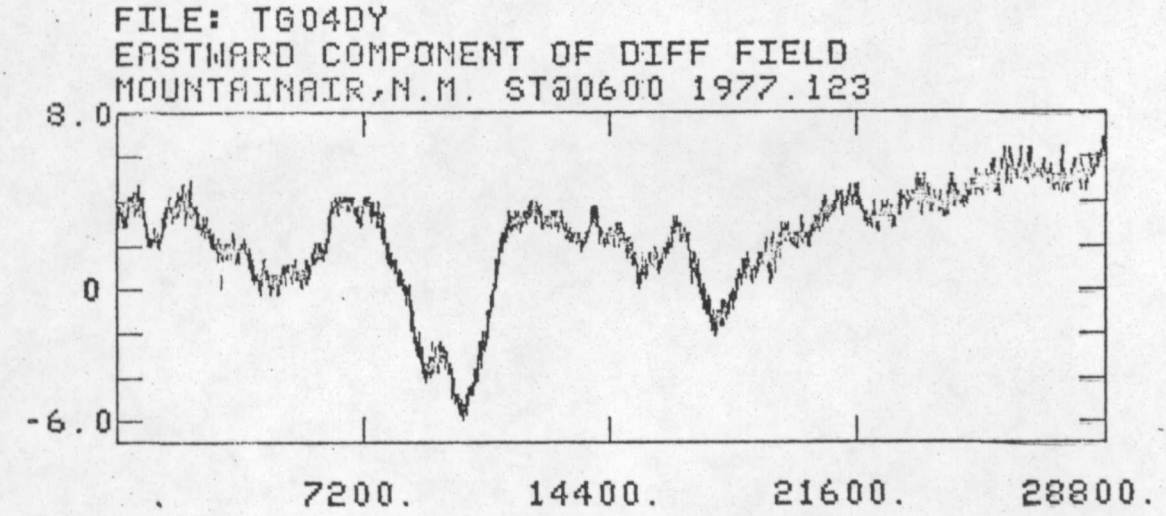
FILE: TG04DY
EASTWARD COMPONENT OF DIFF FIELD
MOUNTAINAIR,N.M. ST@0600 1977.123
8.0
0
-6.0
7200.
14400.
21600.
28800.

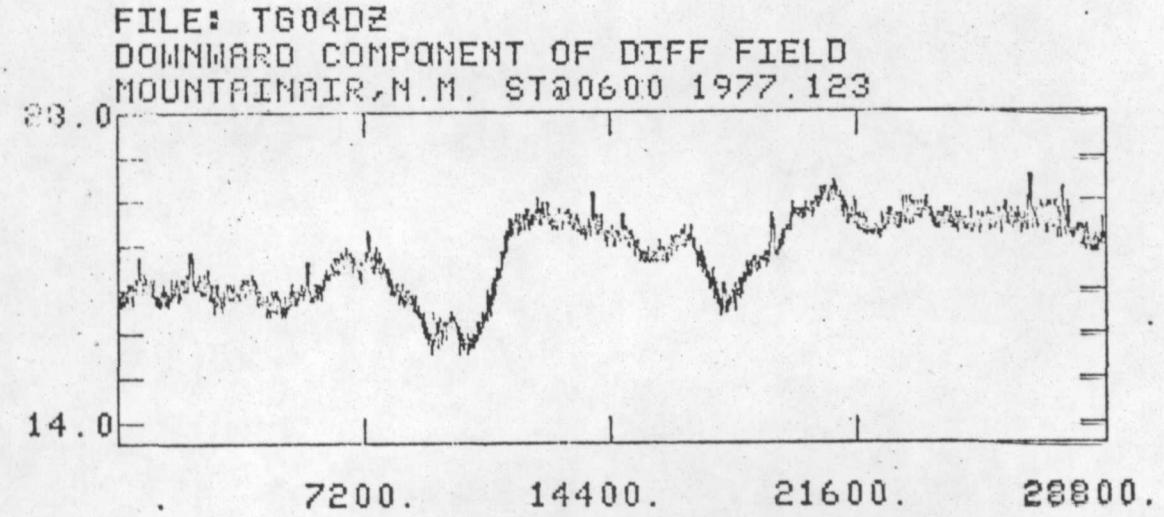
FILE: TG04DZ
DOWNWARD COMPONENT OF DIFF FIELD
MOUNTAINAIR,N.M. ST@0600 1977.123
23.0
14.0
7200.
14400.
21600.
28800.

Figure B.2.4

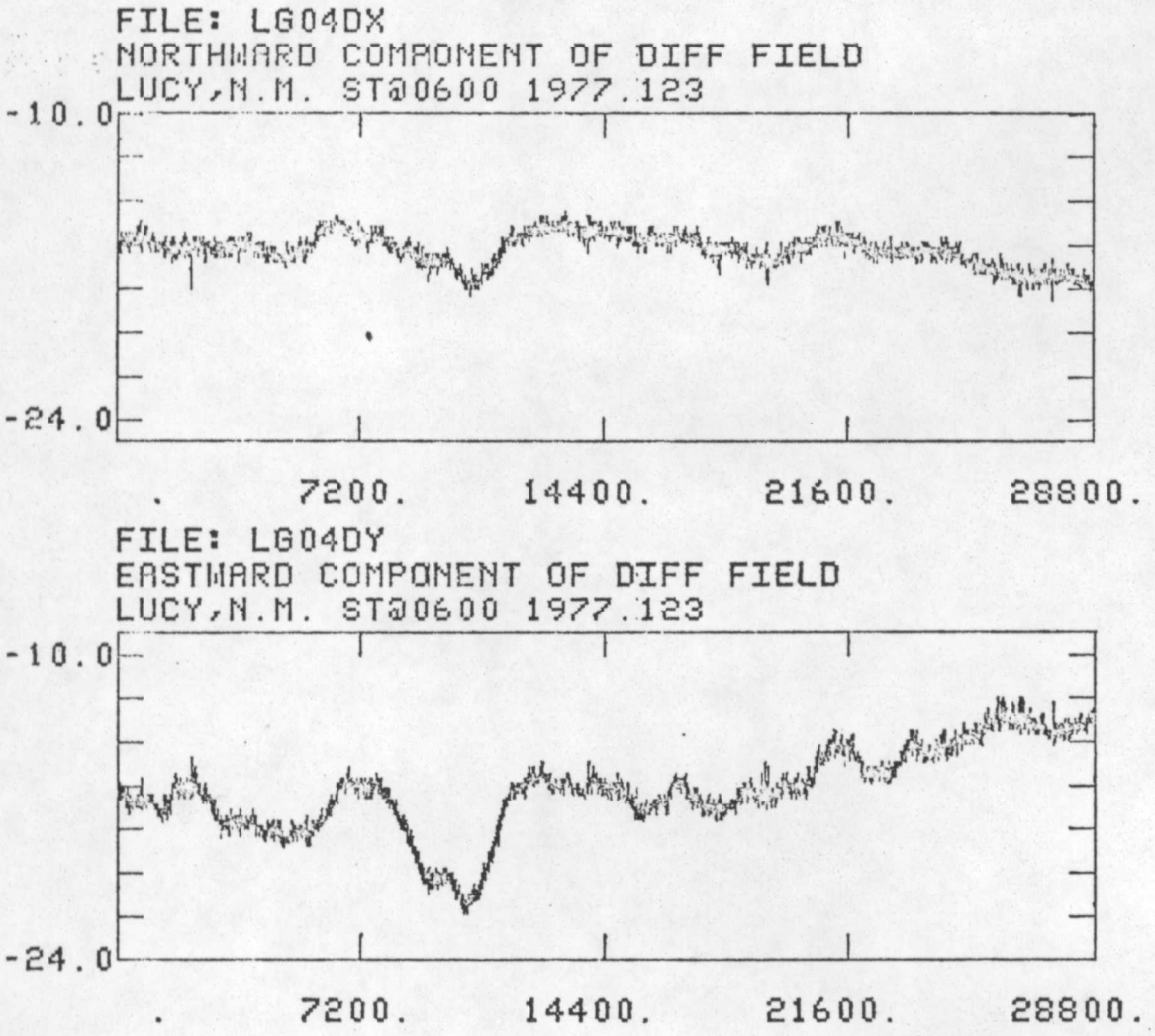
FILE: LG04DX
NORTHWARD COMPONENT OF DIFF FIELD
LUCY,N.M. ST@0600 1977.123
-10.0
-24.0
7200.
14400.
21600.
28800.
FILE: LG04DY
EASTWARD COMPONENT OF DIFF FIELD
LUCY,N.M. ST@0600 1977.123
-10.0
-24.0
7200.
14400.
21600.
28800.

Figure B.2.5

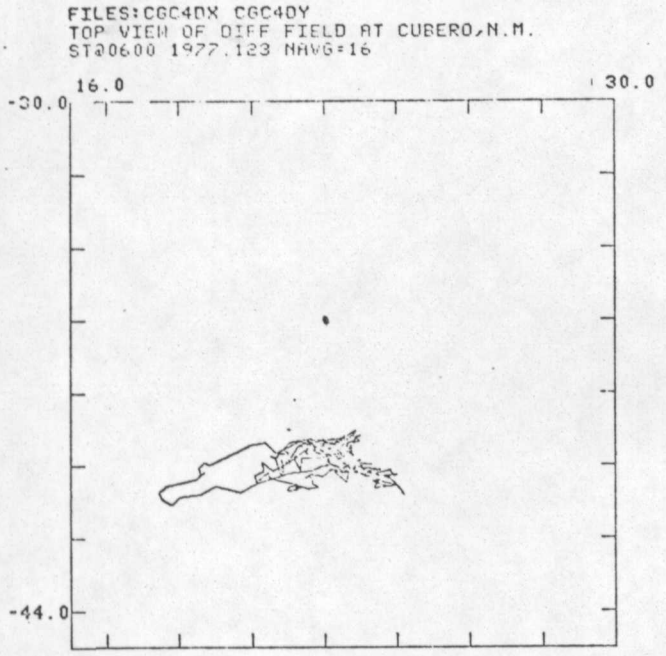
FILES:CGC4DX CGC4DY
TOP VIEW OF DIFF FIELD AT CUBERO,N.M.
ST@0600 1977.123 NAVG=16
16.0
30.0
-30.0
-44.0

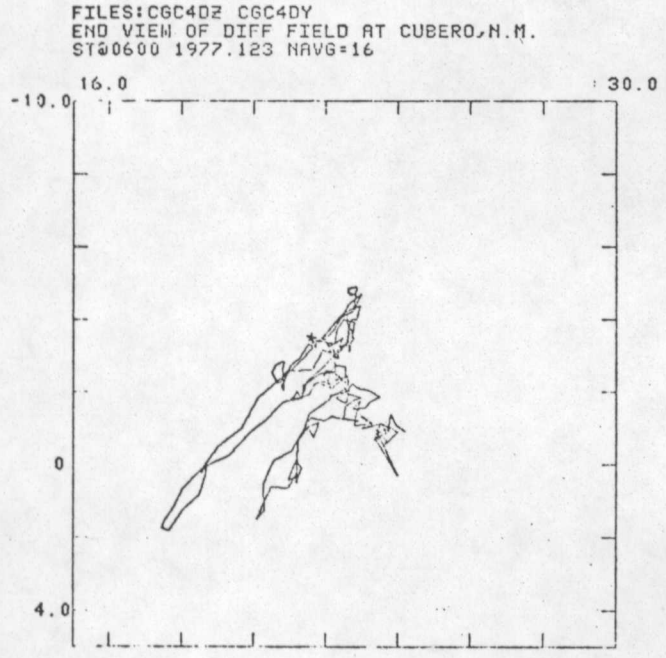
FILES:CGC4DZ CGC4DY
END VIEW OF DIFF FIELD AT CUBERO,N.M.
ST@0600 1977.123 NAVG=16
16.0
30.0
-10.0
0
4.0

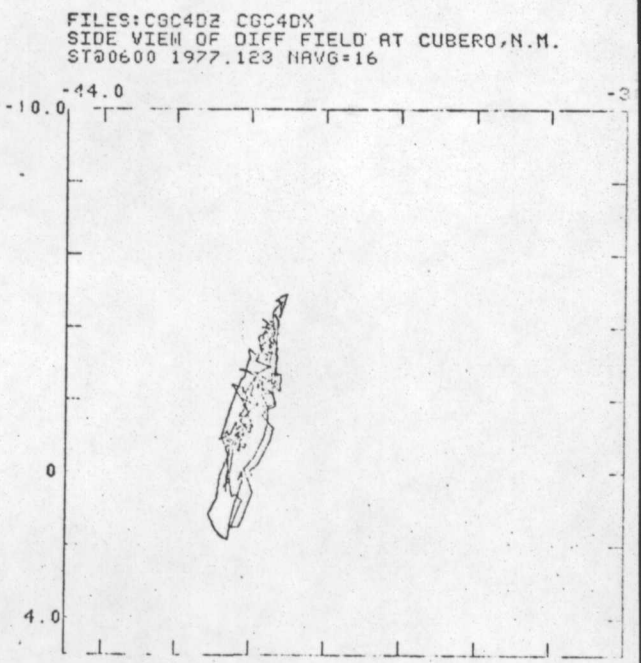
FILES:CGC4DZ CGC4DX
SIDE VIEW OF DIFF FIELD AT CUBERO,N.M.
ST@0600 1977.123 NAVG=16
-44.0
-10.0
0
4.0

Figure B.2.6

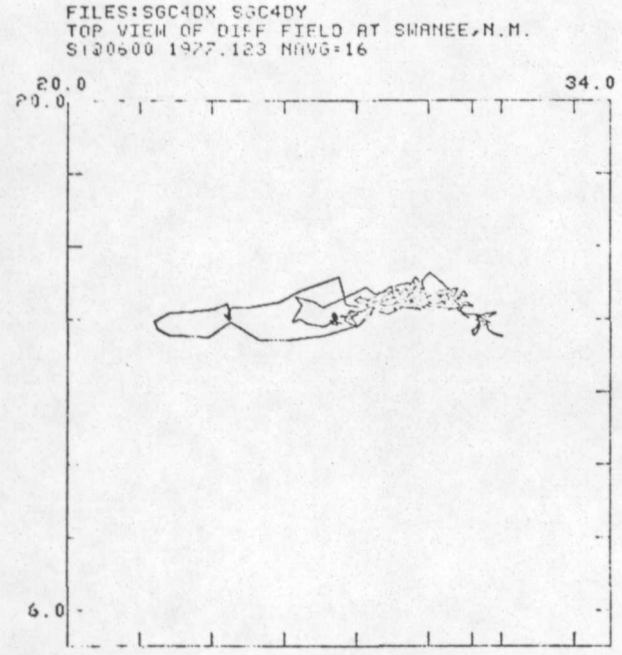
FILES:SGC4DX SGC4DY
TOP VIEW OF DIFF FIELD AT SWANEE,N.M.
ST@0600 1977.123 NAVG=16
20.0
34.0
20.0
6.0

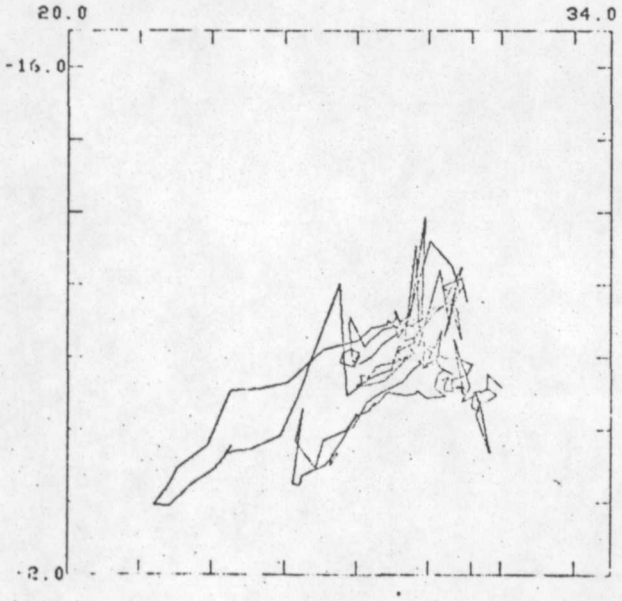
FILES:SGC4DZ SGC4DY
END VIEW OF DIFF FIELD AT SWANEE,N.M.
ST@0600 1977.123 NAVG=16
20.0
34.0
-16.0
-2.0

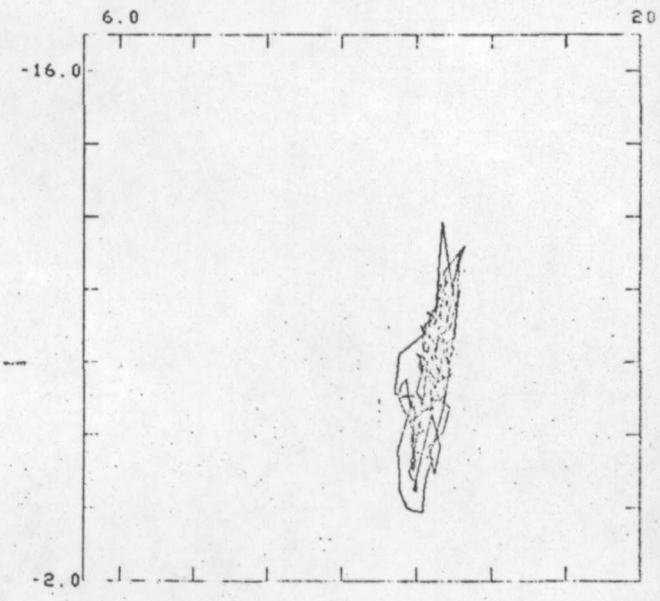
FILES:SGC4DZ SGC4DX
SIDE VIEW OF DIFF FIELD AT SWANEE,N.M.
ST@0600 1977.123 NAVG=16
6.0
20.
-16.0
-2.0

Figure B.2.7

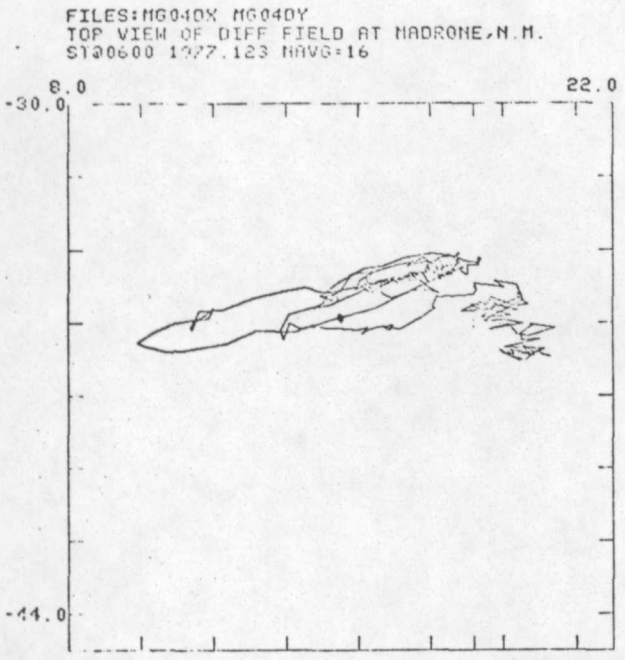
FILES:MG04DX MG04DY
TOP VIEW OF DIFF FIELD AT MADRONE,N.M.
ST@0600 1977.123 NAVG=16
8.0
22.0
-30.0
-44.0

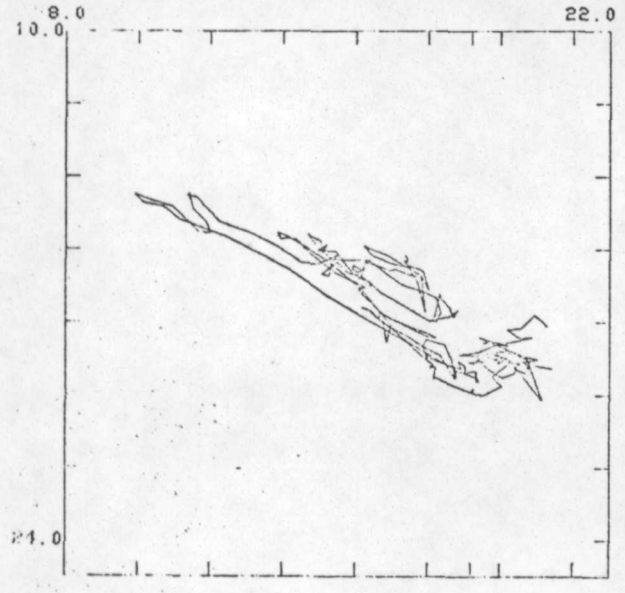
FILES:MG04DZ MG04DY
END VIEW OF DIFF FIELD AT MADRONE,N.M.
ST@0600 1977.123
8.0
22.0
10.0
24.0

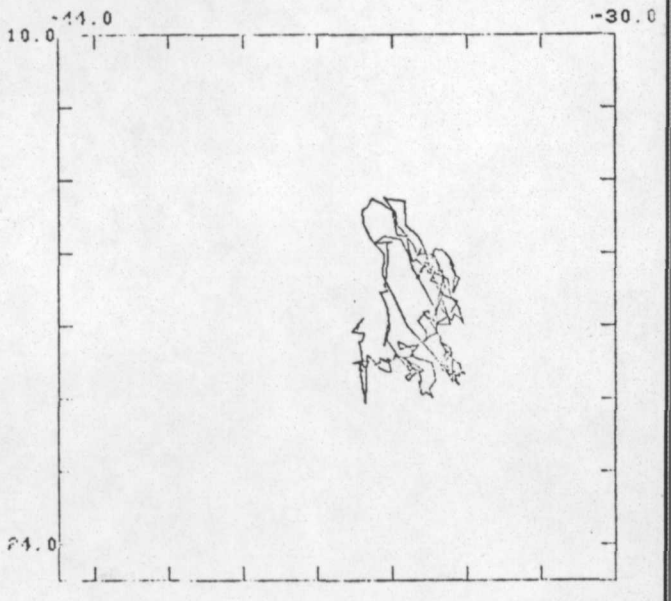
FILES:MG04DZ MG04DX
SIDE VIEW OF DIFF FIELD AT MADRONE,N.M.
ST@0600 1977.123 NAVG=16
-44.0
-30.0
10.0
24.0

Figure B.2.8

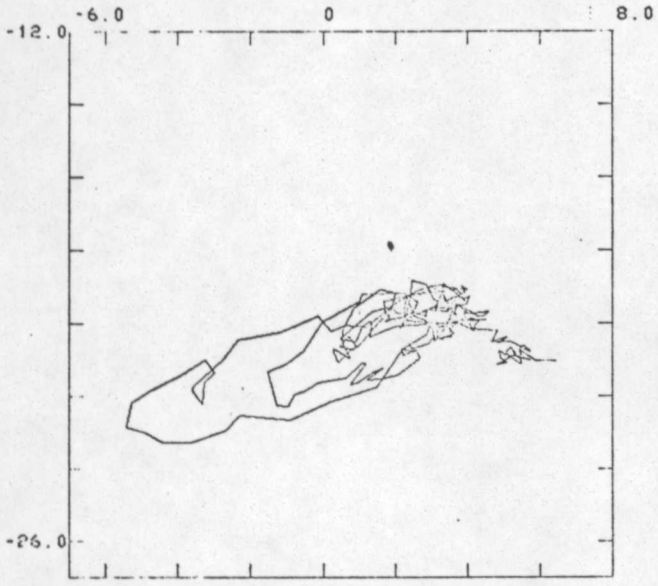
FILES:TG04DX TG04DY
TOP VIEW OF DIFF FIELD AT MOUNTAINAIR,N.M.
ST@0601 1977.123 NAVG=16
-6.0
0
8.0
-12.0
-26.0

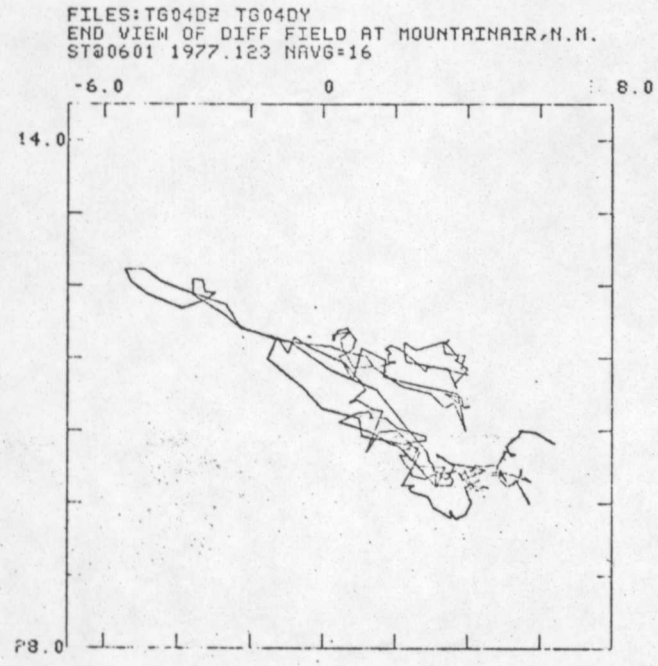
FILES:TG04DZ TG04DY
END VIEW OF DIFF FIELD AT MOUNTAINAIR,N.M.
ST@0601 1977.123 NAVG=16
-6.0
0
8.0
14.0
28.0

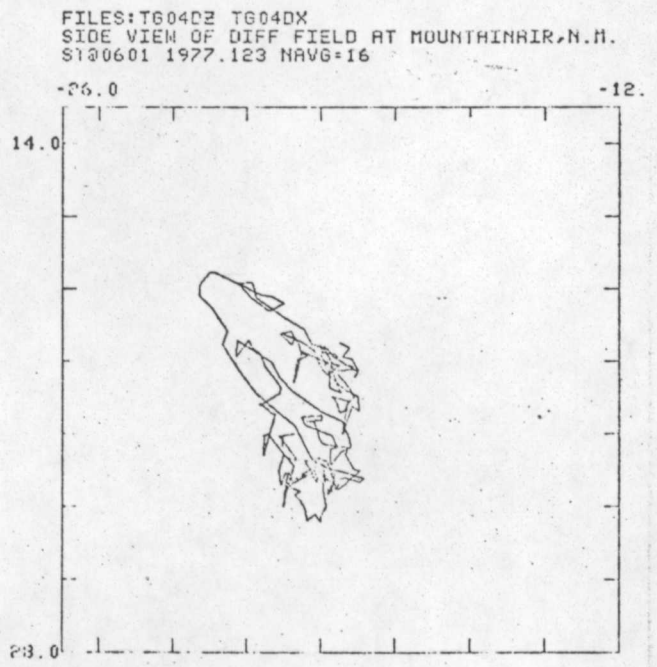
FILES:TG04DZ TG04DX
SIDE VIEW OF DIFF FIELD AT MOUNTAINAIR,N.M.
ST@0601 1977.123 NAVG=16
-26.0
-12.
14.0
28.0

Figure B.2.9

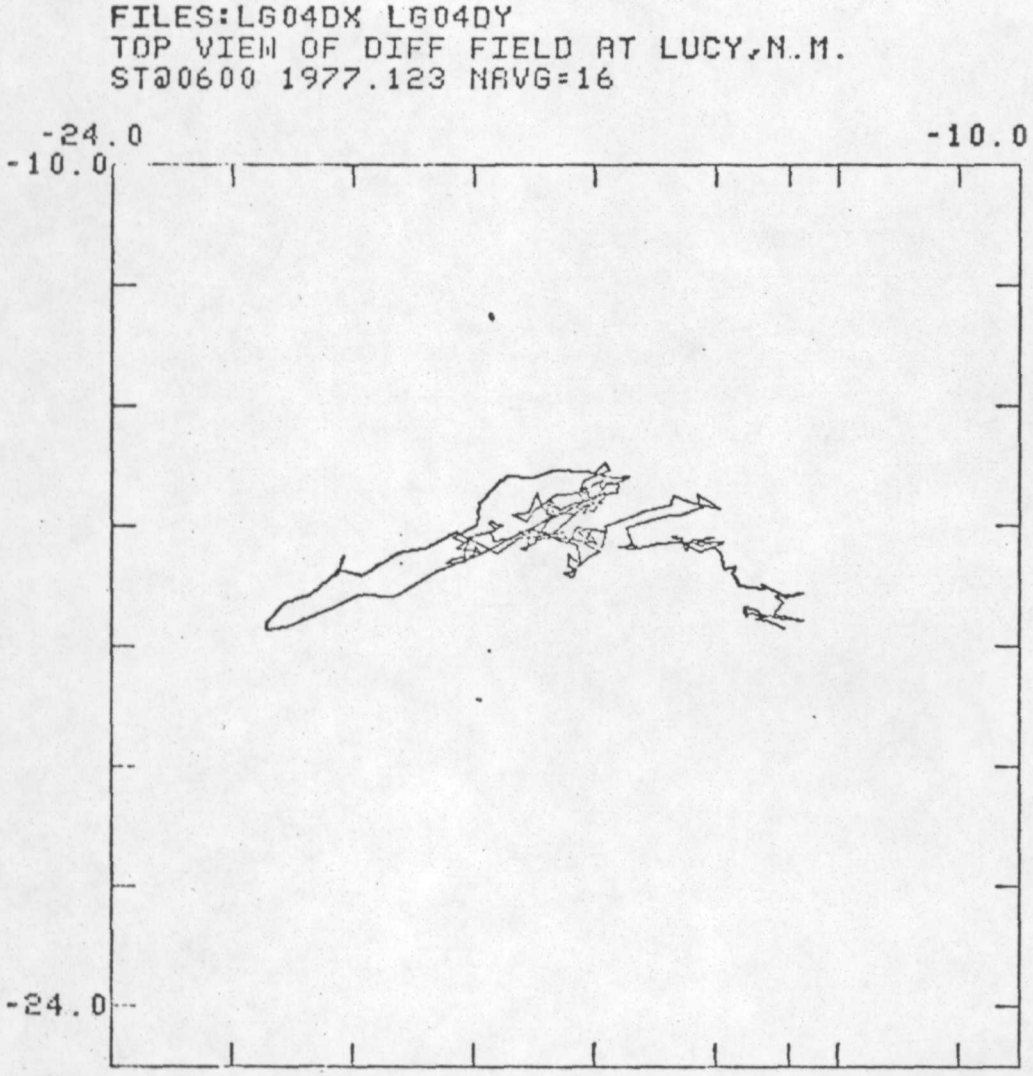
FILES:LG04DX LG04DY
TOP VIEW OF DIFF FIELD AT LUCY,N.M.
ST@0600 1977.123 NAVG=16
-24.0
-10.0
-10.0
-24.0

Figure B.2.10

Differential geomagnetic field variations during Event 3

Figures B.3.1-B.3.5 Differential geomagnetic fields during Event 3. Reference station is Gallup, N. Mexico {GAL}. Vertical tick interval is 2nT. Horizontal scale in seconds.

Station	Figure
CUB	B.3.1
SWE	B.3.2
MAD	B.3.3
MTA	B.3.4
LUC	B.3.5

Figures B.3.6-B.3.10 Hodographs of differential geomagnetic field during Event 3. Reference station is Gallup, N. Mexico {GAL}. Both horizontal and vertical intervals are 2nT.

Station	Figure
CUB	B.3.6
SWE	B.3.7
MAD	B.3.8
MTA	B.3.9
LUC	B.3.10

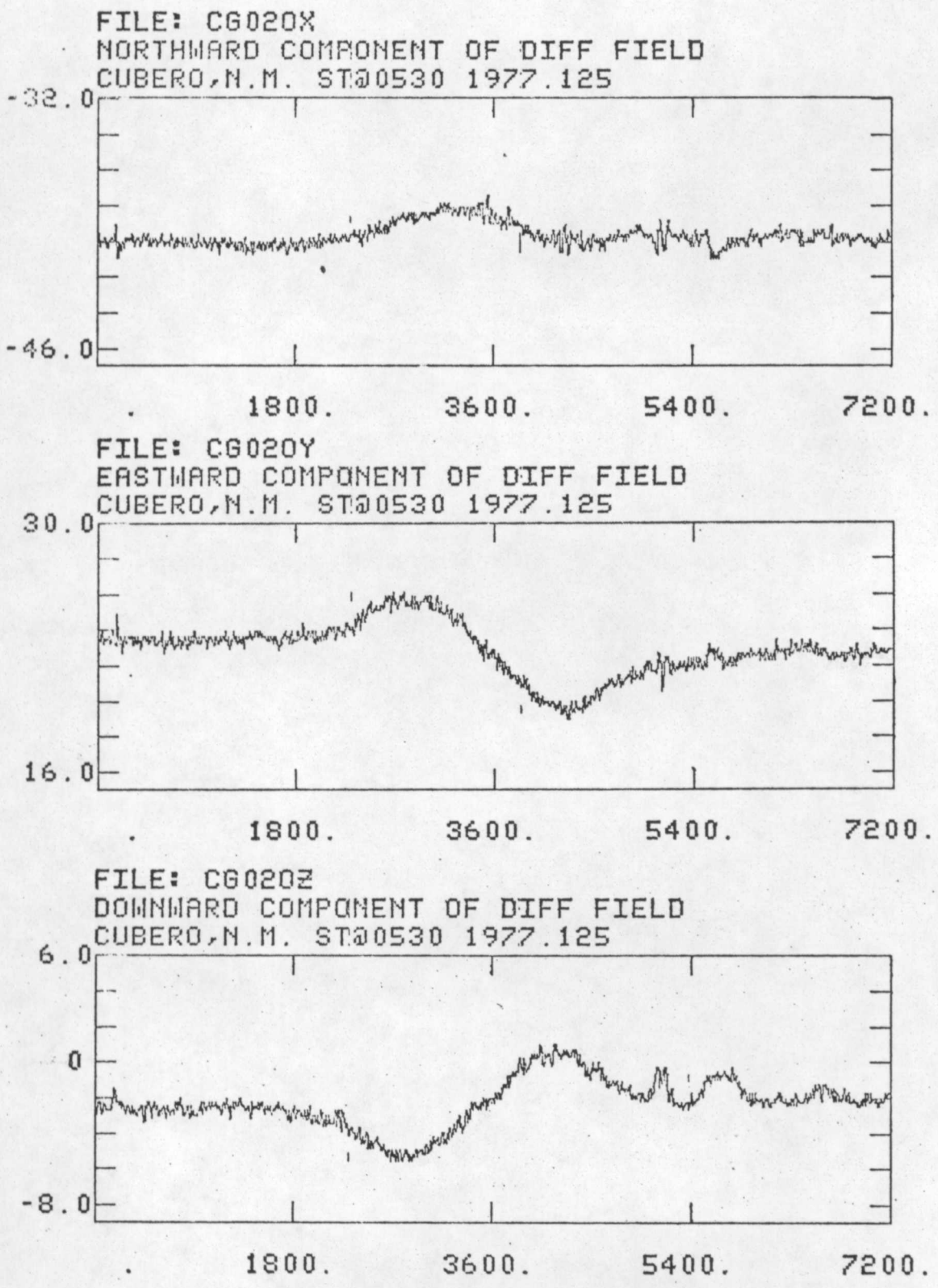
FILE: CG020X
NORTHWARD COMPONENT OF DIFF FIELD
CUBERO,N.M. ST@0530 1977.125
-32.0
-46.0
1800.
3600.
5400.
7200.
FILE: CG020Y
EASTWARD COMPONENT OF DIFF FIELD
CUBERO,N.M. ST@0530 1977.125
30.0
16.0
1800.
3600.
5400.
7200.
FILE: CG020Z
DOWNWARD COMPONENT OF DIFF FIELD
CUBERO,N.M. ST@0530 1977.125
6.0
0
-8.0
1800.
3600.
5400.
7200.

Figure B.3.1

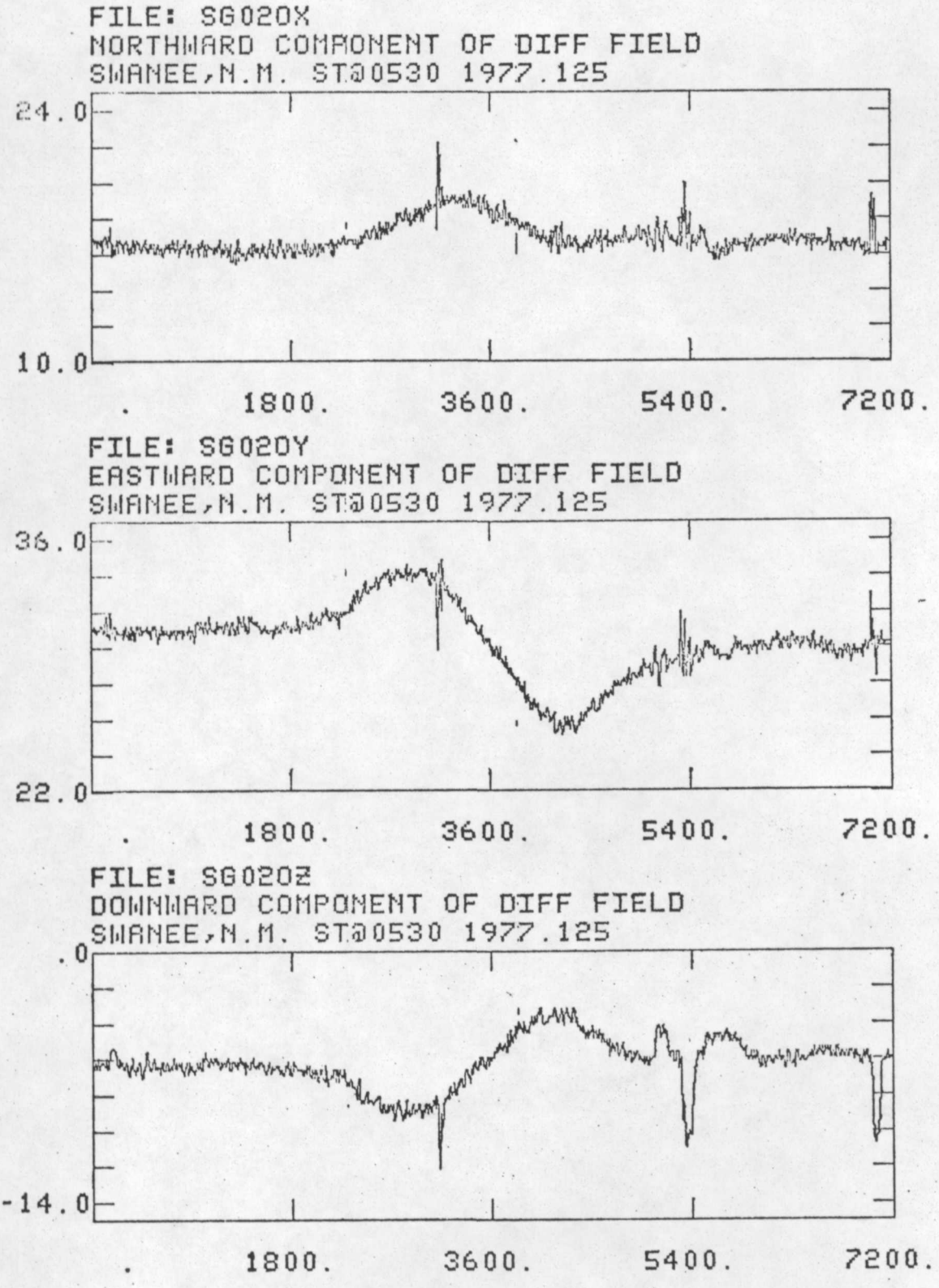
FILE: SG020X
NORTHWARD COMPONENT OF DIFF FIELD
SWANEE,N.M. ST@0530 1977.125
24.0
10.0
1800.
3600.
5400.
7200.
FILE: SG020Y
EASTWARD COMPONENT OF DIFF FIELD
SWANEE,N.M. ST@0530 1977.125
36.0
22.0
1800.
3600.
5400.
7200.
FILE: SG020Z
DOWNWARD COMPONENT OF DIFF FIELD
SWANEE,N.M. ST@0530 1977.125
.0
-14.0
1800.
3600.
5400.
7200.

Figure B.3.2

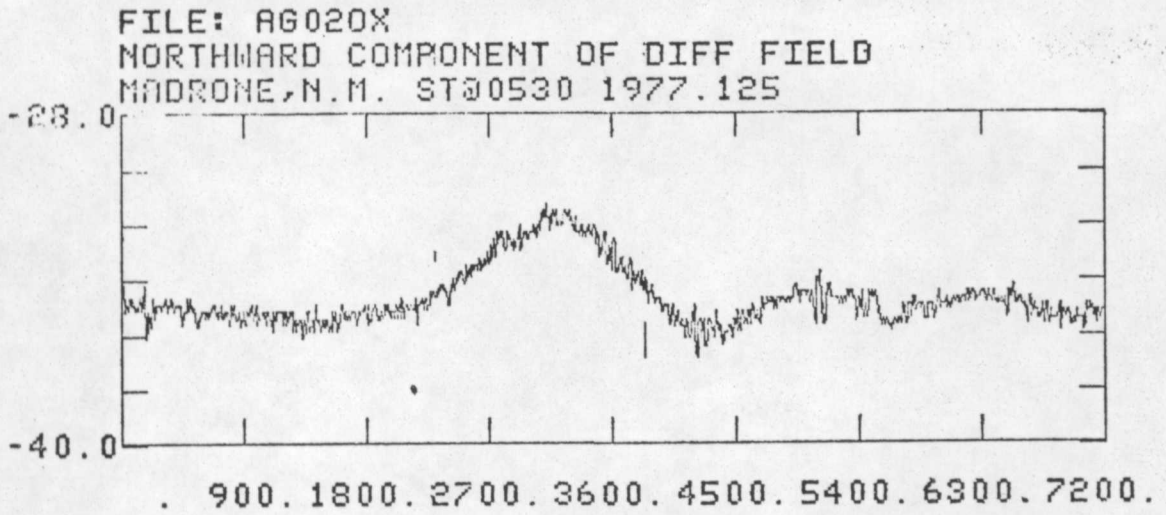
FILE: AG020X
NORTHWARD COMPONENT OF DIFF FIELD
MADRONE,N.M. ST@0530 1977.125
-28.0
-40.0
. 900. 1800. 2700. 3600. 4500. 5400. 6300. 7200.

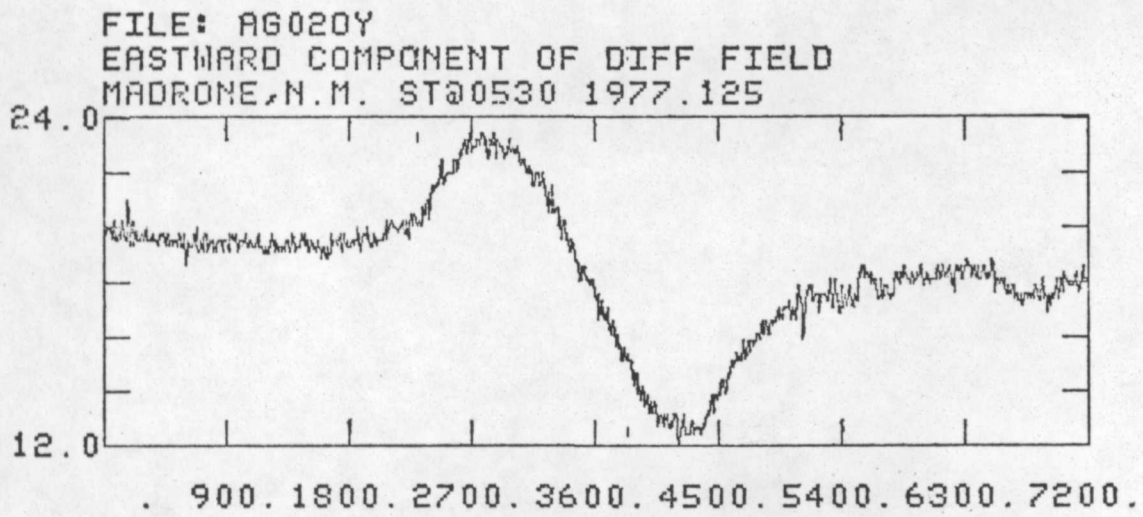
FILE: AG020Y
EASTWARD COMPONENT OF DIFF FIELD
MADRONE,N.M. ST@0530 1977.125
24.0
12.0
. 900. 1800. 2700. 3600. 4500. 5400. 6300. 7200.

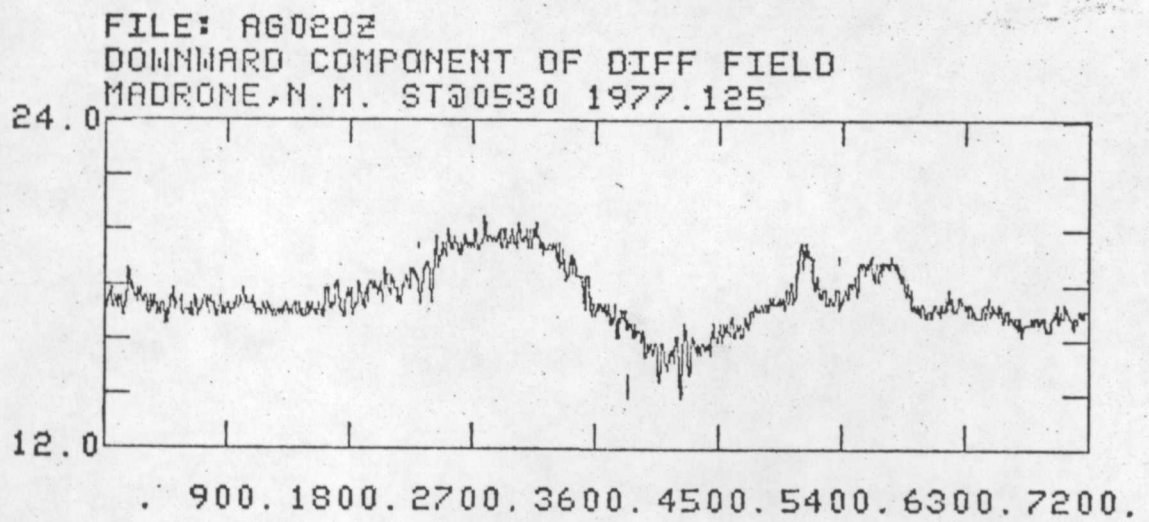
FILE: AG020Z
DOWNWARD COMPONENT OF DIFF FIELD
MADRONE,N.M. ST@0530 1977.125
24.0
12.0
. 900. 1800. 2700. 3600. 4500. 5400. 6300. 7200.

Figure B.3.3

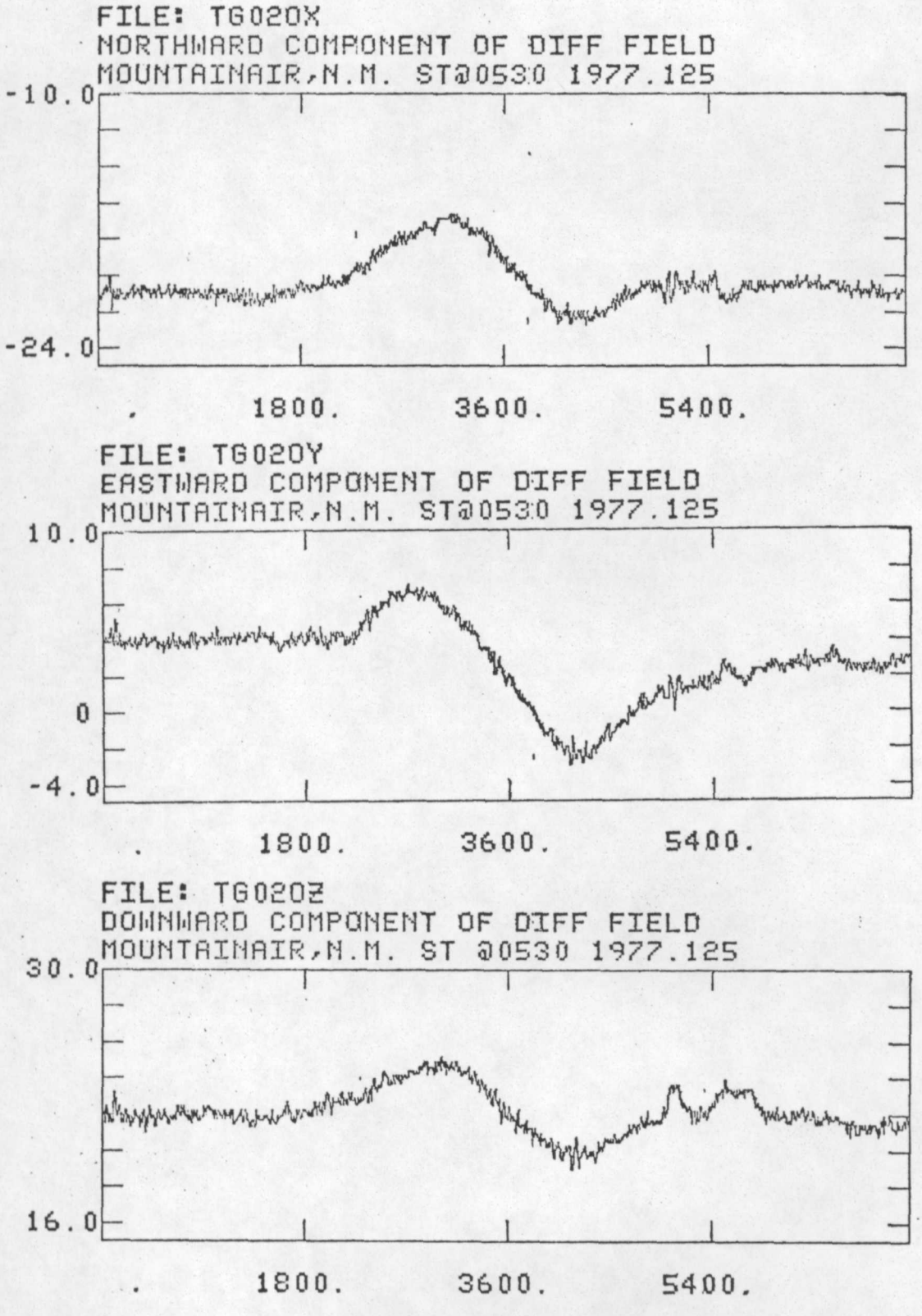
FILE: TG020X
NORTHWARD COMPONENT OF DIFF FIELD
MOUNTAINAIR,N.M. ST@0530 1977.125
-10.0
-24.0
1800.
3600.
5400.
FILE: TG020Y
EASTWARD COMPONENT OF DIFF FIELD
MOUNTAINAIR,N.M. ST@0530 1977.125
10.0
0
-4.0
1800.
3600.
5400.
FILE: TG020Z
DOWNWARD COMPONENT OF DIFF FIELD
MOUNTAINAIR,N.M. ST @0530 1977.125
30.0
16.0
1800.
3600.
5400.

Figure B.3.4

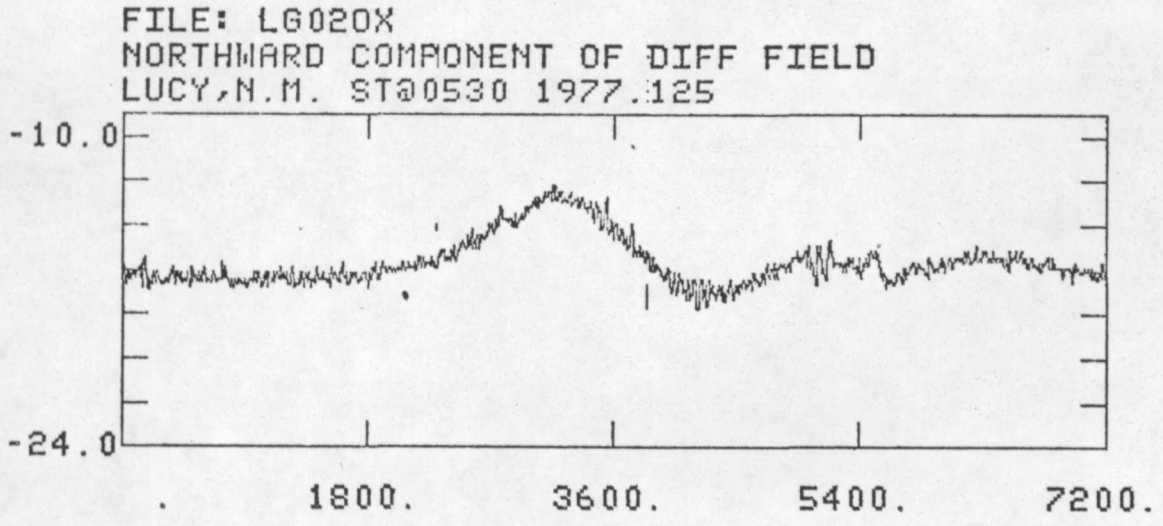
FILE: LG020X
NORTHWARD COMPONENT OF DIFF FIELD
LUCY,N.M. ST@0530 1977.125
-10.0
-24.0
1800.
3600.
5400.
7200.

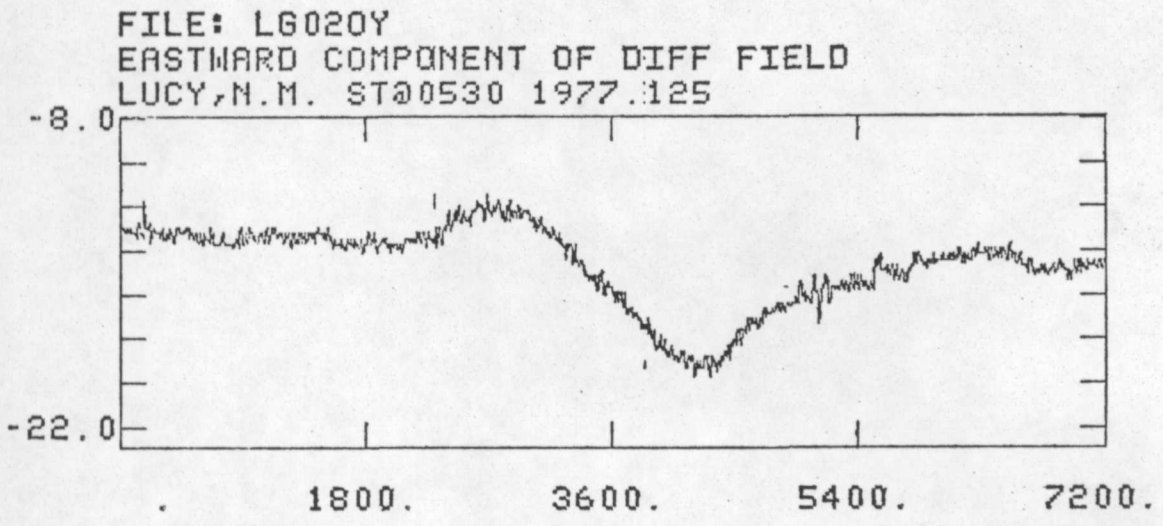
FILE: LG020Y
EASTWARD COMPONENT OF DIFF FIELD
LUCY,N.M. ST@0530 1977.125
-8.0
-22.0
1800.
3600.
5400.
7200.

Figure B.3.5

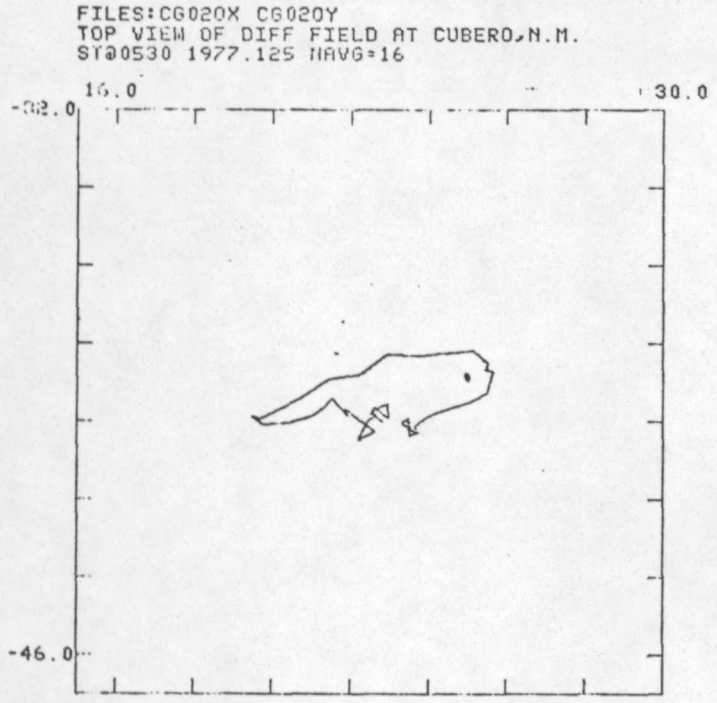
FILES:CG020X CG020Y
TOP VIEW OF DIFF FIELD AT CUBERO,N.M.
ST@0530 1977.125 NAVG=16
16.0
30.0
-32.0
-46.0

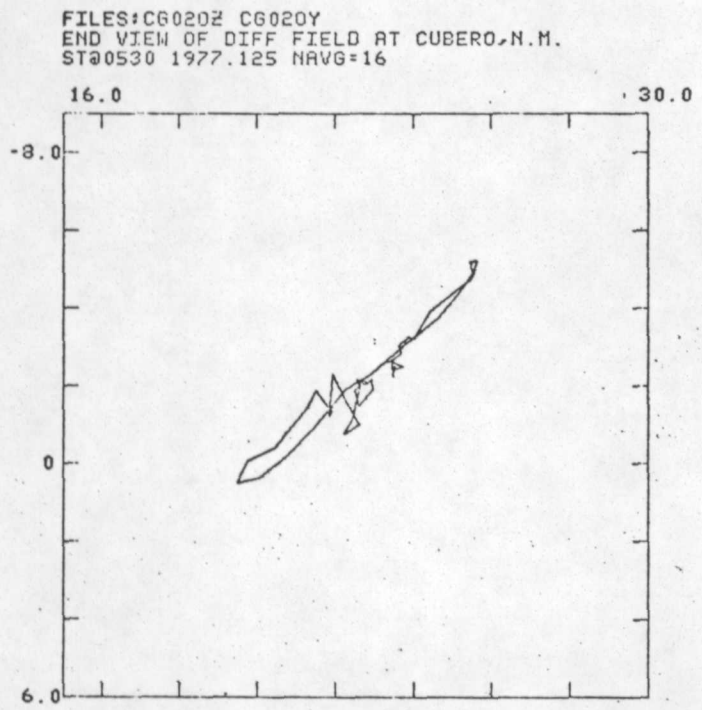
FILES:CG020Z CG020Y
END VIEW OF DIFF FIELD AT CUBERO,N.M.
ST@0530 1977.125 NAVG=16
16.0
30.0
-8.0
0
6.0

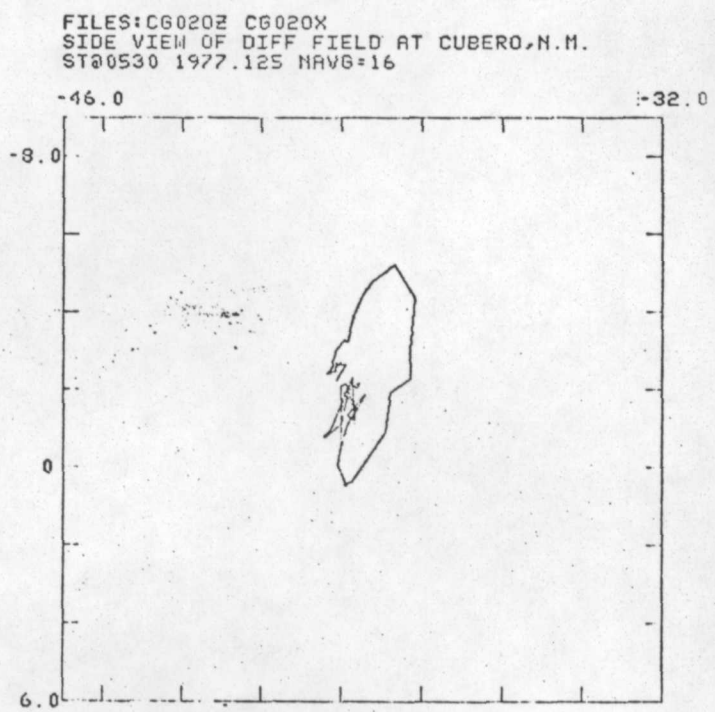
FILES:CG020Z CG020X
SIDE VIEW OF DIFF FIELD AT CUBERO,N.M.
ST@0530 1977.125 NAVG=16
-46.0
-32.0
-8.0
0
6.0

Figure B.3.6

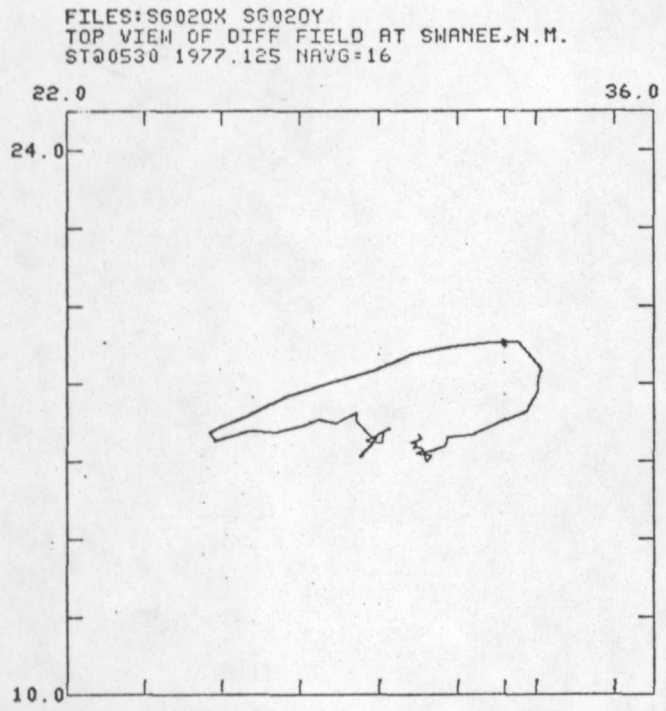
FILES:SG020X SG020Y
TOP VIEW OF DIFF FIELD AT SWANEE,N.M.
ST@0530 1977.125 NAVG=16
22.0
36.0
24.0
10.0

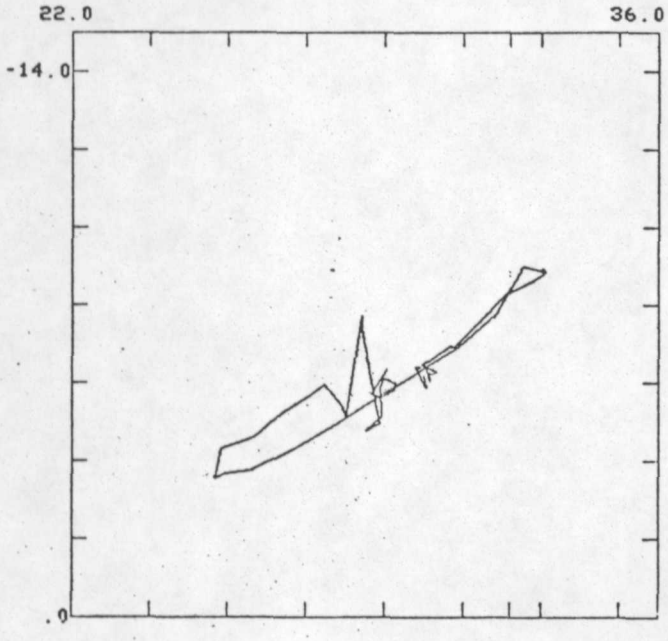
FILES:SG020Z SG020Y
END VIEW OF DIFF FIELD AT SWANEE,N.M.
ST@0530 1977.125 NAVG=16
22.0
36.0
-14.0
.0

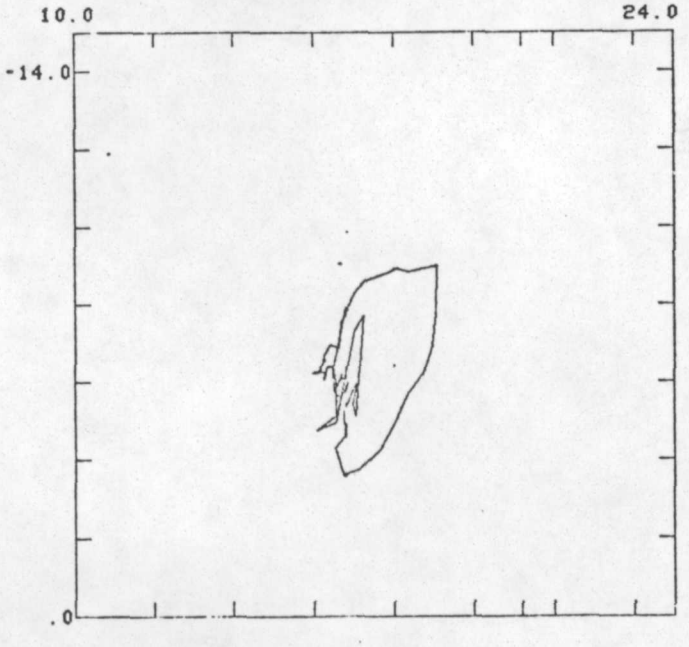
FILES:SG020Z SG020X
SIDE VIEW OF DIFF FIELD AT SWANEE,N.M.
ST@0530 1977.125 NAVG=16
10.0
24.0
-14.0
.0

Figure B.3.7

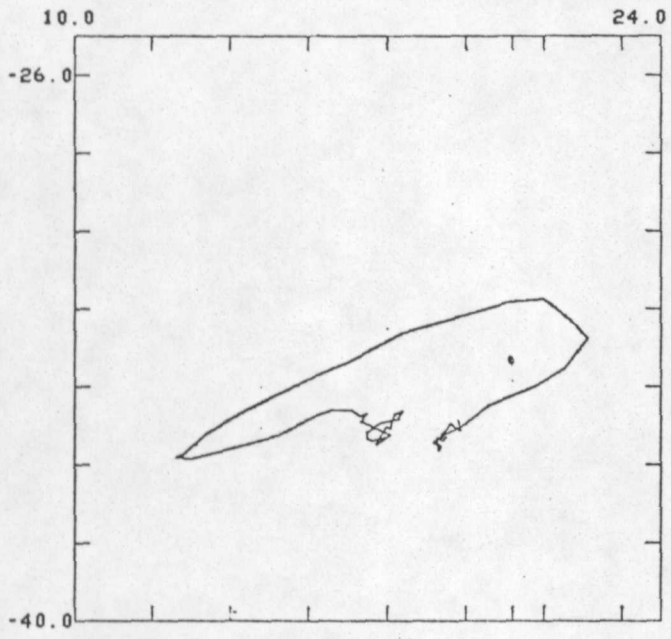
FILES:AG020X AG020Y
TOP VIEW OF DIFF FIELD AT MADRONE,N.M.
ST@0530 1977.125 NAVG=16
10.0
24.0
-26.0
-40.0

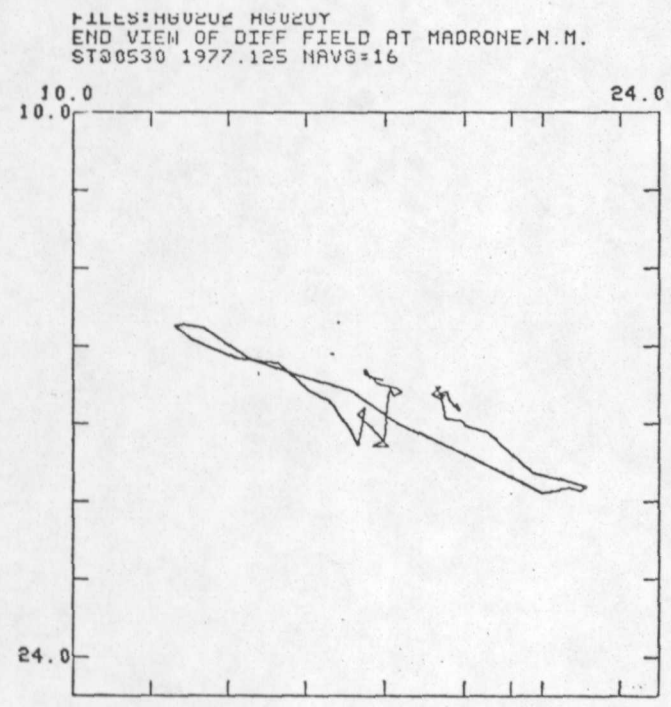
FILES:AG020Z AG020Y
END VIEW OF DIFF FIELD AT MADRONE,N.M.
ST@0530 1977.125 NAVG=16
10.0
10.0
24.0
24.0

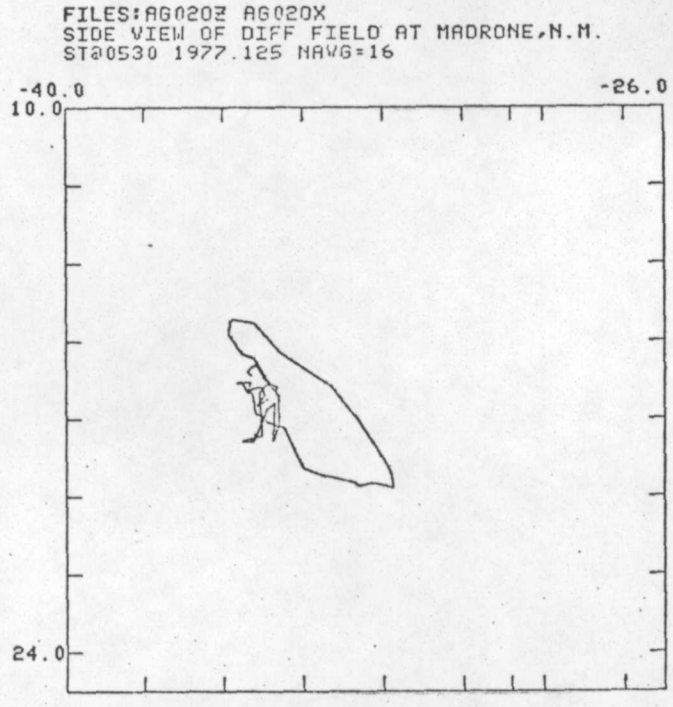
FILES:AG020Z AG020X
SIDE VIEW OF DIFF FIELD AT MADRONE,N.M.
ST@0530 1977.125 NAVG=16
-40.0
-26.0
10.0
24.0

Figure B.3.8

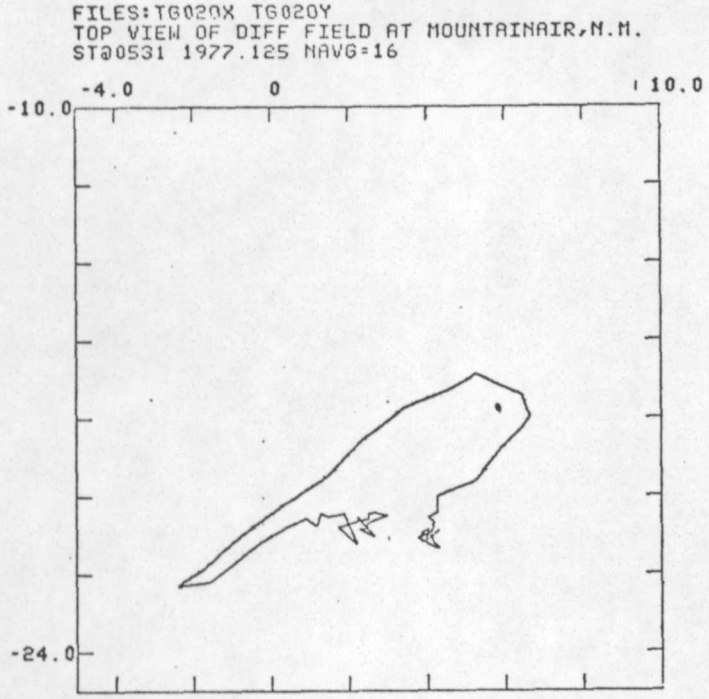
FILES:TG020X TG020Y
TOP VIEW OF DIFF FIELD AT MOUNTAINAIR,N.M.
ST@0531 1977.125 NAVG=16
-4.0
0
10.0
-10.0
-24.0

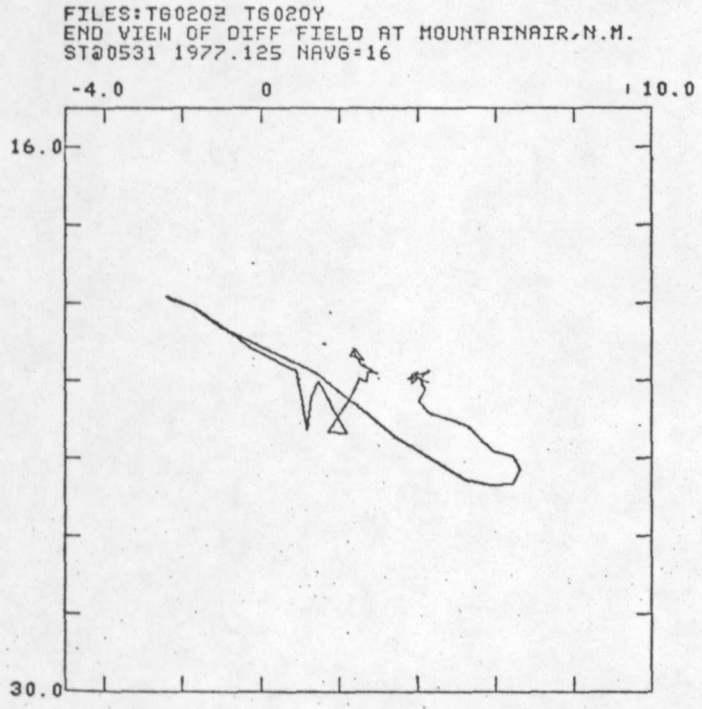
FILES:TG020Z TG020Y
END VIEW OF DIFF FIELD AT MOUNTAINAIR,N.M.
ST@0531 1977.125 NAVG=16
-4.0
0
10.0
16.0
30.0

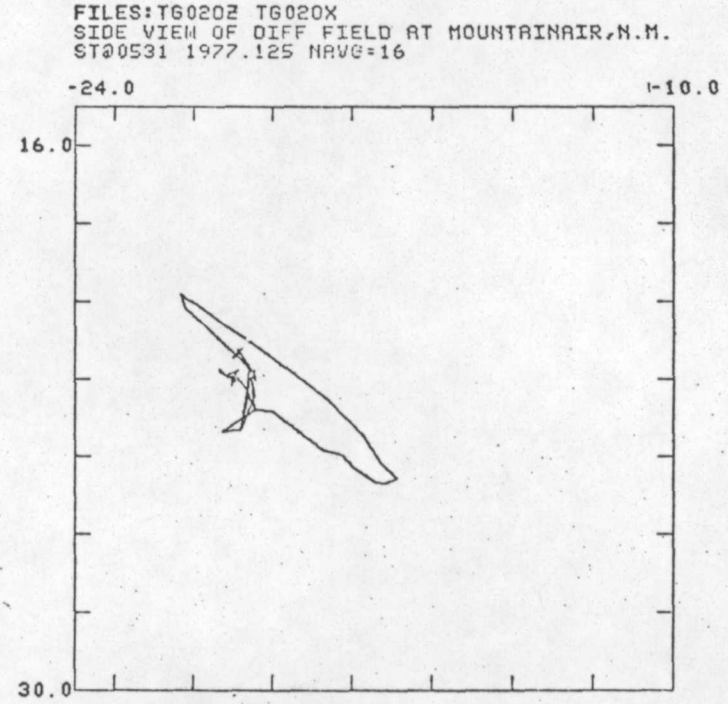
FILES:TG020Z TG020X
SIDE VIEW OF DIFF FIELD AT MOUNTAINAIR,N.M.
ST@0531 1977.125 NAVG=16
-24.0
-10.0
16.0
30.0

Figure B.3.9

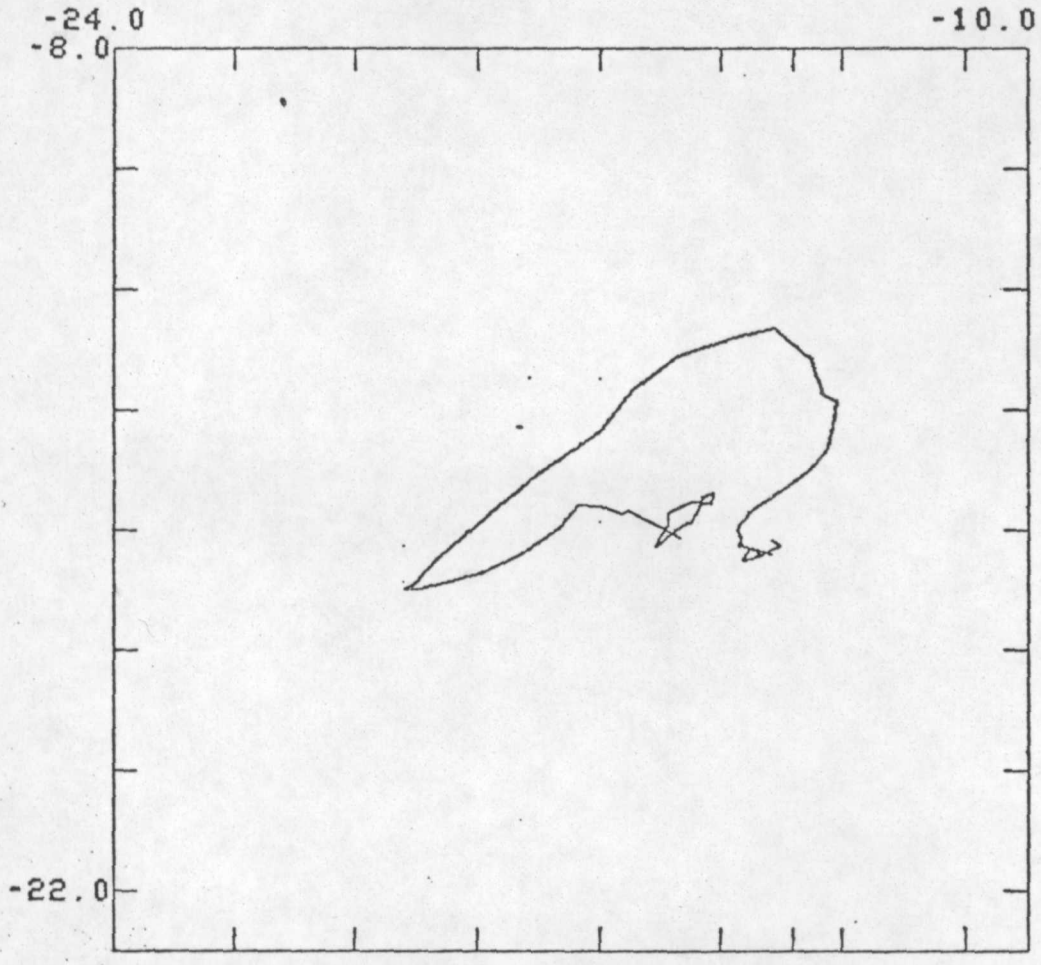
FILES:LG020X LG020Y
TOP VIEW OF DIFF FIELD AT LUCY,N.M.
ST@0530 1977.125 NAVG=16
-24.0
-10.0
-8.0
-22.0

Figure B.3.10